Øystein Rolstad

Orientation effects on energy dispersive spectroscopy in TEM

Master's thesis in MTFYMA
Supervisor: Antonius T.J van Helvoort
Co-supervisor: Dipanwita Chatterjee

June 2020

Master's thesis

NTNU
Norwegian University of Science and Technology
Faculty of Natural Sciences
Department of Physics

NTNU
Kunnskap for en bedre verden

Øystein Rolstad

Orientation effects on energy dispersive spectroscopy in TEM

Master's thesis in MTFYMA
Supervisor: Antonius T.J van Helvoort
Co-supervisor: Dipanwita Chatterjee
June 2020

Norwegian University of Science and Technology
Faculty of Natural Sciences
Department of Physics

NTNU
Norwegian University of
Science and Technology

Abstract

Energy Dispersive Spectroscopy(EDX) is the most used technique to determine the composition at the nanometer-scale by Transmission electron microscopy. The results are affected by how the electron beam hits the specimen relative to its orientation. When a crystal is oriented to a zone axis an effect known as channeling occurs which can alter the ratios between the emitted X-rays from different elements elements. This can introduce errors in the EDX quantification. In this thesis the orientation effects on EDX have been addressed. Python code has been developed and incorporated to quantify the channeling effect and to determine the occupation fraction of an impurity atom.

Using III/V nano wires (GaAs/GaAsSb), different setups have been used to evaluate systematically the effect of the relative orientation. Three setups have been utilized to achieve to examine the orientations effects around a channeling zone axis. The techniques to achieve a deviation from the zone axis were 1) physically tilting the specimen around a channeling zone axis. 2) Having a bending specimen. 3) changing the incident angle of the electron beam.

For configuration 1 a set-up with 4 detectors was used. For configuration 2 and 3 a single detector setup was used. In the first set-up it was found that the channeling an area of GaAs ZB and WZ displayed different behavior around [110] zone axis. WZ had a clear channeling effect on the zone axis with a recorded channeling effect of 15%, whilst the ZB structure exhibited the largest difference in composition at off zone orientations, with a recorded channeling effect of 8%. Variations between the detectors are observed and the tilts done were rather corse. At high amounts $(15at\%)$ of an impurity element a clear channeling effect was observed for a ZB, this channeling was asymmetric indicating that channeling occurd in a specific atomic row.

For case 2 bending was more gradual and significant compositional variations were only observed near the ends of the wire. The nanowires length was divided into three sections, and it was observed that the detectors position relative to the area of excitation would result in different strengths (from 5% to 15%) of channeling.

For case 3 there was more control of the relative angle between the beam and the crys-

tal, and finer compositional variations was observed. Channeling up to 15% was observed over the zone axis, it was found that the effect of channeling was highly dependant upon the reference spectra. Atom location by channeling-enhanced micro-analysis(ALCHEMI) provided decent results for this case for one of two reference spectra. Absorption was found to influence the measured channeling effect, by giving an increased difference in the measured elemental X-ray ratios.

ALCHEMI and statistical ALCHEMI was found to be unreliable for large quantities of an impurity element, likely due to a non negligible contribution to the average periodic potential of the crystal. Cases where ALCHEMI and statistical ALCHEMI gave physical meaningfull results were found, but certain aspects of the proceedure were found to be volatile. When utilizing the method of ALCHEMI it should be done with care.

Sammendrag

Energispredningsspektroskopi (EDX) er den mest brukte metoden for å bestemme et materials komposisjon på nanometer-skala ved transmisjonselektronmikroskoper(TEM). Resultatene påvirkes av hvordan den innkommende elektronstrålen treffer prøven relativ til prøvens orientering. Når en krystall er orientert til en sone-akse vil en effekt kjent som "Channeling" forekomme, dette kan påvirke forholdet mellom antall røngtenstråler produsert fra ulike elementer. Dette kan gi feil i EDX kvantifiseringen. I denne oppgaven har orienteringen av en prøves effekt på EDX blitt utforsket. Python kode har blitt utviklet og inkorporert for å kunne kvantifisere Channeling effekten og for å bestemme okkupasjons brøken av et urenhets(doping) element.

III/V nanotråder (GaAs/GaAsSb) ble undersøkt ved hjelp av forskjellige oppsett, for å evaluere den relative orienteringens effekten. Tre ulike oppsett ble brukt for å undersøke orienterings effektene rundt en channeling sone-akse. 1) rotere prøven rundt sone-aksen. 2) ha en prøve som bøyer seg. 3) å endre vinkelen på den innkommende elektronstrålen. For det første oppsettet ble det brukt 4 detektorer. For oppsett 2 og 3 ble det brukt 1 detektor. I det første oppsettet ble det observert at områder for GaAs (zincblende) ZB og (wurtzite)WZ hadde ulik oppførsel rundt [110] sone-aksen. WZ hadde en tydelig channeling effekt rundt sone aksen med en channeling effekt på 15%, i motsetning hadde ZB strukturen størst variasjon i komposisjon for orienteringer vekk fra sone-aksen med en channeling effekt på 8%. variasjoner mellom detektorene ble observert og roteringen av prøven ble gjort relativt røft. Ved høy konsentrasjon av et urenhets element ($15at\%$) ble en klar channeling effekt observert for ZB, denne channelingen var tydelig asymmetrisk og indikerer channeling i ulike atom rekker, avhengig av orienteringen.

For oppsett 2 var bøyningen av nanotråden mer gradvis og store komposisjons forskjeller ble bare observert nær trådens ender. Nanotråden ble delt inn i tre seksjoner og det ble observert at detektorens relative posisjon til røntgenstrålenes opprinnelses punkt ville resultere i en channeling effekt av ulike størrelser(fra 5% til 15%).

For oppsett 3 var det mer kontroll over den relative vinkelen mellom krystallen og den innkommende elektronstrålen. Finere komposisjons variasjon ble observert. Channeling effekten ble målt opp til 15% over sone aksen. Det var tydelig at referanse punktet var svær viktig når det kom til å kvantifisere channeling effekten. ALCHEMI ga ganske bra resultarer for dette oppsettet for 1 av 2 referanse spektrum. Absorbsjon ga store utslag i målt channeling, ved å skifte de elementale røntgenstråle forholdene.

ALCHEMI og statistisk ALCHEMI ble funnet upålitelige for store kvanta av et urenhets element, dette er sannsynligvis grunnet et ikke neglisjerbart bidrag til de gjennomsnittlige periodiske potensialet til en krystall. Målinger hvor ALCHEMI og statistisk ALCHEMI ga fysiske meningsfulle svar ble funnet, men visse aspekter ved ALCHEMI prosedyren ble funnet svært flyktige. Når man tenker å bruke ALCHEMI metoden burde dette gjøres med forsiktighet.

Preface

This master thesis is part of the 5 year study program "Physics and Mathematics" at the Norwegian University of Science and technology (NTNU). The thesis has been supervised by Professor Dr. Antonius T.J. van Helvoort and co-supervised by Postdoctoral Dipanwita Chatterjee. The data has been aquiered by Professor Dr. Antonius T.J. van Helvoort and Postdoctoral Dipanwita Chatterjee. This Master's thesis is a continuation of the work done in TFY4510 (Physics, project assignment). The main focus in this study have been on data analysis. I have attended one experimental session on the STEM JEOL 2100F at TEM Gemini Centre.

A special thanks to Dr. Antonius T. J. van Helvoort who's childlike enthusiasm for the subject matter never failed to motivate me in times of frustration and confusion. Another special thanks to Postdoctoral Dipanwita Chatterjee without whom this thesis would be a mess. Their insight in discussions and their appreciation for the subject matter have helped alot during this past year. Also a thanks to my parents for supporting me throughout all these years.

I hereby declare that this thesis is my own independent work and is in accordance with the regulations for the Master's degree program in Physics and Mathematics at NTNU

Øystein Rolstad

Table of Contents

Abbreviations

ADF   -   annular dark-field

ALCHEMI   -   atom location by channeling-enhanced micro-analysis

BF   -   bright field

CBED   -   convergent beam electron diffraction

CL   -   Cliff-Lormier

DF   -   dark-field

DP   -   diffraction pattern

EDX   -   energy-dispersive X-ray spectroscopy

EELS   -   electron energy loss spectrometry

FEG   -   field-emission gun

HAADF   -   high-angular annular dark-field

ICP   -   incoherent channeling patterns

ROI   -   region of interest

STEM   -   scanning transmission electron microscopy

TEM   -   transmission electron microscopy

WZ   -   wurtzite

Z   -   atom number

ZB   -   zinc blende

Chapter 1

Introduction

In materials, properties can be altered by slightly changing the composition or structure of the material. For example a B atom introduced to a Si system with the ratio 1 Br per 10^5 Si atom, gives a conductivity increase at room temperature by a factor of 10^3.[1]. Introductions of one or more elements in small amounts, are known as doping, and is the basis of our modern society based on silicon technology and optoelectric devices. In some cases doping of the material can enhance the properties of the material e.g making it more conductible (electrically and/or thermally), more structurally sound, changes to optical properties, chemical properties and so on. If new materials with such novel properties are discovered it could grant things like vastly more efficient semiconductors and stronger super alloys. Hitherto most of these material properties have been synthesized either by accident or by trial and error which can be very time and financially consuming [2]. A better understanding of the underlying atomic structure of materials and where subsidiary doping atoms position themselves can help to systematically predict enhanced material properties. This requires charachterization tools with sufficient accuracy and sensitivity, Like having a flashlight to illuminate gold in a dark room, instead of randomly stumbling upon it in the dark.

Only in the recent century has technology evolved to the stage where we can directly look into the atomic world [3],[4]. To look at this unit of length which is vastly smaller than the wavelength of visible light, high energy electrons ($> 100keV$) with a small wavelength are utilized. By utilizing Transmission Electron Microscopy (TEM) the observer can look at length scales down to Ångstroms which measure in at $10^{-10}m$, by having thin electron transparent samples.

With TEM a variety of different signals are produced as the incident electron beam interacts with the specimen. One interaction is the production of charachteristic X-rays. These can be counted and used to qualify and quantify the elements present in the specimen at a nm scale.. This method is known as Energy-dispersive X-ray spectroscopy (EDX). As established earlier the introduction of dopants in materials can have a major impact on the material properties. For small amounts of dopants ($\approx < 2at\%$), it's possible to determine the occupancy of a dopant on an atom column, by utilizing EDX. By doing multiple EDX scans at certain tilts, the ratio between emitted X-rays may shift due to an effect known as channeling. These ratios displacements can also be utilized to determine the occupancy of dopant's as demonstrated by Taftø and Spence [5]. This method is known as Atom Location by Channeling-Enchanced Micro-analys(ALCHEMI) and can be utilized to confirm that structures syntetize in a predicted matter, or to gain insight into how they syntezie. Hence, channeling (i.e an increased number of X-rays created in an atomic row) affects spectroscopic results, but can be utilized to improve the compositional characterization. This correlates back hvaing the characterization tools to develop materials with more novel properties a reality.

The datasets from the TEM microscope can be very large and in the last decades with the emergence and rise of computers and the vast increase in computational power available, processing and treatment of large datasets have become more tangible. Much of what makes computers so powerful is the software, which can automatise much of the data processing thus giving interpretable results in a relatively short time span. In principle, these treatments should be tracable and transparent. Unfortunaty much of the software commonly used by TEM operators for electron microscopes are commercial software, and come at quite a hefty financial cost. In addition some variables in these software are mere approximations and the routines which makes up the functionality of the software are hidden from the user. An alternative to commercial software are Open-Source software which are freely available for everyone and anyone can contribute to further develop the software, by making it more efficient or adding new functionality. It gives the user access to all the routines underlying the functionality, which allows users to examine where unexpected results stems from. This allows errors to be found and corrected, resulting in a good end product with an open and transparent community.EDX analysis is deceptively hard as a multitude of the signals counted are stemming from sources other than the material, in addition things like X-ray matter interactions and specimen orientation can decrease the accuracy of the analysis. Thus interpreting the EDX results correctly can prove quite challenging, and some knowledge are required to analyse the data correctly. The purpose of this thesis is to try to improve EDX by utilizing Hyperspy and add functionality for AL-

CHEMI and Statistical ALCHEMI into code so that it can be utilized by others with ease, comparing these with other EDX quantification methods and discuss the validity of the results with and without preprossesing of data.

Chapter 2

Theory

2.1 TEM

This section will give a brief overview of Transmission electron microscopy (TEM) and technique relevant for this report.

A TEM utilizes the low wavelength of electrons to give high resolution images of sufficiently thin speciments (<100 nm), the specimen must be thin enough for the electrons to be transmitted through. It utilizes a set of electromagnetic lenses to guide the electron beam as illustrated in figure 2.1. The set of electromagnetic lenses can be adjusted to manipulate the probe size of the incident electron beam.

The TEM has an electron gun which is situated at the top of the TEM and directs the created electrons down the instrument column. The two most utilized sources for TEM is a thermionic gun and an field-emmision gun (FEG). The Thermionic guns utilizes a LaB_6 crystal as a cathode, this cathode is connected to a metal wire. This metalwire is connected to a high voltage power supply which resistitivly heats the wire. At sufficient temperatures the energy becomes large enough to overcome the work function i.e electrons can escape the cathode surface. The electrons then have a negative potential of the accelerated voltage relative to the grounded anode i.e they will be accelerated to relative speeds (at sufficient voltage). A controllable beam is acquired by applying a small negative bias to a Wehnelt cylinder (electrode which guides the electron beam into the microscope itself.) The electron beam leaves the electron gun with energies ranging from 100-300 keV . As explained in Williams and Carters book[7].
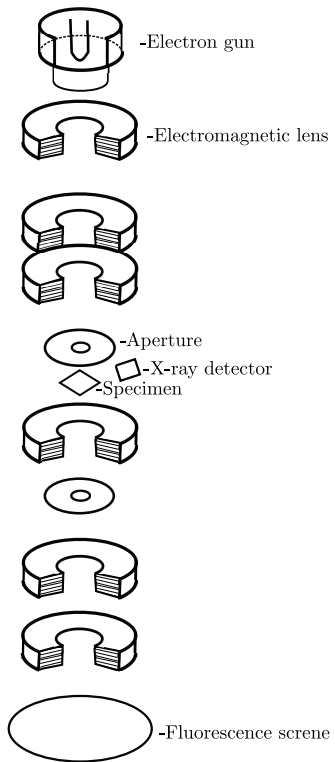
Figure 2.1: Schematic of a TEM adapted from [6]

A FEG utilizes a cathode which generates an intense electric field, due to it being charged with several kV. This field is strong enough to enable electrons to tunnel out of the tip. In addition to the cathode, the FEG also has two anodes, one providing extraction voltage for tunneling to occur whilst the second one accelerates the electrons to the accelerated voltage. The positions of these anodes also allows it to function as a lens, although incorporation of an additional electromagnetic lens provides a more controllable beam.

The lenses in the TEM are electromagnetic and made from copper coils. They are fixed, but the current induced in the lenses can be adjusted, which makes manipulation of the incident electron beam possible. Two common ways to illuminate the sample are with a parallel incident electron beam and with an convergent incident electron beam, these are refereed to as TEM mode and Scanning transmission electron microscopy(STEM) mode respectively. For STEM the intensity of the beam can be focused on a small area down to 0.5 Å. The convergent beam angle is very small $< 10^{-4}$ rads (0.0057) outlined in Williams and Carter book [7].

To reduce the intensity and change the convergence angle of the electron beam through the TEM, aperatures are utilized to block parts of the incident beam, if the intensity is to large it can cause damage to the specimen and the multitude of different detectors. In addition it can prevent over saturation.

As the incident electron beam hits the specimen, several plausible interactions can happen (see section 2.2) e.g some electrons are scattered and some are absorbed. When electrons are absorbed X-rays are created, which can be detected by an X-ray detector.

Once a X-ray reaches the Si-based detector, it will shut down and process the incident X-ray by assigning it to an energy channel. This is done by the X-ray creating electron hole pairs in the detector and measuring the current. As soon the energy of the X-ray is measured, the detector will turn back on ready to process another X-ray. One X-ray assigned to an energy channel is called a count. Ideally X-rays should be detected and processed one at the time, however in a not so ideal reality there are certain complications to detecting the X-rays, these can be read about in section 2.2.3. It is important to have a detector/software which can process X-rays fast to improve the accuracy and computation time.

Post interacting with the specimen the transmitted and scattered electrons are manipulated by a new set of electromagnetic lenses onto a fluorescent screen. The strength of the

lenses and height of the screen can be manipulated to display the real space image or the reciprocal image.

Heavier atoms scatter at an angle greater than lighter atoms and some scattering cases loses energy to inelastic effects like absorption. If much of the scattering is inelastic, electron energy loss spectroscopy (EELS) can be utilized to correct results. There are also High angle annular dark field (HAADF) which looks at electrons scattered at an even higher angle, it is very sensitive to the atomic number(Z) ($I \propto Z^5$) and for a specimen with even thickness gives a qualitative picture of the average Z at the probing position. When using a dark field the interaction of interest is any or all of the scattered electrons. In STEM this is done by an annular detector which in short is a circular detector which lets the direct beam i.e the bright field (BF) beam pass through. It measures electron scattered over larger angles for each illuminated point. The large scattering angle and the large detector makes it very unlikely that the detected electrons are in phase.

2.2   Electron matter interaction

An incident electron can interact with a specimen in three ways

- it can be transmitted trough the material without interacting with anything.

- it can scatter elastically on an atom's electron cloud or atom core.

- it can scatter inelastically losing a portion of its energy to other interactions in the system.

All these interactions between the speciment and the electron gives rise to different effects which when detected can reveal properties of the specimen. For a thin specimen (< 100 nm) the interactions in figure 2.2 are expected.
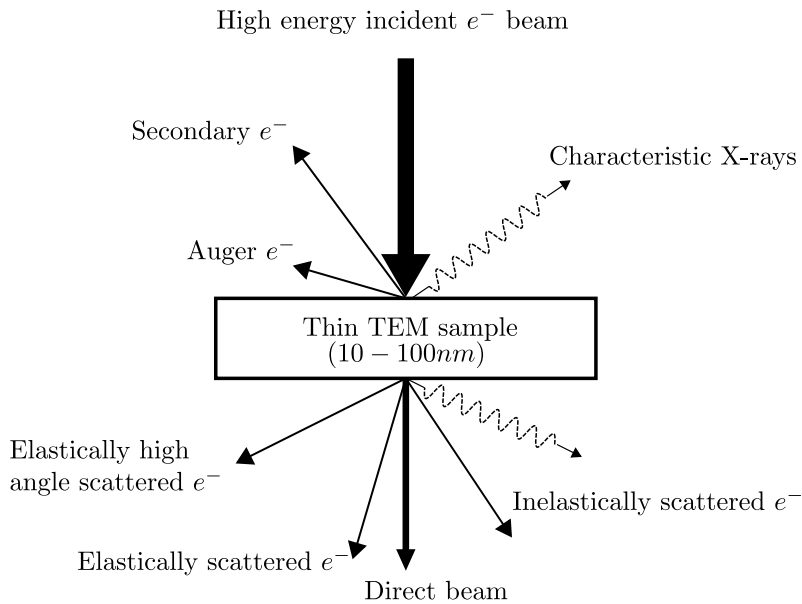
Figure 2.2: Electron matter interactions for a thin specimen

- The secondary electrons are ejected from an atoms conduction or valence band, they are generally considered free electrons within the specimen, they originate from the specimen surface and can provide high resolution images in STEM.

- Kinematic scattered electrons, which will give rise to electron diffraction. This is very telling about the weight ratio and crystal structure of the specimen.

- Elastically high angle scattered electrons can give information like mass thickness contrast and making up the dark field, useful for Z-contrast imaging.

- Inelasticlly scattered electrons will lose energy to the system whilst traversing the specimen, this energy loss will be of a characteristic nature and allows for analysis on the chemical composition of the specimen. This method is known as EELS.

- Characteristic X-rays are the result of inelastic scattering where an X-ray of specific energy can be emitted upon de-excitation of an excited atom. Further explained in [2.2.1].

- Auger electrons are secondary electrons with specfic energy. They can be created when inelastic scattering happens, where loosely bound outer electrons can be emitted upon de-excitation of an excited atom.

- Bremsstrahlung X-ray are produced when the electron scatters on the nuclei.

2.2.1 Characteristic X-rays

An incident electron with energy higher than an atoms inner-shell critical ionization energy, may scatter inelastically on one of said shells electrons, effectively knocking it out of the atom, leaving the atom in an ionized state.The chance for an incident electron ionizing the atom is given by the ionization cross section.

$$\sigma_T = \left(\frac{\pi e^4 b_s n_s}{E_0 E_C} \right) \log \left(\frac{C_s E_0}{E_C} \right) \tag{2.1}$$

The relationship between an atoms critical ionization energy and the atom number Z, can be described by the empirical Moseley's law

$$\lambda = \frac{B}{(Z - C)^2} \tag{2.2}$$

Where B and C are constants, and Z the atomic number. This then gives an estimate for the number of excited X-rays E_C values and their related characterisitc X-rays are not quite identical due to charachteristic X-rays from the different atom shells being invariably less than E_C. This difference increases with Z.

Post electron removal the atom will now have a lower energy state available from the vacant electron and the atom will be in a state it can not contain.
The atom returns to its lowest energy state by having an electron from a higher energy shell replace the vacant electron. The excess energy of this de-excitation will result in the emission of either an X-ray or an auger electron, as seen in figure 2.3. Through a similar process which involve significantly lower energies the atom relaxes back to its original state by interacting with the sample's free electrons. These "lower" energy interactions may emit lower energy photons or generate phonons but these will not be detected in the X-ray Si detector.

The energy de-excitation to the lower shells will be dependent on a couple of factors. The atom weight which is Z dependant, the shell in which an electron has been removed and the shell from which an electron de-excites. This released energy will be unique for the different parameters, which in turn allows for identification. The only energy shells which will be of interest in EDS are the three lowest energy shells K,L M in ascending order. In addition, the L and M shells containing subshells as can be seen in figure 2.3. It is worth noting that some energy transitions between shells/subshells are quantum mechanically illegal and will not happen. The X-rays created from interactions in the K shell are refereed to as K X-rays. If the vacant electron spot is filled with an electron from the shell above
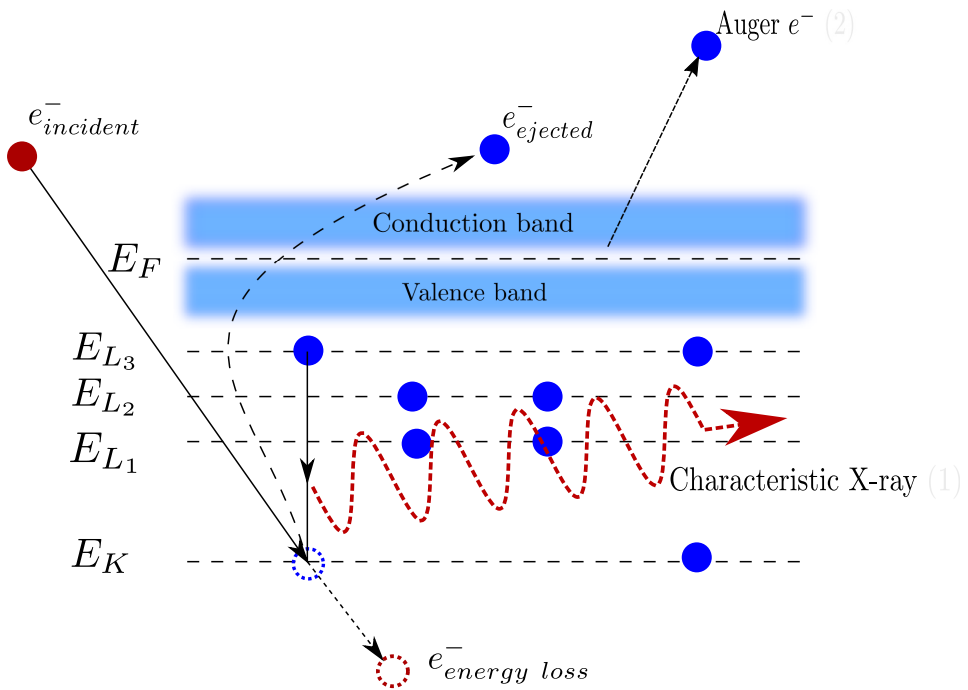
Figure 2.3: An inner shell electron is ejected out of the atom, as an upper shell electron takes the vacant electron's place two things can happen (1) an X-ray is emitted, or (2) an auger electron is emitted.

we denote the it as, α, the one above that one β these are subscripted with $_{1,2}$ ... for the different subshells.As an example a Ga with a knocked out K shell electron filled by an L shell electron (the only one quantum mechanically allowed) will be written as Ga_α.

Although electron transitions from all upper level shells can happen, they are not equally probable. In addition to this the atom might not excite an X-ray at all, it might emit an auger electron instead. The probability of X-ray vs Auger is known as the atoms fluorescence yield, and it has a strong Z dependence. It is usually plotted in relation to de-excitations to the K-shell against Z. It is given as

$$\omega = \frac{Z^4}{a + Z^4} \tag{2.3}$$

where $a \approx 10^6$. As the atoms below $Z = 5$ don't have outer shells, they will always emit an auger electron. Whilst the probability for X-ray emission goes drastically up for higher Z.

In addition to scattering on the electron cloud, the incident electrons can get scattered by the nuclei of the atom. This interaction can cause a large change in the incident electrons momentum releasing a photon in the process. The resulting intensity of these scatterings are modeled by

$$N(E) = \frac{KZ(E_0 - E)}{E} \tag{2.4}$$

K is known as Kramers constant, E_0 is the incident electron energy and N is the number of counts for a given energy X-ray.

Absorption

X-rays can interact with matter, but this interaction is not nearly as strong as the electron matter interaction. Nevertheless X-rays created inside a material will have to traverse said material before it can reach a detector, during the traversal X-rays have a probability of being absorbed. Which in turn will yield lower counts in the detector. In addition the rate at which X-rays are absorbed are dependant on the energy of the incident/created X-ray, the material and the length traversed within the material. The intensity of an X-ray can thus be modeled as

$$I(x) = I_0 e^{-\mu x} \tag{2.5}$$

The factor μ is known as the attenuation coefficient, which is the accumulated effect from the scattering processes, the transmission and the absorption i.e material and energy dependant. x is the length traversed through the material. A typical behavior of the attenuation coefficient can be seen in figure 2.4. Spikes in absorption coefficient are located at
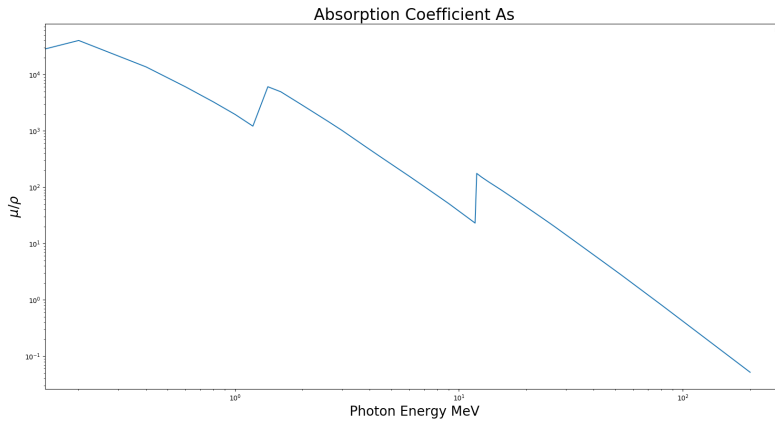
Absorption Coefficient As

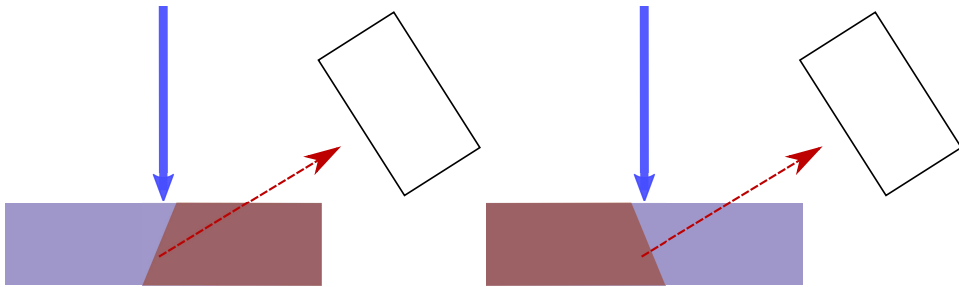**Figure 2.4:** Attenuation coefficient of As for energies between 0 KeV and 200 KeV

Figure 2.5: The type of material an X-ray traverses can affect the resulting intensity

energies similar to the characteristic X-rays. The attenuation coefficient is unique for each element and can be found in an online database[8].

If an X-ray traverses more pure element materials layered after each other, the resulting intensity can be modeled as

$$I(x_1, x_2, ..., x_n) = I_0 \Pi_i^n e^{-\mu_i x_i} \tag{2.6}$$

As the penetration power varies with energy, the resulting intensity of some X-rays will be lower as they are more easily absorbed by a material.

For materials composed of n number of elements the attenuation coefficient is set to be.

$$\mu = \frac{1}{n} \sum_{i=0}^{n} \mu_i \qquad (2.7)$$

The material traversed can be different for the same area scanned, due to the manner in which the specimen is oriented or the detector position. The different path-lengths through the material will thus cause a difference in intensity recorded.
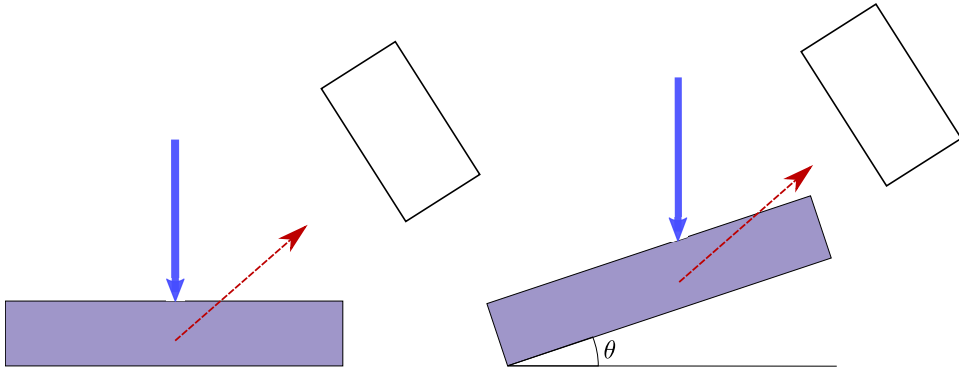

Figure 2.6: The length of material an emitted X-ray will cause a decreased intensity

2.2.2 Shadowing

In regards to produced X-rays being intercepted on its way to the detector, the specimen holder can completly block the X-rays path to the detector. This is known as shadowing, and it will result in a reduced number of X-rays reaching the detector. Shadowing is illustrated in figure 2.7a.
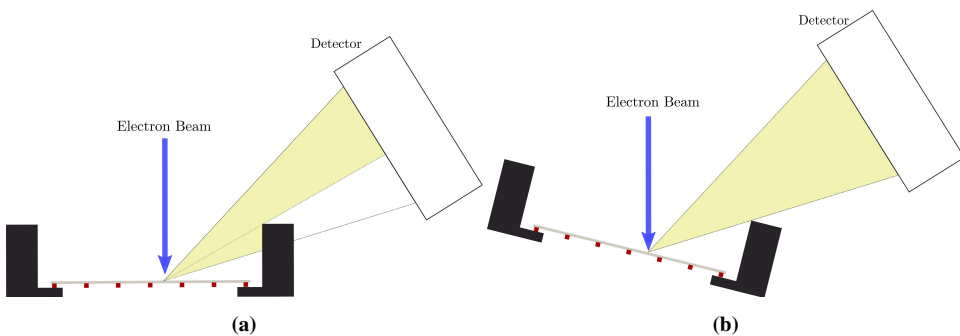

Figure 2.7: a) Shadowing of the detector, blocking parts of the incident signal, b) Shadowing avoided, by tilting the detector

2.2.3 Artefacts

As seen in section 2.2 the emitted X-rays may interact with matter and be absorbed, reflected or give rise to new characteristic X-rays, thus the path the X-rays take to the detector matter. If the detector is placed in such a manner that the X-rays will have to penetrate part of the sample to reach the detector, it can interact with parts of the sample which one does not wish to probe.

In addition the vacuum in the TEM microscope isn't perfect and might contain oxygen as well as the sample interacting with oxygen under preparation/transportation, which can cause oxidisation of the sample. Even if oxygen has a low fluorescence (not many X-rays are created), one can still expect that it has a non-negliable contribution to the spectrum.

Due to the nature of how X-rays propagate from the specimen they will also hit parts of the instrument, which will cause the elements of which the instrument is constructed off to produce characteristic X-rays. Common artifact peaks of this type originate from Fe and Cu.

As mentioned in section 2.1 the detector is composed of Silicon and if the X-rays have sufficient energy, they can interact with the silicon to produce characteristic Si X-rays, in addition to this the incident X-ray will loose the energy required to produce a Si_{k_α} X-ray.

In the section 2.1 the closing time of the detector was briefly discussed. If the detector doesn't close fast enough, an additional X-ray may enter the detector which in turn will create additional electron hole pairs and give a count in the wrong energy channel, as more electron hole pairs will be formed.

In some cases the bremsstrahlung can cause a background noise in the EDX spectra, but with clever positioning of the detector this can be mostly avoided. A typical EDX spectra can be seen in figure 2.8.
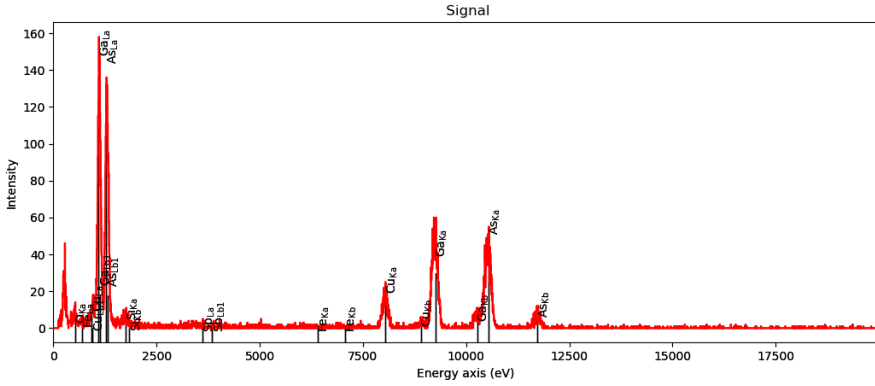
Figure 2.8: A raw EDX spectra. The nanowire in this particular consist of Ga,As and Sb. It is possible to deduce alot of the artefacts from this plot. The Bremssthralung is negligibly small in this particular spectrum.

2.3 Crystallography

Crystallography is the description of the arrangement of atoms in a crystal. The definition of a crystal is a three dimensional periodic array of identical building blocks (here building blocks are referred to as atoms or groups of atoms).

Crystallography is the description of a periodic arrangement of identical crystal basis (atoms or groups of atoms) in a crystal, apart from occasional impurities and imperfections present throughout the specimen. The translation between crystal basis's are given by the lattice vectors $\vec{a_1}, \vec{a_2}, \vec{a_3}$, which does not necessarily need to be orthogonal to each other.Thus any one basis position can be represented by R (in equation 2.8) from a given basis within the crystal. A structure where this applies for all positions is known as a Bravais lattice.

$$R = m \cdot \vec{a_1} + n \cdot \vec{a_2} + o \cdot \vec{a_3} \tag{2.8}$$

The lattice vectors constitute a parallelepiped containing one crystal basis known as a unit cell. Thus many properties of the crystal can be deduced from examining one unit cell. The volume of a unit cell is given as

$$V = \vec{a_1} \cdot \vec{a_2} \times \vec{a_3}$$

(2.9)

In figure 2.9a schematic of a unit cell's dimensionality, in figure 2.9b the unit cell for GaAs is visualized.
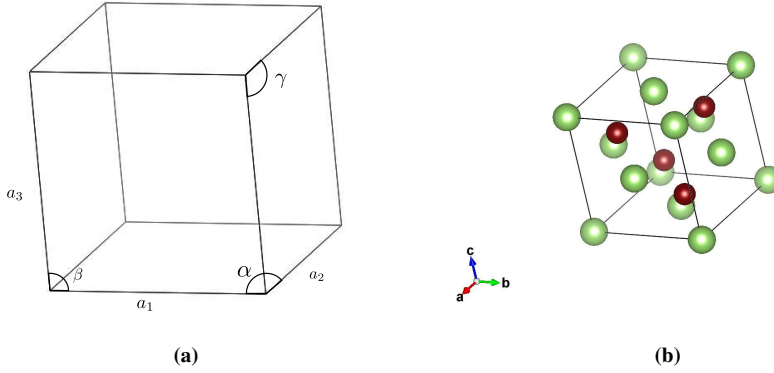

Figure 2.9: a) Dimensionality of a unitcell, b) GaAs (ZB) unitcell

For GaAs the particular unit cell construction is known as a Zinc Blende (ZB), which has a diamond cubic structure with alternating atoms.

In crystallography and solid state physics in general it is of great importance to know the relation between the real space and the reciprocal space (which is the fourier transformation of real space). The reciprocal lattice vectors can be given as a combination of the their real space counterparts $\vec{a_1}$, $\vec{a_2}$ and $\vec{a_3}$.

$$\vec{\mathbf{b_1}} = 2\pi \frac{\vec{a_2} \times \vec{a_3}}{V} \quad \vec{\mathbf{b_2}} = 2\pi \frac{\vec{a_3} \times \vec{a_1}}{V} \quad \vec{\mathbf{b_3}} = 2\pi \frac{\vec{a_1} \times \vec{a_2}}{V} \tag{2.10}$$

The lattice representation in reciprocal space can be represented by the miller indices (h,k,l) and the reciprocal vectors $\vec{\mathbf{b_1}}, \vec{\mathbf{b_2}}, \vec{\mathbf{b_3}}$. Any point in the reciprocal lattice can be represented by the reciprocal lattice vector $\mathbf{G}$.

$$\mathbf{G} = h\vec{\mathbf{b_1}} + k\vec{\mathbf{b_2}} + l\vec{\mathbf{b_3}} \tag{2.11}$$

When examining a crystal orientation of the specimen is of great importance. As the different orientations will yield different electron paths throughout the specimen. The effects of orientations are plentiful, but examples such as different diffraction patterns and intensities are expected at different orientations. The way the orientations are defined are through a plane orthogonal to the lattice vectors in which direction we observe the spec-
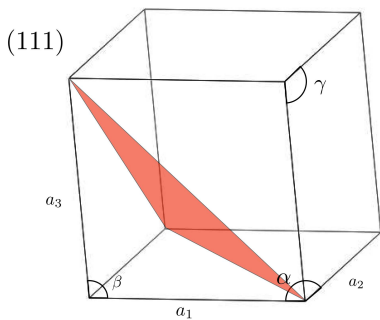
imen, meaning by the miller indices. A few schematics of an GaAs unit cell at different orientations are presented in figure 2.10.
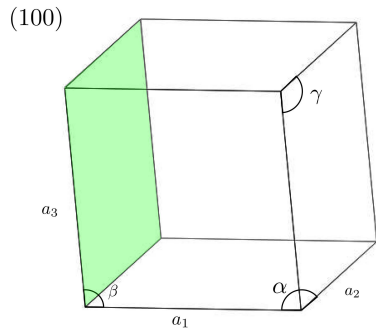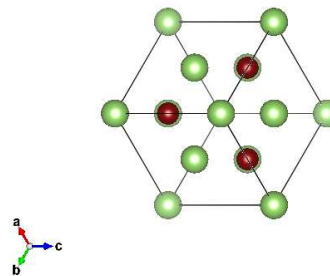

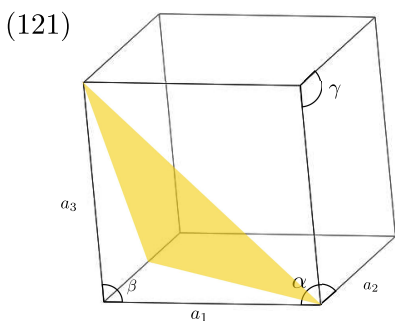(a) The [001] plane illustrated
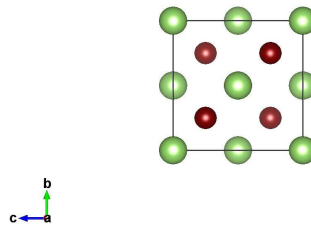
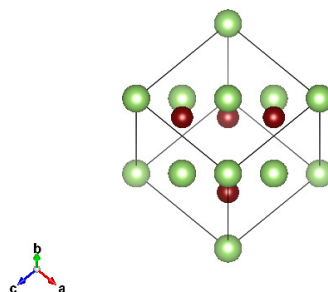(b) GaAs visualized the (001) direction

(c) The [111] plane illustrated

(d) GaAs visualized the (111) direction

(e) The [121] plane illustrated

(f) GaAs visualized the (121) direction

Figure 2.10: Schematic of different planes and how that orientation looks for GaAs

From the unitcell a crystals structure factor (F) can be determined. The definition of the

structure factor is the sum of atomic scattering factors for all atoms in a unit cell, multiplied with a phase factor. This in turn can determine where one can expect constructive and destructive interference.

$$F(\theta) = \sum_i^\infty f_i e^{2\pi i(hx_i + ky_i + lz_i)} \tag{2.12}$$

Here f_i is the i'th atoms scattering power where h,k and l are the miller indices (depending on orientation) and x,y,z are the atom positions within the unitcell. The θ is represents orientation (h,k,l). This in turn can be used to determine where diffraction can be expected. In the case of GaAS the structure factor becomes.

$$F_G = \begin{cases} 0 & \text{hkl mixed} \\ 4(\text{f}_{Ga} + if_{As}) & \text{h+k+l=odd} \\ 4(\text{f}_{Ga} + f_{As}) & \text{h+k+l=2n, n=even} \\ 4(\text{f}_{Ga} - f_{As}) & \text{h+k+l =2n, n=odd} \end{cases}$$

This will then yield information on where one can expect diffraction peaks, the structure factor is also crucial in determining the extinction length of a specimen (see Appendix A.1).

2.4 Diffraction

Wavelike spherical phenomena can be modeled as $E(r,t) = E_0 e^{i(kr - \omega t)}$ where E_0 is the amplitude, k the wave vector and ω the phase factor. When the two waves phases are off by a factor π it causes an amplitude extinction. This effect is known as interference. The part that can be observed is the intensity, given by

$$I = |\boldsymbol{E}(r,t)^2| \tag{2.13}$$

$\boldsymbol{E}$ is the super position of the wave i.e $\boldsymbol{E} = E_1 + E_2$. The phase information is lost when the intensity is measured. The electron has a particle/wave duality, and can be modeled as a wave. An incident electron can scatter elastically on an atom plane and it was shown by Bragg that this interaction behaved as a wave being reflected. He formulated his findings in Braggs' law, which states the conditions for constructive interference.

$$n\lambda = 2d\sin\theta_B \tag{2.14}$$

Where n is the n'th atom plane, λ the wavelength of the incident beam, d the spacing between atom planes. This is visualized in figure 2.11.
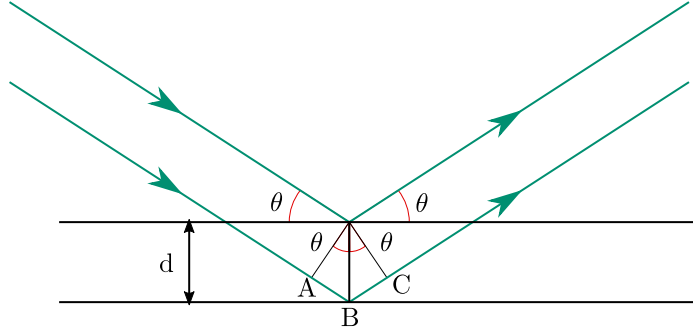

Figure 2.11: Visual representation of Braggs law, where θ is the angle between the incident wave and the lattice plane, d is the spacing between atomic planes.

What this means in practical terms is that if the length $AB + BC$ is such that the reflected beam from one atom plane has the same phase as the reflected beam from the plane above it, constructive interference will occur.

$$AB + BC = n\lambda \tag{2.15}$$

This is valid for multiple consecutive atom planes, as each plane reflects a small amount of the incident beam $(10^{-3} - 10^{-5})$ i.e this effect can have a contribution from $10^3 - 10^5$ atom planes. Bragg's law thus is a consequence of the lattice periodicity.

This collection of intensity maxima will make up what we call the diffraction pattern. This is pattern resides in the reciprocal space, which is the fourier transformation of the real space. The way we navigate the reciprocal space is with $\vec{Q}$ which is analogous to the real space $\vec{r}$.

$$I(Q) = |\mathcal{F}(\rho(r))|^2 \tag{2.16}$$

I(Q) being the intensity at a given position Q, $\mathcal{F}(\rho(r))$ is the fourier transformation of the electron density.

2.4.1 Ewalds sphere

The diffraction conditions formulated by braggs can be described in the reciprocal space by the Laue condition. The incident wavevector $\vec{k}$ and the scattered wavevector $\vec{k'}$ amplitude is given by the wavelength λ.

$$|k| = \frac{1}{\lambda} \tag{2.17}$$

The position in the reciprocal space is given by $\vec{Q} = \vec{k} - \vec{k'}$. The condition for diffraction is fulfilled when the reciprocal lattice vector $\vec{G}$ to equal the $\vec{Q}$.

$$\vec{Q} = \vec{G} \tag{2.18}$$

The positions in reciprocal space which fulfill the requirements for diffraction in reciprocal space can be vizualised with the Ewalds sphere. The sphere has a radius which relates to the incident electrons wavelength λ as such $r = 2\pi/\lambda$. This in turn makes the points satisfying the diffraction conditions in all practical conditions to lay on a line.
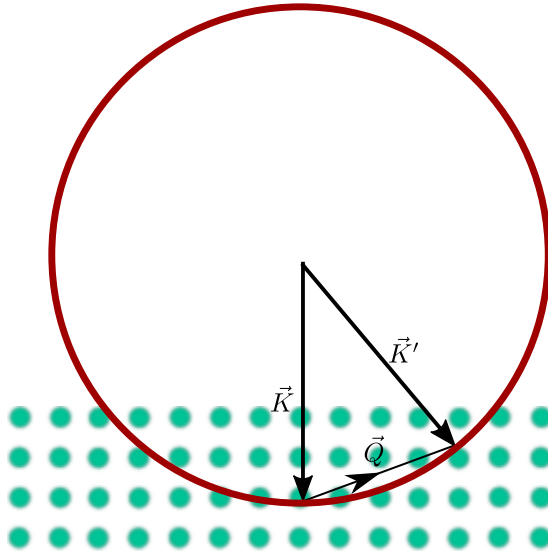

Figure 2.12: Schematic of Ewald sphere in 2d (red) with a reciprocal lattice (green)

The incident wave will not have an exact set λ and will have a deviation from the average wavelength $\Delta\lambda$, this will give a thickness to the Ewalds sphere. In addition, small deviation from the zone axis will also give diffracted points, these intensities are correlated to how far off the Bragg condition they are. The effect of this in regards to EDX analysis are briefly explained in section 2.4.2 and the calculations can be found in the appendix.

This deviation from the Bragg condition is known as the excitation error/deviation parameter and is denoted as s. s is a vector and its sign indicated whether or not the position is inside the ewalds sphere (s is positive) or outside (s is negative).
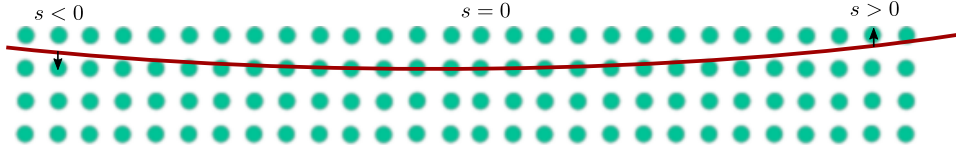

Figure 2.13: The offset s visualized, here diffraction can be expected even though the diffraction conditions aren't completely satisfied

Note that these figures are over exaggerated to better demonstrate how this works. In reality the radius will be very large and lay almost "flat" over a lattice (given a propper lattice orientation).

2.4.2 Channeling

The following section is based on chapter 13 of Transmission Electron microscopy book[6] by Fultz and Howe. Calculations and a deeper explanation of the subject can be found in the appendix A.1. A high energy electron will experience a change in its wavevector as it traverses a material, due to the average periodic potentials of the specimen. This potential is constituted by the materials structure factor, which again is dependant on the orientation of the unit cell relative to the incident electron beam.

The changes in the electron beam throughout the specimen can be represented by breaking the incident electron wavefunction ϕ into two parts the direct beam ϕ_0 (which is a continuation of the incident beam) and the diffracted beam ϕ_g. Which helps in keeping track on how the original amplitude is distributed throughout the specimen at a given depth. These beams can also be represented by a combination of bloch waves and spherical waves in such a manner

$$\Phi_0 = \frac{\phi_0}{\sqrt{V}} e^{ik_0 r} = C_0^0 \Psi^{(1)} + C_0^1 \Psi^{(2)} \tag{2.19}$$

$$\Phi_g = \frac{\phi_g}{\sqrt{V}} e^{i(k_0+g)r} = C_0^0 \Psi^{(1)} + C_0^1 \Psi^{(2)} \tag{2.20}$$

Where V is the unitcell volume, k_0 is the incident wavevector, g is the reciprocal lattice vector and Ψ is the solution of a bloch wave .

For a slight excitation error s around the zone axis, the average periodic potential will alter the incident blochwaves. If the specimen consists of two elements, and these line up in elemental rows. One of the blochwaves will have its amplitude maximized over a given atomic row. This effect is known as channeling.
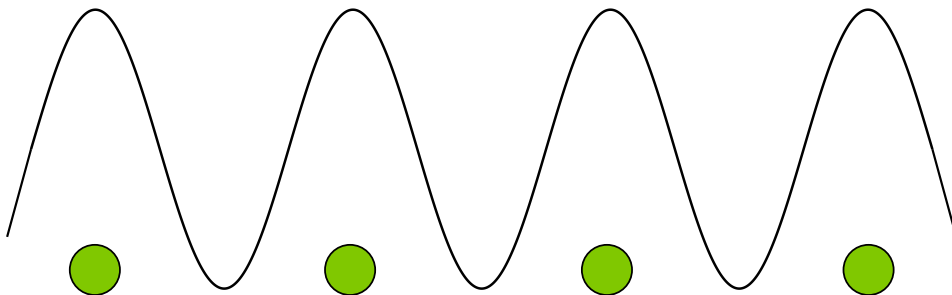

Figure 2.14: Bloch wave maximized over an atom row

The strength of channeling is defined by [9], [10] as

$$E = \frac{|Y^C - Y^0|}{Y^0} \tag{2.21}$$

Where $Y^r = \frac{N^r_{el_1}}{N^r_{el_2}}$, is the ratio of the number of X-ray counts from element 1 ($N^r_{el_1}$) divided by the number of X-ray counts from element 2($N^r_{el_2}$) at an orientation r. The subscripts 0 and C, stands for referance (non channeling condition) and channeling condition respectively. This effect is only relevant when the specimen thickness is larger than the extinction distance, which depends on the structure factor. It also encourages a higher excitation of X-rays, the reason is explained in the appendix A.1. When the deviation from the zone-axis is too great or the thickness too thin, dynamical theory will exhibit the same behavior as kinematical theory.

2.5   Qualitative X-ray analysis

A qualitative analysis of an EDX spectra requires every X-ray peak to be determined. This requires a proper calibration of the system,which can be done by using known materials, localizing their characteristic peak in the spectra and moving/resizing the energy channels accordingly, so they match up with the tabulated values. After the system has been properly calibrated, one can analyse the spectra from a specimen. By considering the aforementioned artefacts, one can deduce which peaks stem from these and treat them accordingly, in most cases they will be ignored. The background will also have to be

subtracted from the spectra. After doing these steps the elements in the specimen can be deduced by analysing the remaining peaks.

2.6   Quantitative X-ray analysis

The EDX spectra can qualitativly tell what elements resides inside the specimen, but the EDX spectra can also be utilized for quantitative analysis. In section 2.2.1 the creation and counting of characteristic X-rays were detailed and intensity peaks defined. In 1951 Castaing[11] assumed that the concentration of an element within a speciment could be given by the generated intensity $I_{(i)}$, however its difficult to achieve in practice. The suggestive fix proposed by Castaing

$$C_i/C_{(i)} = [K]I_i/I_{(i)} \tag{2.22}$$

This fix takes the difference between the generated and measured count for element i, K is a factor with contributions from Z, the absorption and the fluorescence. Given a standard composition $C_{(i)}$. However the calculations of the correction term K are exceedingly complex. With the emergence of TEM, Cliff and Lorimer[12] showed that a modified version of Castaings equation could be used to determine quantification on thin speciments (i.e making the absorbtion and flourescence negligable).

$$\frac{C_A}{C_B} = k_{AB}\frac{I_A}{I_B} \tag{2.23}$$

This shows how the weight percentage concentrations of the elements (C_A, C_B) relate to the each other vs how measured intensity peaks relate to each other times a sensitivity term reliant on the Z of element A and B. This can be extended to all elements present in the specimen (given the conditions for Charachteristic X-rays are meet). The $k-$factors for elemental pair are related in the following manner for element A, B and C.

$$k_{AB} = \frac{k_{AC}}{k_{BC}} \tag{2.24}$$

The combined weight percentage of the entire specimen will naturally add up to 100%.
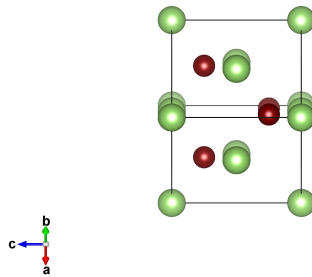
$$\sum_i C_i = 100\% \tag{2.25}$$

Figure 2.15: GaAs unit cell tilted slightly of the [110] direction, to illustrate the atomic rows.

The use of this method requires that the k factor be determined, either experimentally or by calculation. There is also the ZETA-factor method which utilize pure-element standards to determine the zeta factors, which serves the same purpose as the k factors. The quantitative methods are done off zone to prevent the effects of channeling.

2.7   ALCHEMI

Atom Location by Channeling Enchanced Microanalysis (ALCHEMI) is a quantitative techinque that can determine the atom crystallographic sites, distribution and types of substitutional impurities in small quantities as reported in the book by Williams and Carter[7] and the papers by Spence, et al[9], [10]. It is performed by taking EDX-scans of a crystal at a tilt close to a channeling zone axis (usually a very small tilt is required) and quantitatively comparing the resulting EDX spectra against a non-channeling spectra. The theory of ALCHEMI was deduced by Spence and Taftø [5]. From section 2.4.2, it was established that the incident and diffracted beam could be represented as a collection of bloch waves. The shape of the bloch waves are affected by the average periodic potential.

When an atomic row consist of one element and channeling occurs over that row, a bloch wave can have its wave crest over said atom row. In section 2.4.2, it was stated that a bloch wave maximized over an atomic row causes an increase in the number of excited X-rays. Small amounts of an impurity atom ≈ 2 or less atom $\%$ [10],[13] would not alter the average periodic potential in any significant manner, thus if channeling occurs in a row with impurities a linear increase in the X-rays from the impurity and host atom are expected. This type of blochwave maximization is illustrated in figure 2.16.
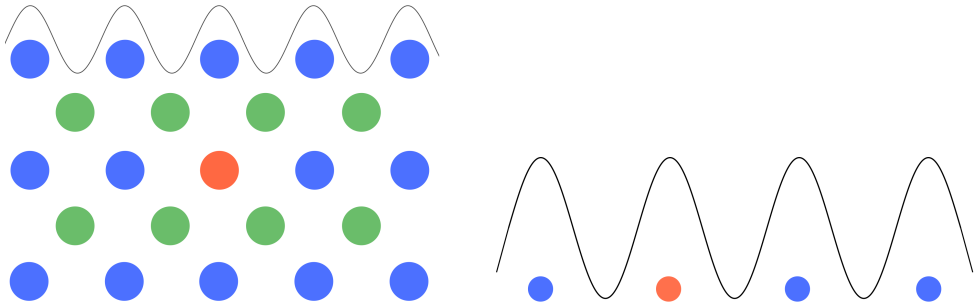
Figure 2.16: Small amount of an impurity element will not change the average periodic potential in any significant way, thus the blochwave will maximize over all the elements in the atom column

The atom column that will experience a bloch wave maximization during a channeling condition, is determined by excitation error s and the unit cell form factor.

(1)   (2)   (3)

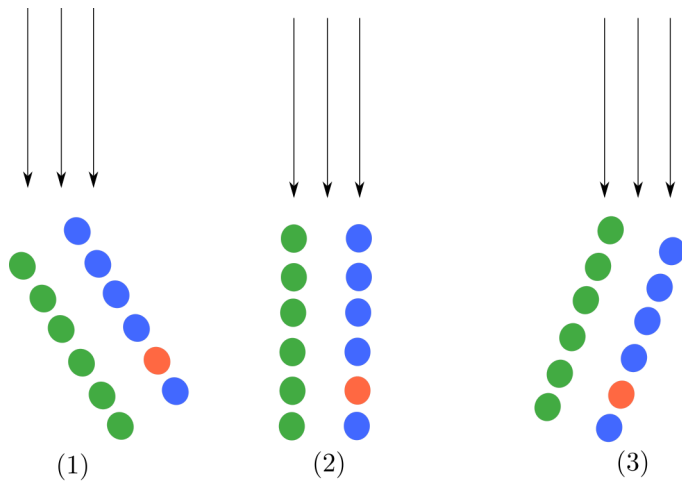**Figure 2.17:** Two atom rows at -s, 0 and +s. The different tilts can lead to the blochwaves maximizing over different atom rows.

The next subsection will go through the steps and equations to perform ALCHEMI and find the impurty occupation fraction on the different atomic rows.

2.7.1 A thought experiment on ALCHEMI

For a material consisting of three different elements A,B and C two different EDX scans at different tilts are performed, one slightly off zone and one off zone i.e under kinematic conditions. The number of counts under each line of interest e.g Si_K, is counted up. A fraction p of the C atoms is assumed to line on the A atoms sublattice, and a fraction of (1-p) on the B sublattice. By taking the number of counts of atom C in measurement 1 and 2, with the atom sublattice occupancy p.

$$I_{C_2} = I_{C_1}p + I_{C_{tot}}(1-p) \tag{2.26}$$

Where the subscript of I_C dictates which measurement the count was taken at. $I_{C_{tot}}$ is the added sum of the C counts from the different measurements. Thus the occupation fraction p can be calculated. A schematic of two X-ray spectra at different tilts are illustrated in 2.18. Using the relative ratio between the counts of the different measurements, the dose

Figure 2.18: Schematic of EDX spectra of a material at different tilts
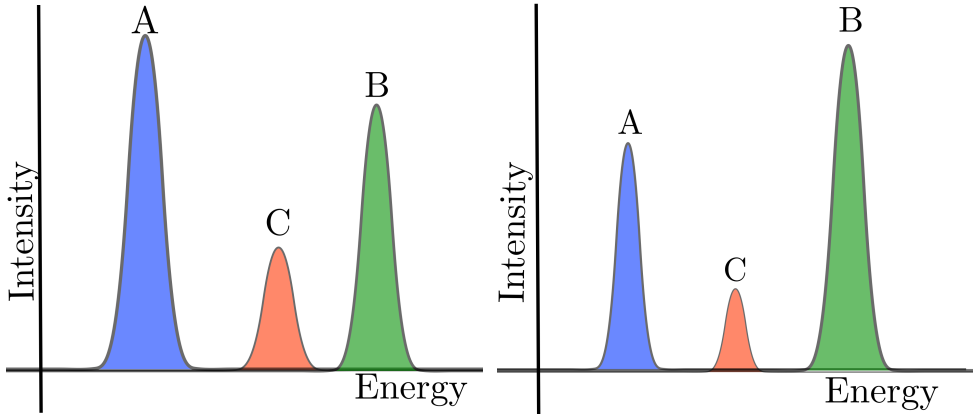
ratio R_X for an element X are defined as.

$$R_X = \frac{R_{X_C}}{R_{X_0}} \tag{2.27}$$

Here R_{X_C} are the counts of element X under a channeling condition and R_{X_0} are the X counts from a non-channeling condition.

The occupation fraction are then defined from the dose ratio of the three elements.

$$p = \frac{R_C - R_B}{R_A - R_B} \tag{2.28}$$

If $p = 1$, then C resides solely on sublattice A and for $p = 0$ it resides on the B sublattice. If p=0.5, half of C resides on A and half on B and so on. The fraction is only physical for values between 0,1. There have been reports of varying results by the utilization of AL-CHEMI [10],[9],[14] , and an alternative method which seems to produce more accurate results compared to standard ALCHEMI is the method of statistical ALCHEMI presented in a paper by Rossouw et.al[15].

Statistical ALCHEMI

A multitude of papers (for example Pennycook et.al[14] and Turner et.al[16]) reported on the shortcomings and varying success's of ALCHEMI, as a response to this a statistical approach to ALCHEMI. The method known as statistical ALCHEMI, calculates the occupation fraction from multiple channeling spectras against a reference non-channeling spectra. The occupation fraction is then plotted against number of counts from the tertiary impurity element. An element C present in two sublatices A and B with each their own intensity count, can be used to determine α_A and α_B which is essentially the contribution to the C counts related to the measured A and B counts from their respective sublattices. In statistical ALCHEMI (Rossouw [17]), the results are plotted against the strength of channeling and a plane is fitted to the data points through regression.[18] The α coefficients can be determined by a least square fit.

$$I_C = \alpha_A I_A + \alpha_B I_B \qquad (2.29)$$

It can then be shown that p can be expressed by the α_A coefficient and the K-factors from equation 2.22.

$$p = \frac{\alpha_A}{\alpha_A + \frac{k_A}{k_C}} \qquad (2.30)$$

In papers by Spence et.al [9],[10] the statistical ALCHEMI is performed by plotting the alchemi results of different tilts (excitation errors) by rocking the incident beam to get an incoherent channeling pattern (ICP). The results are usually plotted as a function of the ALCHEMI results p against the number of counts from the host element of an atomic row, then a regression line is drawn through these points. The coefficient determining the slope will thus grant our result. In a paper from Spence et.al[9] the statistical ALCHEMI was performed with a constant C, which is gained by doing a matrix multiplications of the p result of length N against a 1 x N matrix containing 1.

2.8 Data processing

The lines in the EDX spectra most suitable for analysis is the K_α lines as the L and M lines have many closely spaced subpeaks which often overlap, due to the resolution limitations of the detector. But in cases where the K_α are outside the spectrum ranger or too energetic to be detected i.e will penetrate the detector, the L and/or M lines may be utilized. But as the L and M lines have low energy and usually overlaps, deconvolution it is of great importance when analysing these peaks. The general approach to interpret EDX signals is depicted in the flow chart in figure 2.19. Each of these steps will be further elaborated later in the section.
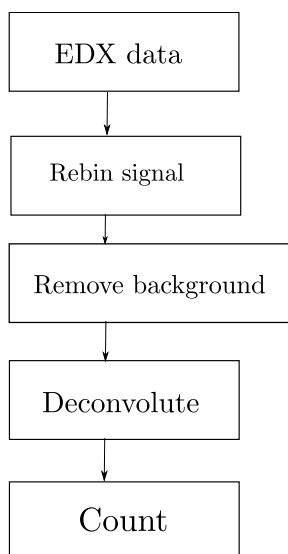
```
┌──────────────────┐
│     EDX data     │
└──────────────────┘
         │
         ▼
┌──────────────────┐
│   Rebin signal   │
└──────────────────┘
         │
         ▼
┌──────────────────┐
│ Remove background│
└──────────────────┘
         │
         ▼
┌──────────────────┐
│   Deconvolute    │
└──────────────────┘
         │
         ▼
┌──────────────────┐
│      Count       │
└──────────────────┘
```

Figure 2.19: Flow chart representing how raw data is converted to counts, which can be used to deduce composition.

2.8.1 Raw data

When recording EDX in scanning transmission electron microscopy (STEM), each pixel of an image will have its own spectra, this is schematically shown in figure 2.20 with a corresponding spectra .
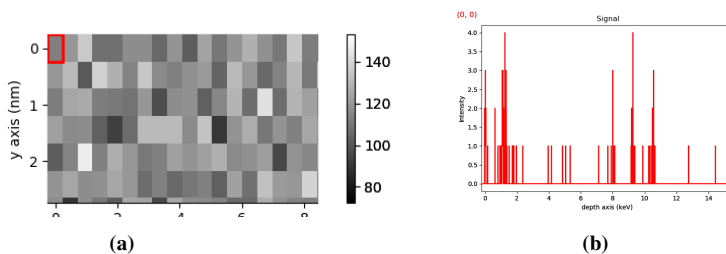
Figure 2.20: a) pixel map, b) Corresponding EDX spectrum from highlited area in Figure 2.20a

As the reader might observe, this might be quite hard to interpret. So the trick here is to add the contribution of multiple pixels to gain greater insight into the composition of the material. The pixels added have to be in the same region of interest (ROI). The summed spectras from a larger region will then yield a spectrum which is easier to analyse, as can be seen in figure 2.21.
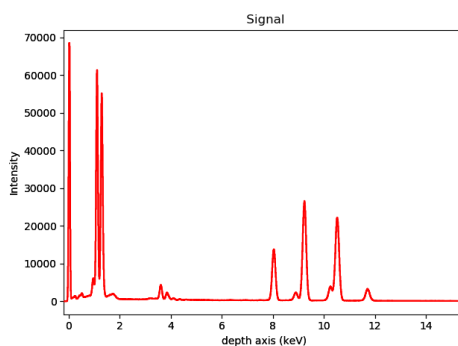

Figure 2.21: Example of a summed EDX spectra.

Background removal is done by estimating the background from equation 2.4, for the background to be visible in figure 2.21 it would have to be plotted in a log scale. If it is very prominent the background can be removed by approximation of equation 2.4.

From Figure 2.21 we observe a Gaussian tendency of the peaks. Missing "counts" can thus be reintroduced by fitting a Gaussians to each of different peaks. This is primarily done for two reasons:

- To account for irregularities in the counts (to make it a perfect Gaussian).

- To better deal with overlapping peaks (making the deconvolution process easier).

As observed in Figure 2.22 there are peaks overlapping. Whilst fitting the model to a Gaussian, it separates each peak into separate Gauss functions, making it easier to estimate the actual counts. This process of separating Gaussian curves is known as deconvolution, and the deconvoluted peaks of figure 2.21 can be seen in figure 2.22.
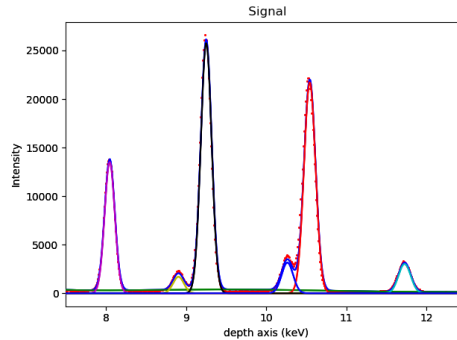

Figure 2.22: Gaussian fitted to the different peaks, And the deconvolution of the peaks. Red dots are the data points and the colored lines are element specific (Cu_K-purple, Ga_K blue, As_K red and so on)

Some peaks coincide and will have to be handled as twin peaks, this requires some additional processing, but it is essential as twin peaks will give a wrong answer.

The counting then simply becomes a matter of finding the area under the curve for the respective peaks and their width i.e integrating the deconvoluted peaks over an appropriate width.

2.8.2   Fallacy of the "Software Blackbox"

Often much of this functionality for EDX analysis is included in commercial software. The problem however is that people tend to trust the software a bit to much. Many of the calculations done by these softwares are unavailable to the consumer, which ultimately means that it is a black box. Preset values which may not apply to the consumers instruments (like the k-factors), functionality for preset absorption effects and so on, may actually end up hurting the end result, by incorrectly altering it. This in turn justifies the effort of making an open source firmware, which can implement the same functionality as the commercial software and make it transparent to the consumer whats really being calculated and so on. EDX is deceptivly hard and wrong interpretation of the data (or the conditions at which the measurements were taken) can cause the end result to be wrong.

Chapter 3

Experiment

According to theory, there should be an orientation effect when performing an EDX analysis on and around a zone axis with channeling atom columns. To see how large of an effect an on zone EDX analysis yields, three different experimental cases were set up. One where the specimen is rotated, one where the specimen bends and one where the incident beam is manipulated to hit an area at different angles.

3.1 Material and specimen preparation

For all experiments self-catalyzed GaAs/GaAsSb heterostructured nanowires are used. The nanowires are grown by molecular beam epitaxy on 111-Si. As the growth is random, there is some variation in nanowire diameter and length. The nanowire has a ca. 1 um segment of GaAs in the zinc blende (ZB) structure. Adding 1 min Sb-flux, an axial ZB GaAsSb insert forms (100-200 nm long). After closing the Sb-flux, a segment of GaAs in the wurtzite (WZ) structure is formed. After 5 min the growth is terminated by closing the Ga and As fluxes. For further growth details, see Munshi[19]. The ZB GaAs has some twin planes and the WZ GaAs stacking faults. The insert has a varying Sb-content, with a max. plateau around its middle[20]. The nanowires are assumed to have a hexagonal cross-section, with (110)-facets for ZB and (1120)-facets for WZ segments. A schematic nanowire is shown in Figure 3.1. For the final studied case, beam rocking, a GaAsSb between highly GaAs regions with high stacking fault density was use. This is initially a small diameter ($<$ 100 nm), but growth after this insert leads to radial GaAs overgrowth to a thickness of ca. 400 nm. The total nanowire growth details and structure are described in [21] and chosen to have a stronger signal given a small (ca. 4 nm, more parallel but weaker beam) and an overall low Sb content.
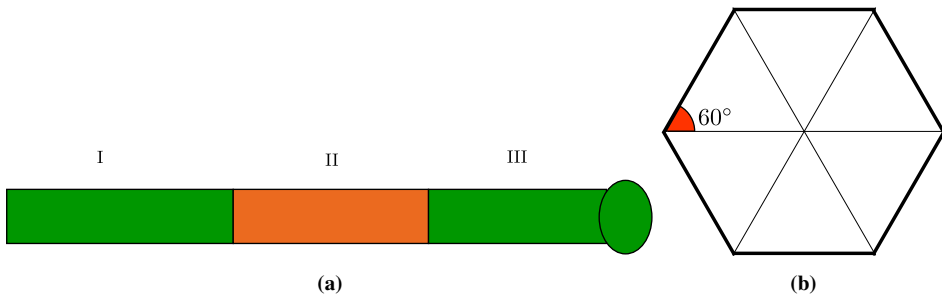
Figure 3.1: a)Schematic of nanowire Area I ZB GaAs, area II ZB GaAsSb insert and Area III GaAs WZ. On top is a Ga-droplet
b)Schematic of the wire dimension viewed from the [111] orientation

The nanowires are scraped off with a fine diamond scriber and transferred onto a 300 mesh Cu grid with a holey carbon film (ca. 20 nm thick). Nanowires in the middle of the grid are selected away from Cu grid bars.

3.2 Data acquisition

The nanowires are studied in three different set-ups representing three different series of varying beam-lattice orientation approaches. These three cases will be separately be presented together with some images and different patterns of the studied nanowires.

3.2.1 Case 1: Sample tilt series:

The EDX data are collected on an FEI Osiris at 200 kV with a four $30mm^2$ SDDs (i.e. Chemistem) by Z. Saghi and A. van Helvoort at the University of Cambridge. All three areas/regions labeled in Figure 3.1 are probed scanning a 10x10 area using a 1 nm probe at the middle of the nanowire. The nanowire is tilted around the nanowire axis, with the 0-tilt when the middle of the ZB insert is at [110] zone. In this study the tilt range -5 to +5 degrees is used and a standard double tilt holder. The set-up is schematically depicted in Figure 3.2. Data is collected for 1 min live time and with each of the four detectors separately. The scanned area is summed and a model for the area is created. The used k-factors are given in Table 3.1
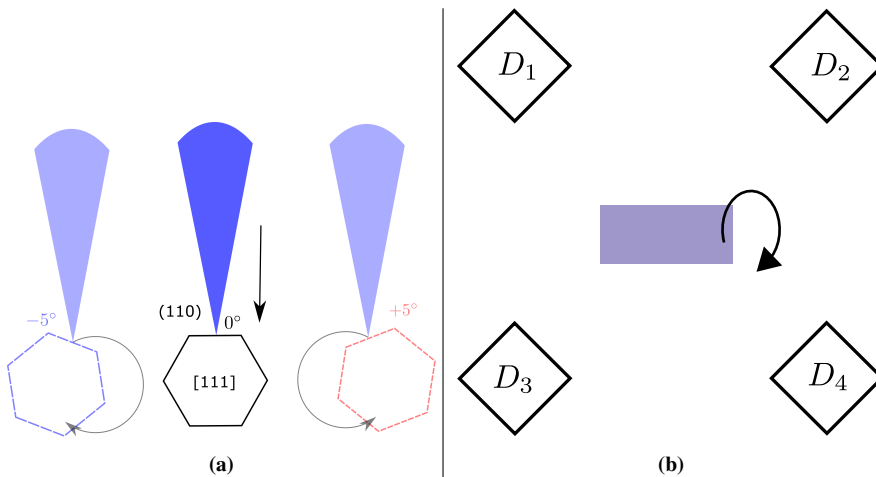

Figure 3.2: a) Schematic of the tilting of the nanowire
b) Schematic of experimental setup, with 4 detectors. Tilting directions in regards to the detectors are depicted by curving arrow.

3.2.2 Case 2: Bended nanowire segment

The EDX data are collected on a JEOL 2100F at 200 kV in STEM mode and with an 80mm2 Oxford Instrument SDD, placed perpendicular to the low-background double tilt TEM holder, by D. Chatterjee. Scan was over a nanowire similar with a structure similar to area I (ZB GaAs, see Figure 3.1, middle on ca. [110] zone, bending over scanned area) will be studied. The schematic set-up and the nanowire are shown in Figure 3.3. EDX collection was done by Oxford Instrument Aztec software and converted to .hdf5 format using a script made by D. Lundeby[22]. The used k-factors are given in Table 3.1
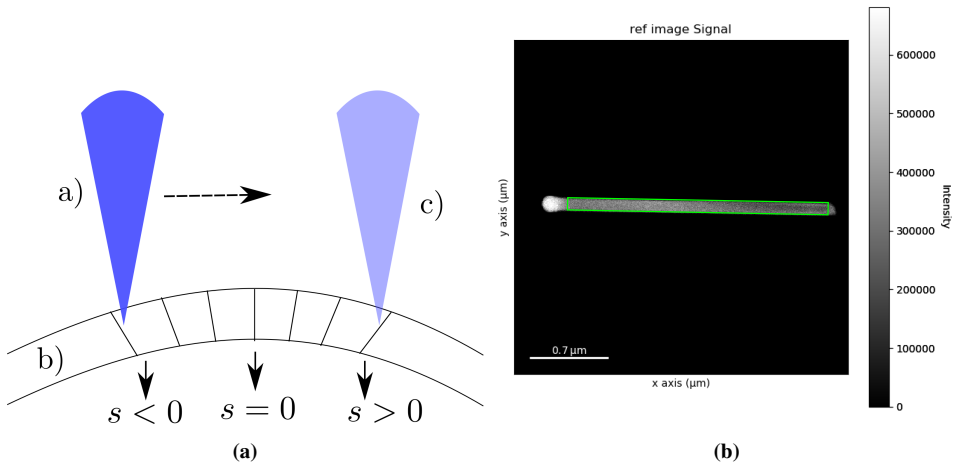

Figure 3.3: a) Schematic of The incident convergent elecron beam and the nanowire b) The GaAs nanowire, area examined with highlighted by the green rectangular

3.2.3 Case 3: Rocking beam:

The EDX data are collected on a JEOL 2100 at 200 kV in STEM mode and with an 80mm2 Oxford Instrument SDD, placed perpendicular to the TEM holder X-axis, by A. van Helvoort. Here a thicker nanowire was studied with a lower Sb content as a less bright source and a weaker but more parallel probe was used. The schematic of the process is shown in Figure 3.4 and the structure together with the diffraction pattern is shown in Figure 3.5. The labeling in Figure 3.5b refers to the different tilts of the incoming beam. The convergence angle was XYZ mrad and the beam tilt steps are given in Table 3.1
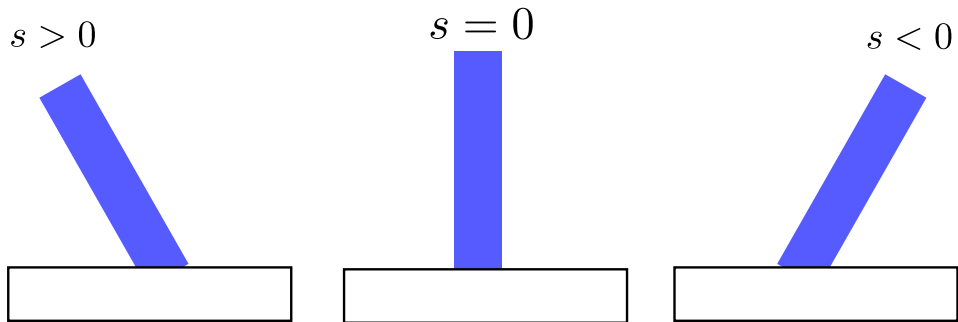

Figure 3.4: Schematic of the electronbeams incident
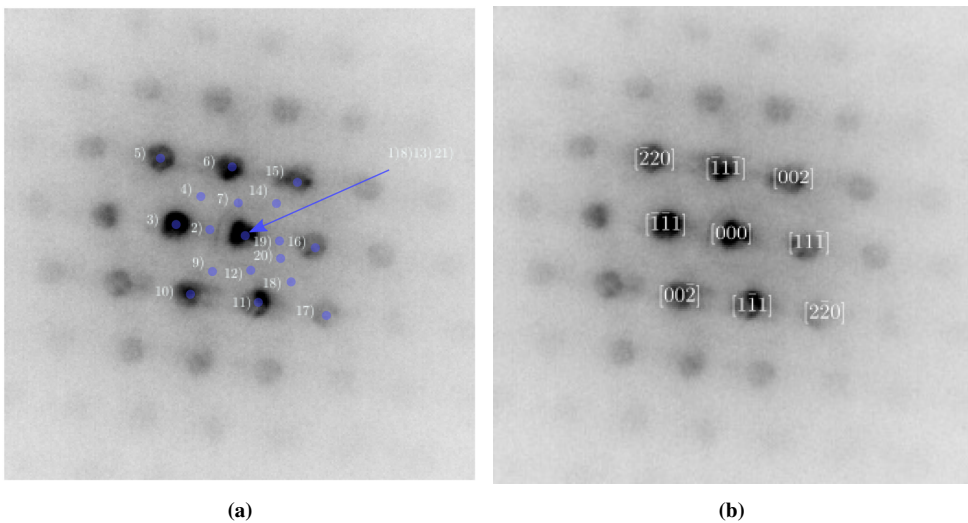

| (a) | (b) |

Figure 3.5: a) The beam rocking were performed on the highlighted areas and indexed.
b) Indexing of the orientations in the diffraction pattern

EDX collection was done by Oxford Instrument Aztec software and converted to .hdf5 format using a script made by D. Lundeby[22]. The used k-factors are given in Table 3.1.

Table 3.1: Convergence angle's for selected zones in Figure 3.5b

Zone	angle(mrad)
[111]	3.84
[002]	4.36
[220]	6.28

Table 3.2: K-factors utilized in the different experiments

Case	$As_{K\alpha}$	$Ga_{K\alpha}$	$Sb_{L\alpha}$	$Ga_{L\alpha}$
Tilt series:	2.225	1.930	2.873	-
Bended wire:	2.835	2.4919	3.976	-
Rocking beam:	1.502	1.346	1.948	1.713

3.3 Data processing

The computation was performed in python3.0 in a jupyter notebook, utilizing the following libraries. The source code for constructing the results, can be found in the appendix A.2.

- hyperspy.api (version 1.5.2) for the implemented was off handling EDS data like the actual loading and processing of the data i.e modeling and fitting. As well as visualization of the data in question.

- numpy is used for mathematical functions.

- os for getting directory path.

- pandas for management of data when needed.

- operator for list item sorting and item localizations.

- matplotlib used to visualize the results.

The code wich is included in the appendix, was performed on a Huawei Matebook X pro laptop sporting 8 GB RAM and an intel i5-8250U processor.

Chapter 4

Results

4.1 Case 1: Sb insert in GaAs with 4 detectors

The dataset was taken on three different areas of a nano wire. As illustrated in Figure 3.1, area I consist of Ga and As in a ZB structure, area II has the same structure as area I, but with a Sb insert and area III consisting of Ga and As in a WZ structure. The areas are outlined in Figure 4.1.
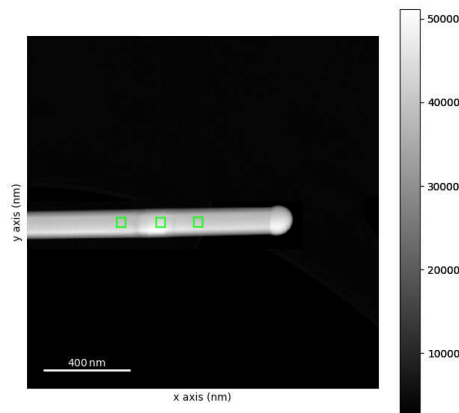

Figure 4.1: Image of the nanowire. From left to right area 1,2,3

The data was collected using four detectors and data collection was performed at different tilts ranging from 30 to +5 from the [110 zone axis]. All detectors where not used at all the tilt angles, because of shadowing. As the tilts of interest where near the zone axis, only

the tilts from -5 to $+5$ were taken into account when plotting. Every tilt examined were composed of a 10 x 10 pixels, these were then summed together to get a spectra for the given tilt for a given area e.g tilt $5°$ at area 1. The process is shown in Figure 4.2.
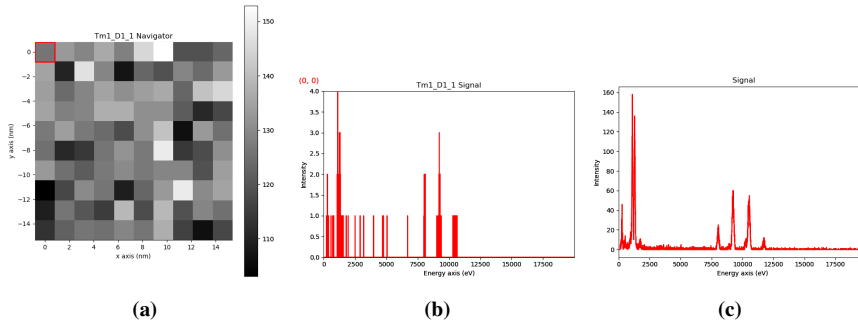

(a) (b) (c)

Figure 4.2: a) Area I at $-1°$ tilt at detector, b) Spectra from one pixel, c) spectra from all pixels

The spectra was modeled with the following elements ["Ga", "As", "Sb", "Si", "Cu", 'Fe','O']. In the following results there will be featured modelfitted (Gausian fit) and un-fitted models(raw counts), modelfitted will have a solid line, whilst non-fitted will have a stippled line. The detectors could not record independently at the time of the acquisition of this particular data so one detector would remain on while the others were turned off. Thus 4 separate measurements were taken for each tilt (except were the detectors where shadowed).

Only one comparision between all the detectors will be showcased in the results. The remaining results can be found in the Appendix A.3. Every pixel in a scan is summed together to make a more statistically significant spectra, which can be made into a model. In the model the peaks can be fitted by gaussian curves to try and account for a lack of counts in the spectra.

4.1.1   Pure GaAs areas(I,III)

First the composition between the pure GaAs areas where examined. These areas (area I and III) should be quantitatively similar i.e 50 at% Ga and 50 at% As. The areas have different atomic structures ZB (area I) and WZ (area III). Its thus of interest to see how the orientation and structures affect the measured composition. The results are presented in figure 4.3 and 4.4.

Figure 4.4: Composition area III
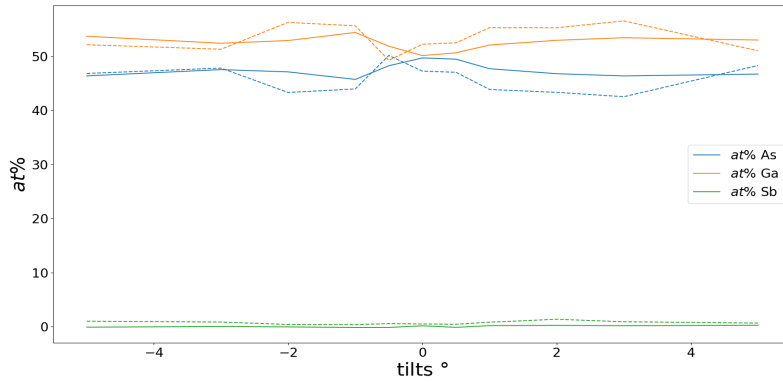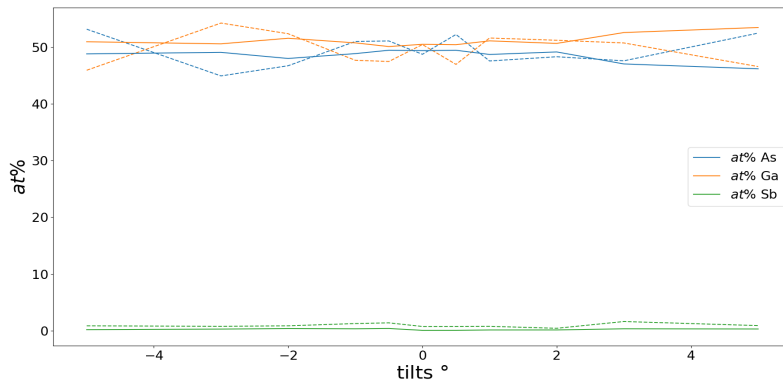

Figure 4.3: Composition area I

The composition at area I and III were expected to be 50 at% Ga, 50 at% As and follow similar trends, but a deviation is observed between the different areas. It is therefor reasonable to assume that these variations originates from the orientation effects. The strength of the channeling at the different tilts are shown in figure 4.5 and 4.6.
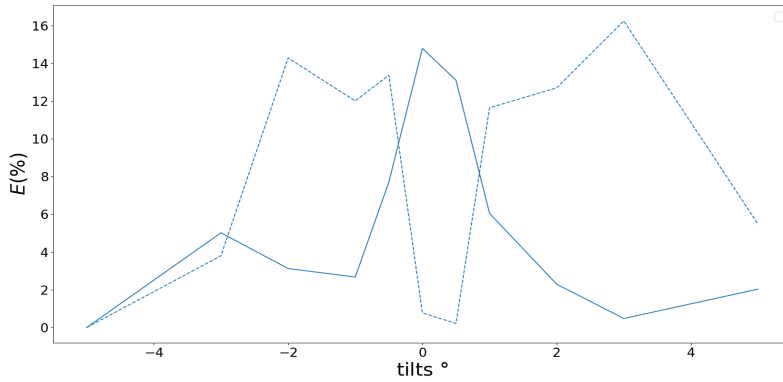
Figure 4.6: Channeling area III (WZ structure).
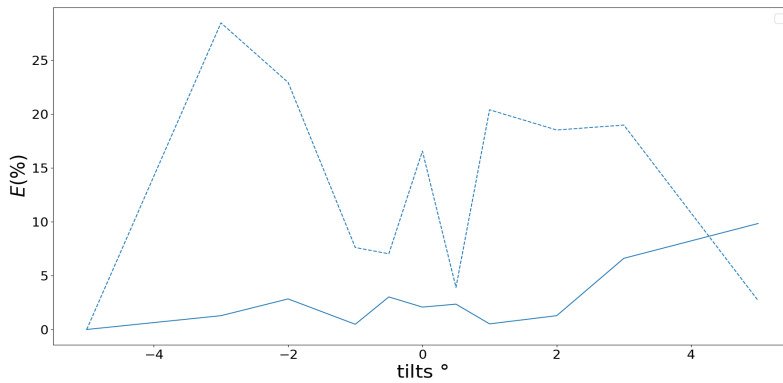
Figure 4.5: Channeling area I (ZB structure).

The channeling appears clear in the WZ strucuture (area III), but the ZB structure is not displaying the expected effects. From section 2.4.2 it was stated that an increased number of X-rays are created when a specimen of sufficient thickness are examined on zone. To check if this is the case the number of counts from area 1 and area 3 are added and plotted. The results of the total counts are presented in figure 4.7 and 4.8.
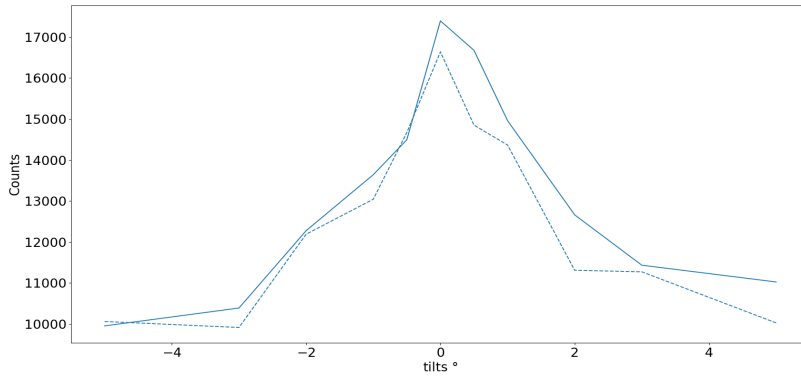
Figure 4.8: Total counts area 3 (WZ structure).
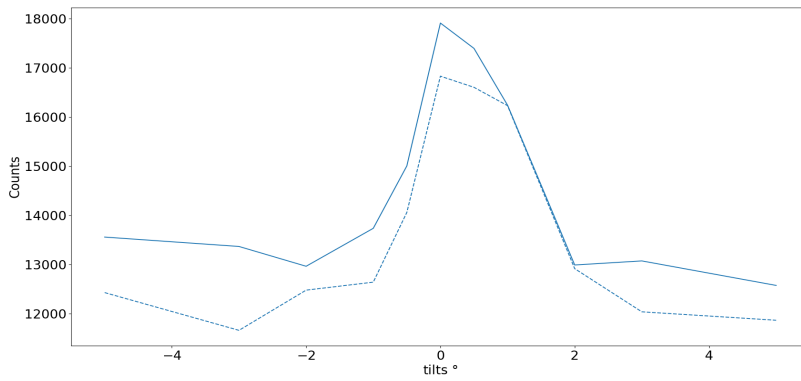
Figure 4.7: Total counts area 1 (ZB structure).

4.1.2 GaAs with a Sb insert

It is now of interest to examine if the introduction of a tertiary element has an impact on the ratios between the emitted X-rays ($Ga_{K\alpha}/As_{K\alpha}$). The composition of area 2 (ZB GaAs with Sb) at the different tilts of the [110] axis are shown in Figure 4.9.
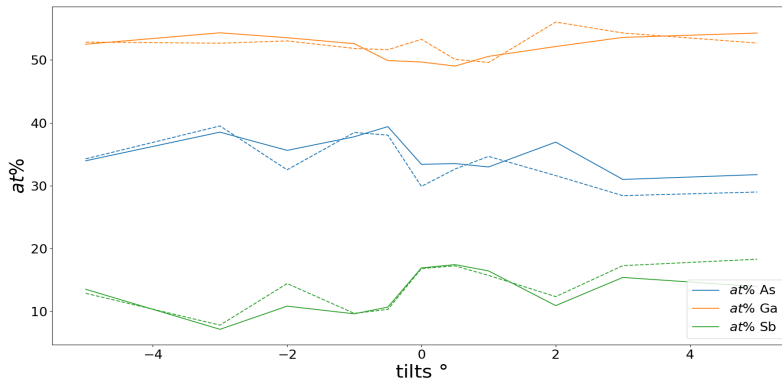
Figure 4.9: Composition area 2 (ZB GaAs with Sb).

The channeling effect for this area is taken between the As and the Ga X-rays, and presented in figure 4.10.
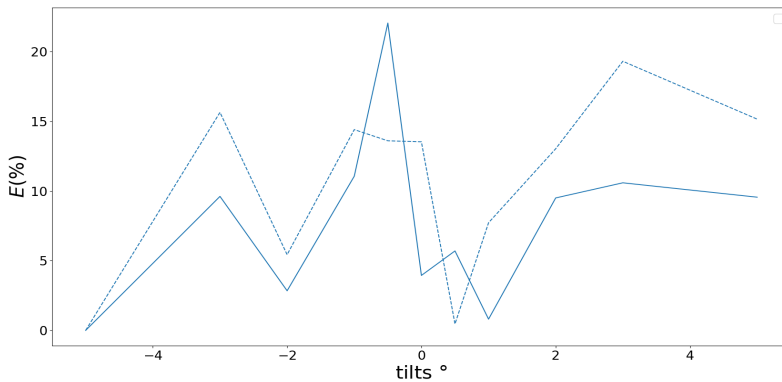
Figure 4.10: Channeling effect area 2 (ZB GaAs with Sb).

The total counts are once again used to verify that an increase in X-rays occurs on zone axis.
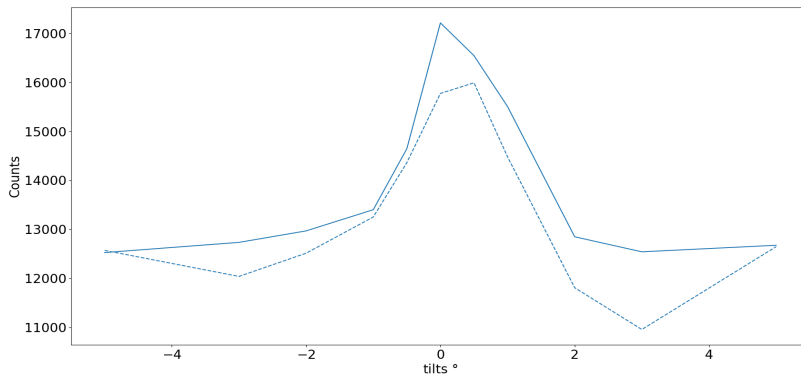
Figure 4.11: Total number of counts area II

ALCHEMI and the consistency of the detectors

All measurements in this experiment was done by 4 detectors. Individual plots for all the 4 detectors can be found in Appendix A.3. Here the channeling from area 2 for the individual 4 detectors are shown in figure 4.12

(a)

(b)

(c)

(d)
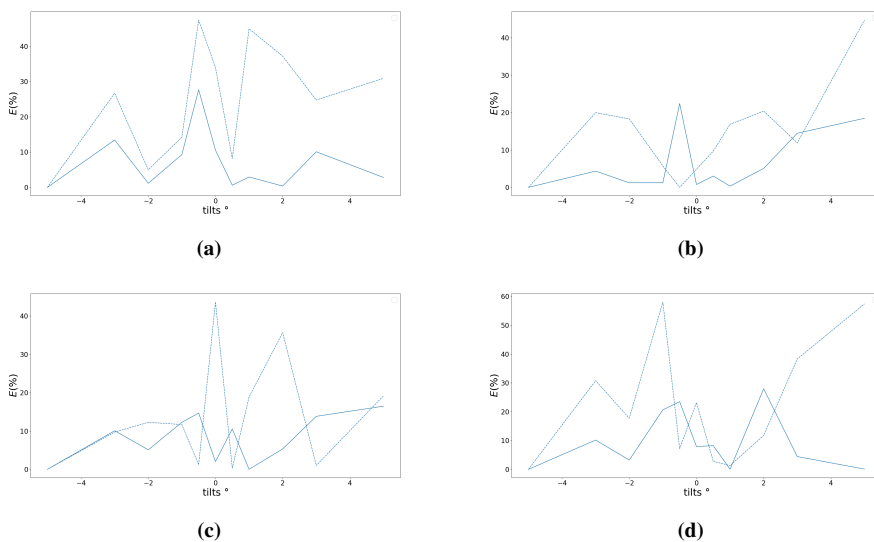
Figure 4.12: a) Channeling of area 2, detector 1. b) Channeling of area 2, detector 2. c) Channeling of area 2, detector 3. d) Channeling of area 2, detector 4

Different detectors give different channeling strengths and tendencies at different tilts.

From figure 4.9, compositional differences are observed and thus it would be of interest to examine if ALCHEMI can be observed, and if the choice of detector will affect the result.

In section 2.5 it was established that ALCHEMI works by taking the count ratio's between a spectra from a channeling condition and a non-channeling condition. Trying a few channeling conditions and comparing the across all detectors, to see if ALCHEMI works and if it is consistent across all the detectors. For area 2 the results tabulated in table 4.1 were obtained, all results here utilized a modelfit.

Table 4.1: ALCHEMI for different detectors at different tilts AREA 2

| Tilt 1	Tilt 2	Det 1	Det 2	Det 3	Det 4	All Det
-1	3	-1.845	-1.907	-1.156	-1.353	-1.502
-1	-3	-18.031	-16.405	12.785	2.949	29.444
-1	5	-2.827	-0.916	-0.764	-1.504	-1.264
-1	-5	-3.146	-21.602	-2.768	-1.208	-2.62
-0.5	3	-0.689	-0.532	-0.806	-0.796	-0.698
-0.5	-3	7.617	4.42	9.971	4.345	5.525
-0.5	5	-0.75	-0.153	-0.451	-0.768	-0.476
-0.5	-5	-0.596	-0.582	-1.735	-0.453	-0.763
0	3	1.011	0.866	1.504	1.294	1.137
0	-3	-94.05	-32.922	-12.105	-65.19	-30.665
0	5	2.38	1.679	2.124	3.054	2.182
0	-5	4.25	-37.651	-11.208	4.526	8.18
0.5	3	2.04	1.132	1.067	1.367	1.304
0.5	-3	-21.448	-143.791	359.938	-76.471	-47.666
0.5	5	9.635	1.806	1.472	3.121	2.28
0.5	-5	74.752	12.915	3.065	4.558	6.688
1	3	0.759	0.76	1.291	1.897	1.027
1	-3	-22.239	-35.319	-14.574	-12.53	-18.283
1	5	3.308	1.568	1.87	308.18	2.316
1	-5	10.362	-83.787	1523.236	-708.701	32.589

4.1.3 Statistical ALCHEMI

As established in section 2.5 statistical ALCHEMI utilizes the alchemi results from multiple spectra and draws a regression line.
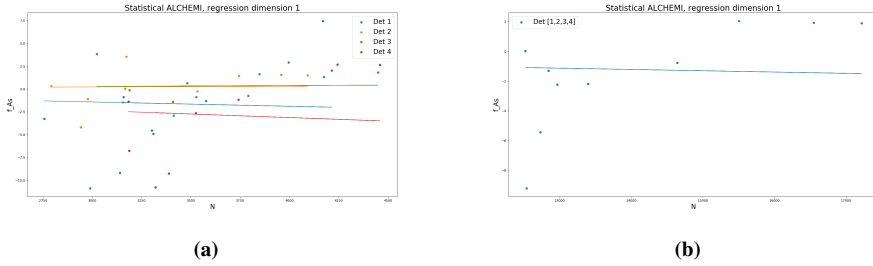
Figure 4.13: a)Statistical ALCHEMI results for the individual detectors, b) Statistical ALCHEMI results for all detectors combined

Table 4.2: Statistical ALCHEMI results for the different detectors

Detector	p_{As}	error
1	0.301	± 0.075
2	-0.29	$\pm - 0.07$
3	-2.848	$\pm - 0.683$
4	2.769	± 0.716
all	-2.313	$\pm - 0.433$

As suggested by Spence et.al[10], the regression can be done with a constant offset. In the results clear outlines in the occupation fraction $p > 20$ are filtered out.

(a)

(b)
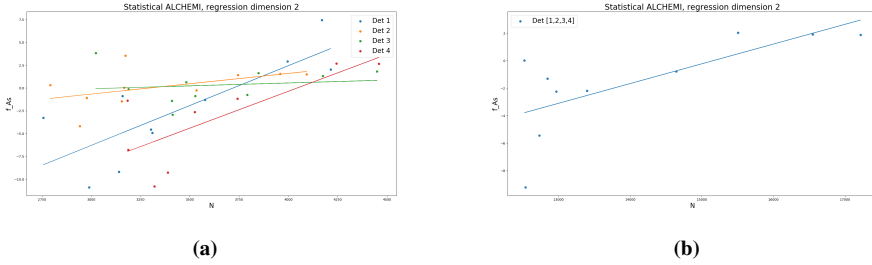
Figure 4.14: a) Statistical ALCHEMI results for individual detectors with a constant offset b) Statistical ALCHEMI results for all detectors combined with a constant offset

Table 4.3: Statistical ALCHEMI results for the different detectors with a constant offset C

Detector	p_{As}	error	C
1	0.107	± 1.012	4.186
2	-0.279	± 0.242	-1.291
3	-2.854	± 0.75	0.277
4	2.936	± 0.947	6.6
all	-2.298	± 0.574	0.769

4.2   Case 2: Bended nanowire segment

Dropcasting of the nanowires on soft Carbon film of the TEM grid should cause the nanowire to bend. If this is the case, it is of interest to set the middle of the wire on zone axis [110] and to a scan the whole nanowire and see if the composition changes . If the wire bends, the other areas of the wire should be slightly off zone.A reference image area where the examined area is highlighted in Figure 4.15.
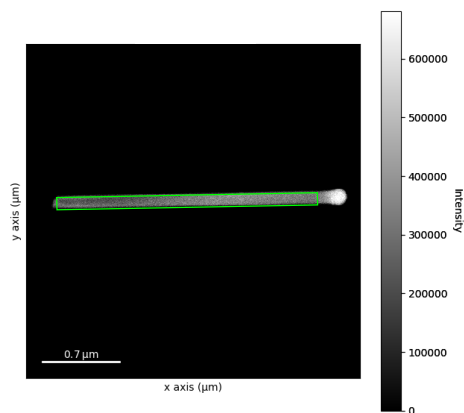
Figure 4.15: HAADF image of the nanowire, the area examined highlighted. The approximate length of the wire is $2.28\mu m$

The map of the area is shown in Figure 4.16
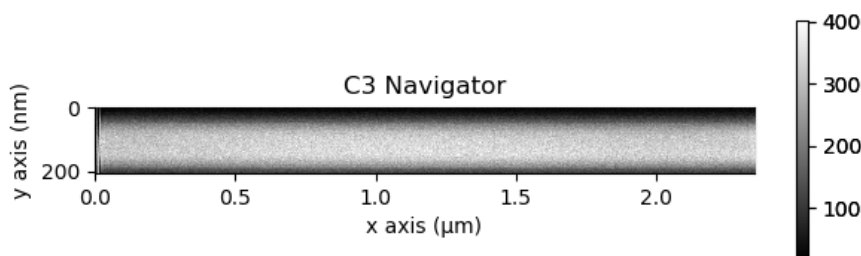
Figure 4.16: Intensity map of the nanowire

All the calculation's in this section are done by doing a model-fitting of the spectra. The composition across the wire with the k-factors in Table 3.2 gives the following result outlined in Figure 4.17. The resolution of a single pixel is not enough to give an interpretable result, thus adding spectras of multiple pixels are required. The compositional variations in the horizontal direction are of interest, a rebinning i.e summing all vertical pixels.
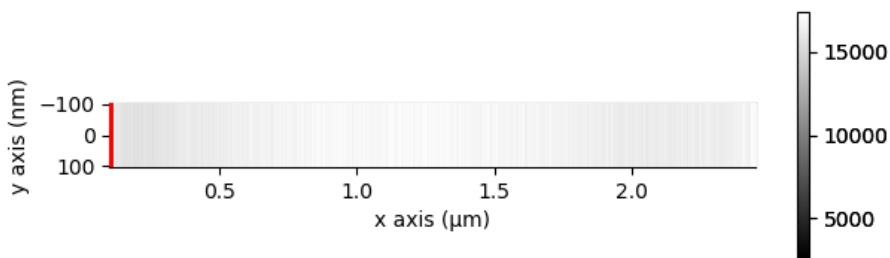
Figure 4.17: The nanowire rebinned in the vertical direction

Which gives the following composition.
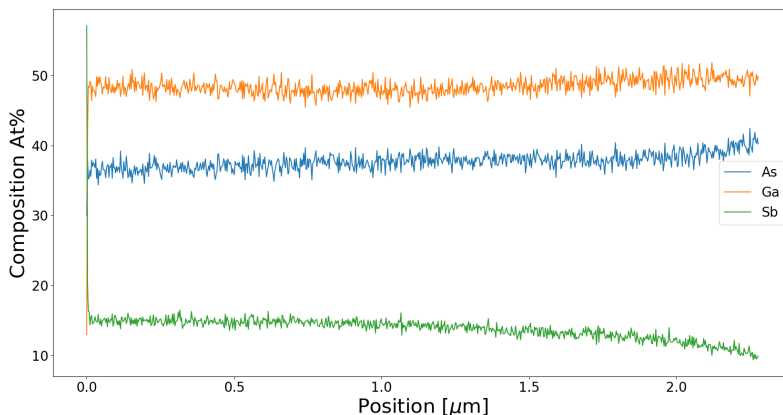
Figure 4.18: Composition of the bent nanowire, with pixels rebinned vertically

The composition has great deviation per pixel step. To reduce this a greater rebinning of greater magnitude is requiered. From the original map in figure 4.16 one edge of the wire appears darker, i.e its facing away from the detector. Thus rebinning to a dimension that segregates the vertical pixels to center of the wire, the edge facing away from the detector and the edge facing the detector. In addition to the relative detector position, the edges of the wire itself will have different thicknesses at the edges (see figure 3.1). The effects of relative detector positions and specimen thickness affects the resulting EDX spectra in channeling and close to channeling conditions. The wire was rebinned to a size of 27 x 3 pixels, as shown in Figure 4.19. The top pixels are labeled as Edge 1. the middle pixels as wire center and the botom pixels as Edge 2.
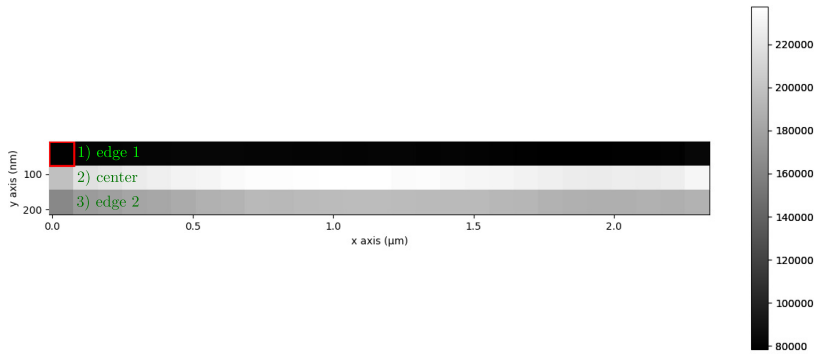
Figure 4.19: The rebinned wire. The darkest part (the top pixels) of the wire is facing away from the detector, the central part in the middle and the edge facing the detector (the bottom pixels)

The compositions for the edges and heights are given in figures 4.20,4.21 and 4.22.
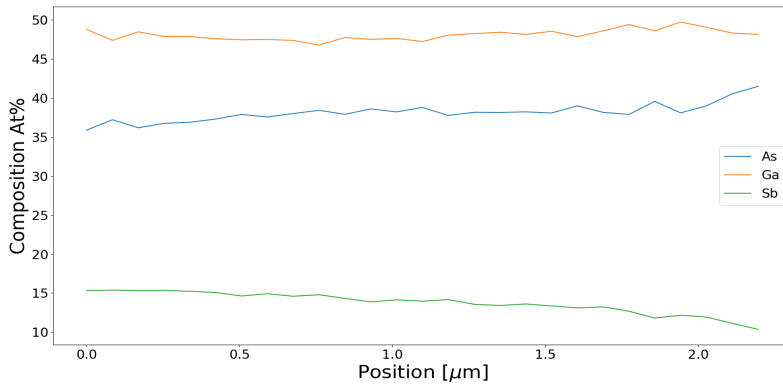
Figure 4.20: Edge 1 (facing away from the detector) , composition
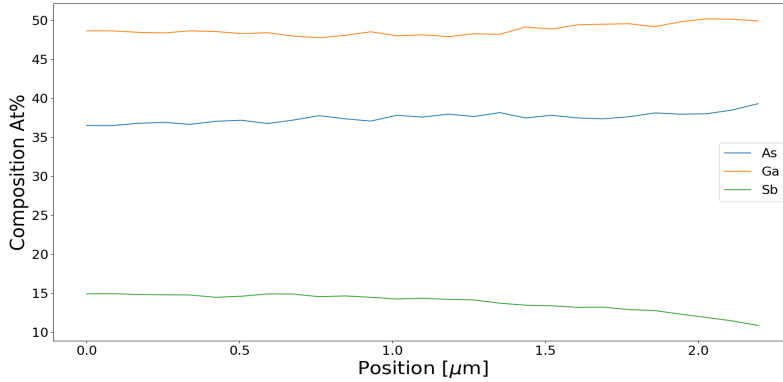
Figure 4.21: The center of the wire, composition
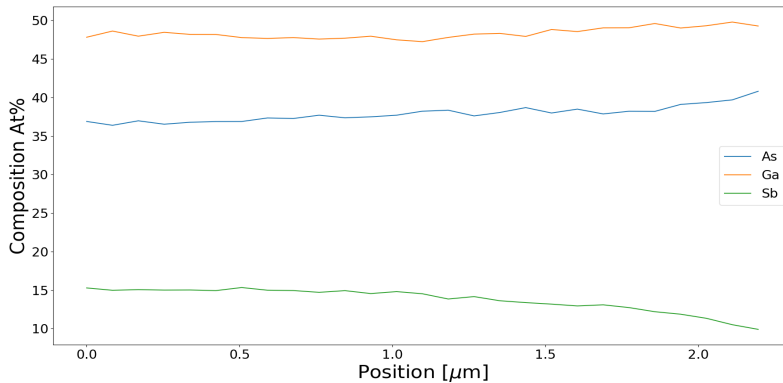
Figure 4.22: Edge 2 (facing the detector), composition

If channeling is occurring an increase in the amount of emitted X-rays are expected. The wire bends and should have positions which are slightly off the zone axis. The on zone was taken around the area in figure 4.23. The counts at the different edges and center are shown in figure 4.25. To see how the relative compositions change across the length of the wire (positions $0 - 2.28 \mu m$). The edges and the center channeling reference point are taken at against its leftmost pixel. The channeling obtained for the different edges and the center are shown in figure 4.24.
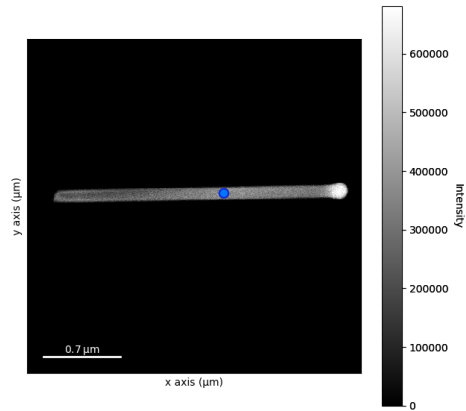
Figure 4.23: Approximate location of the off the [110] zone axis.
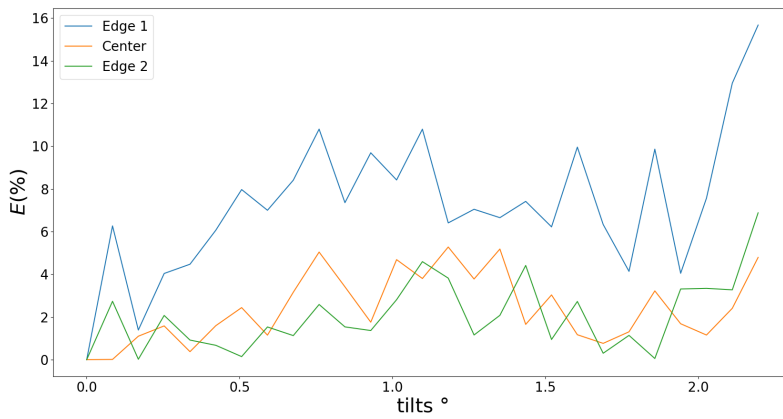
Figure 4.24: Channeling effect at the different edges and the center

The channeling does not appear to reveal the zone axis, thus it is of interest to see if the total counts over the wire will reveal the location of the zone axis.
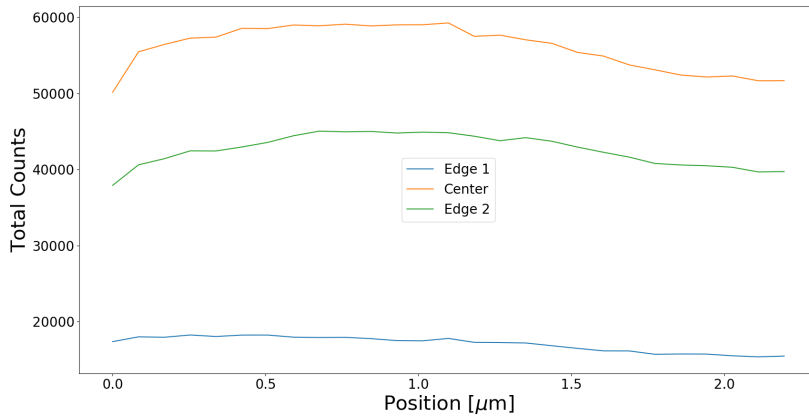
Figure 4.25: The total number of counts obtained for the rebinned areas

For the bent wire experiment it was of great interest to maximize the number of X-rays detected, shadowing (illustrated in schematic 2.7a) will cause parts of the detector to be blocked by the stage which the Cu-grid containing the nanowire's. Thus a specimen which was on zone-axis with a positive tilt (towards the detector as seen in Figure 2.7b) was located, to maximize the number of X-rays detected. It is of interest to try statistical ALCHEMI across the wire and look if the results are consistent across the edges and the center. The results for the different edges are given in figures 4.26, 4.27 and 4.28.
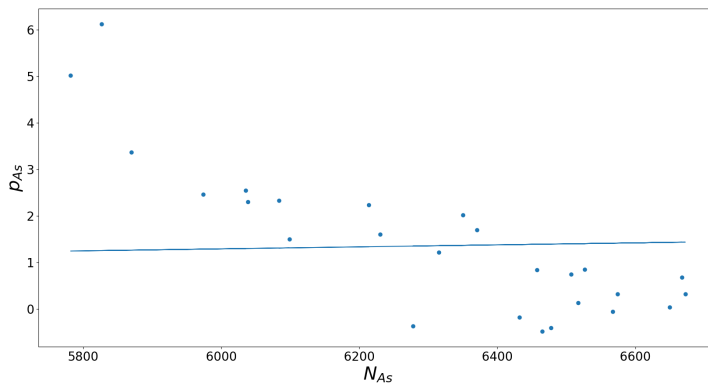
Figure 4.26: Statistical ALCHEMI on edge 1
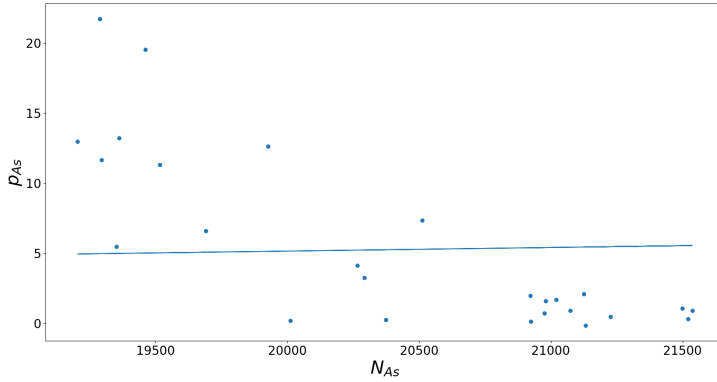
Figure 4.27: Statistical ALCHEMI on center
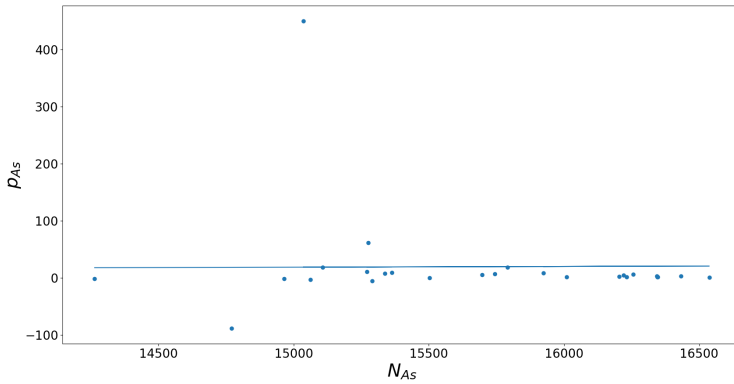
Figure 4.28: Statistical ALCHEMI on edge 2

The statistical ALCHEMI results for the different edges are given in table. All of the statistical ALCHEMI were performed against the same reference point which was chosen as edge 1 pixel 0 (the leftmost pixel). 4.4

Table 4.4: Statistical ALCHEMI performed at the different edges and the center

Edge	p_{As}	error
Edge 1	1.337	± 0.095
Center	5.254	± 0.301
Edge 2	19.249	± 1.421

4.3 Case 3: Beam Rocking

A tilting of the incident beam should cause a change in the excitation error s. The nanowire examined are shown in figure 4.29a.

(a)   (b)
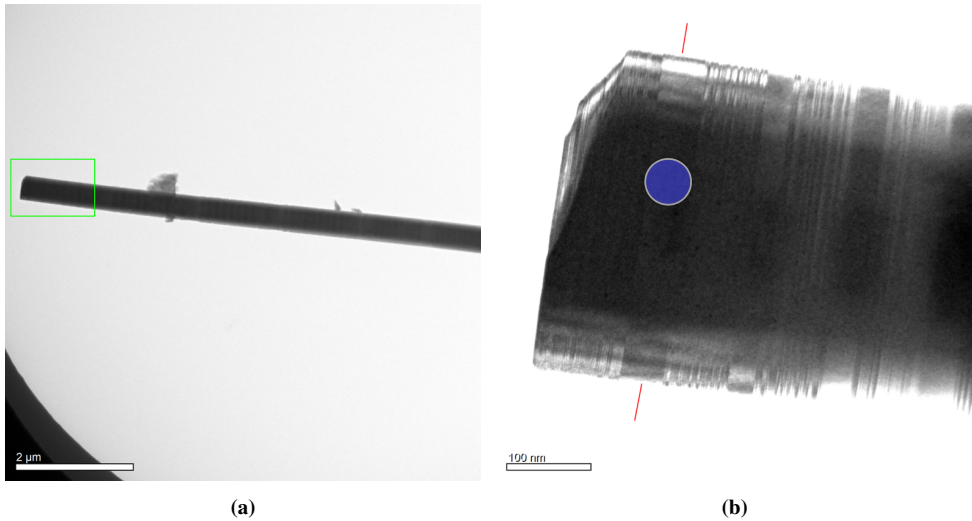
Figure 4.29: a) Nanowire examined, area in green is examined, b) This is the green area from fig4.29a, beam rocking performed approximately on the blue zone

Each index area in Figure 3.5a, has a spectra like the one in figure 4.30. All figures in this section are model-fitted. The nanowire and the area of interest which is analysed is depicted in figure 4.29a.
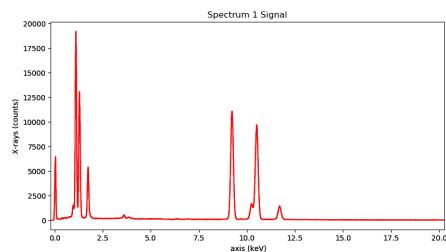
Figure 4.30: The raw spectra from the beam rocking area indexed 1).

The calculated compositions for each area is shown in Figure 4.31
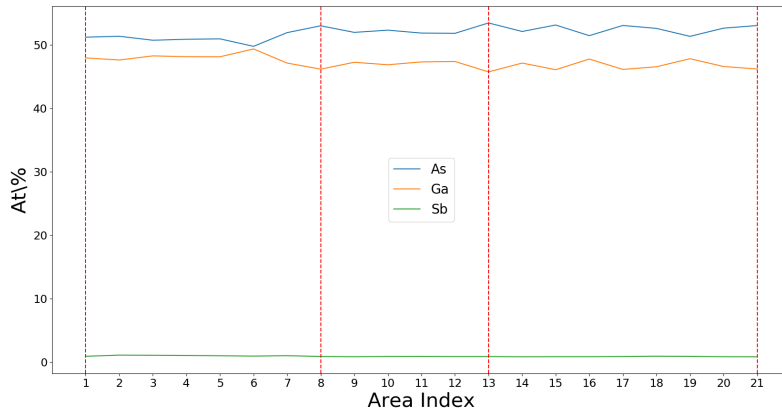
Figure 4.31: Composition for the areas indexed in Figure 3.5a, the [000] area's are highlighted by red lines.

Two off zone spectras were taken as a referance and the compositions for the reference spectras are given in table 4.5.

Table 4.5: Compositions from the reference spectra

	Ga	As	Sb
Referance 1	51.67%	48.10%	0.98%
Referance 2	54.05%	45.83%	0.91%

The channeling effect of the indexed areas against both reference spectras are shown in Figure 4.32 and 4.32,
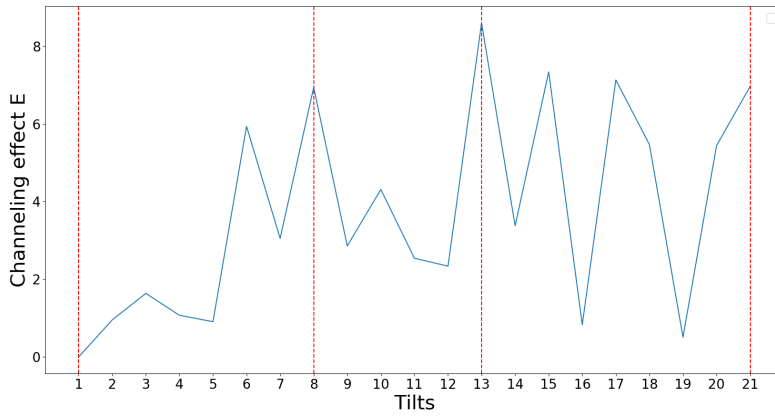
Figure 4.33: Channeling effect of the different areas against reference spectra 2.
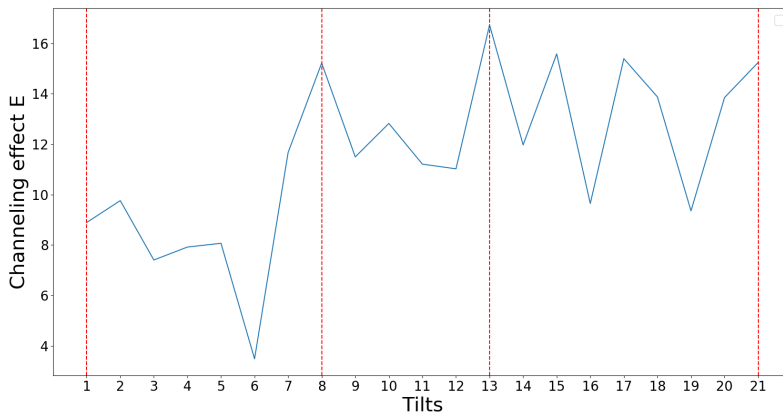
Figure 4.32: Channeling effect of the different areas against reference spectra 1.

It is off interest to see whether the consistency of the emitted K and L lines, and if channeling can have an effect on the K/L ratios.
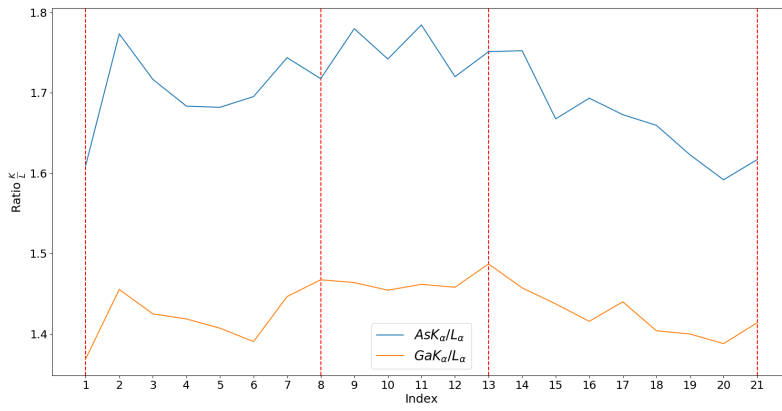
Figure 4.34: K/L lines ratios of Ga and As for the bent nanowire

The tertiary element Sb are present in a low quantity and by utilizing ALCHEMI the occupational rate of the impurity atom on the host atom rows can be determined.

Table 4.6: The ALCHEMI results for the occupation fraction on the As column for reference spectra 1 and 2

Area	p_{As}(ref1)	p_{As}(ref2)
1	1.26	-0.839
2	2.734	-3.5
3	3.26	-2.157
4	2.784	-2.052
5	2.291	-1.651
6	3.279	-0.47
7	1.794	-3.934
8	0.77	-243.378
9	0.432	0.069
10	0.801	-1.856
11	0.941	-1.175
12	0.691	-0.5
13	0.665	3.522
14	0.291	0.484
15	0.527	7.725
16	0.45	0.146
17	0.749	37.249
18	1.061	-6.211
19	1.115	-0.786
20	0.469	-0.801
21	0.345	Null

The ALCHEMI is clearly heavily dependant upon the chosen reference spectra, the occupational fraction was also attempted to be gained by utilizing statistical ALCHEMI. The statistical ALCHEMI was performed against referance spectra 1, the results are displayed in Figure 4.35.
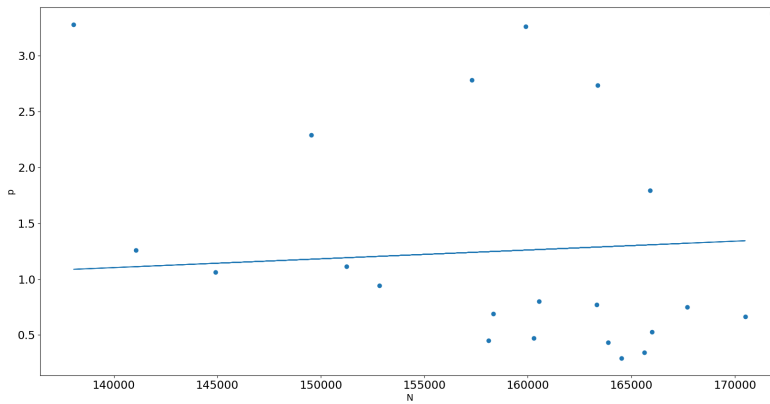
Figure 4.35: Statistical ALCHEMI on Referance area 1

Which gives a occupational fraction $p_{As} = 1.27 \pm 0.11$

Chapter 5

Discussion

In this chapter the obtained results are discussed. Each case of the study will be discussed sequentially and the authors observations about the results will be explored and consequently compared to the literature.

5.1 Case 1: Sample tilt series

The interesting part of this case was that the measurement was taken by four separate detectors, which allows to compare the consistency of the measurements, all plots for individual detectors for all areas can be found in appendix A.3. The EDX acquisition was done at different tilts including the zone axis which is usually avoided due to channeling effects. The goal of the measurements was to explore the effects of EDX-scans on a nanowire in different orientations.

5.1.1 Pure GaAs areas(I,III)

Composition

For both area I and area III in figures 4.3 and 4.4 the composition is known to be $50at\%$ Ga and $50at\%$ As. For Area 1 the composition for the fitted case is as expected i.e within an error of $\pm5\%$. For the given k-factors the most accurate result is observed closest to the zone axis. But for tilts further off zone, a larger quantity of Ga is observed relative to As. This could simply be due to the K-factors not being correct for the material and the instrument, or the fact that the model fit alters the initial data in a manner which could result in inaccurate end result. For the unfitted case deviations are larger than for the fitted case. A shift of the dominating element i.e As $at\%$ Ga $at\%$, is observed for the unfit

model at both $-5°$ and $-5°$. Both the unfit and the fit model the results closest to the real result is found on the zone axis. The reason could be an error in the experimental K-factors or other underlying orientation effects. Between the $5°$ and $-5°$ tilts a relatively large compositional difference is observed, which is unexpected and the origins of this effect might be from some underlying orientation effects. Area III appear to give more consistent results between the fitted and unfitted models at the different tilts, in the sense that Ga is always dominant over As. This likely have origins in the choice of k-factors, as Ga and As are close in the periodic table and their scattering power should not differ to much. In the fitted data, Ga and As appear to be 50/50 composition when on zone. But for the unfitted data, Ga and As appear to be at $-0.5°$. From the unfit case it would be appropriate to assume that the $-0.5°$ was the on zone case. Perhaps this stems from misalignment of the electron beam i.e the scan wasn't done exactly on zone. If this is the case then the fit case would be wrong. But from observations of both the unfit and fit case there is reason to believe that something is occuring around the zone axis. To the

Channeling and counts

For area I there is no apperant channeling around the on zone tilt, and for the fit case the largest channeling effect is observed between the $-5°$ and $5°$ tilts i.e the largest compositional variations are observed between two supposedly non channeling orientations. The total number of counts for area I appears to confirm that the channeling is appearing around the zone axis due to the increased number of counts. The channeling effect equation 2.21 only considers the ratios between counts from different elements. This could imply that composition changes around the zone axis, not necessarily being the clearest indication of on zone EDX analysis and that the relative number of EDX counts detected can be utilized to identify the zone axis by EDX. For area III the channeling and total counts follows a similar trend, the channeling effect and the total number of counts are largest at the zone axis.

5.1.2   GaAs with Sb insert

Composition

For area II the compositional variations at the different tilts are much larger than for the pure GaAs areas. The fit and unfit models follow's each others compositional trends reasonably well, but it is quite clear that a model fit has less overall variability. For the tilts closest to the zone axis different behaviors are observed for negative tilts and positive tilts. This can likely be attributed to channeling, and that one atom column gets a higher excitation than the other. However As and Sb does not increase linearly as stated in the
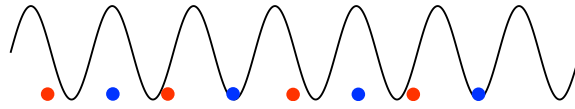
Figure 5.1: Illustration of the blochwave over the As, Sb column

ALCHEMI section 2.5. This is likely due to the quantity of Sb being high enough to alter the average periodic potential in such a manner that the resulting bloch waves not maximizing over the atoms of the impurity column, as illustrated in Figure 5.1.

Channeling and counts

The total counts were highest around the zone axis, which does support the theory in section 2.4.2 which stated that an increased number of X-rays will be emitted for an on zone channeling direction.

ALCHEMI and statistical ALCHEMI

The ALCHEMI procedure was performed against the $-5°$ tilt as the non-channeling orientation, a few negative tilts provided a good result, and for the positive tilt the results were way off. As mentioned in the 2.4.2, the blochwaves will be altered by the average periodic potential. The fact the ALCHEMI only provided some usable results for negative tilts of the zone axis , is likely due the bloch wave maximizing over the Ga column for the correct results and the As/impurity for the incorrect results. Which means that the incident electron beam channeling through the column does not cause a linear excitation of X-rays from elements occupying the atomic column. The amount of Sb in the As column is likely to high and the contribution of Sb atoms to the average periodic lattice potential does not cause a blochwave favorisation in the manner expected. In actuality the ratios between Sb and As are reversed i.e increase in As and decrease in Sb. This is illustrated in figure 5.1.

This is contradictory to the ALCHEMI theory which states that the ratios should be more or less equivalent for the impurity and host atom (according to the theory). When the blochwave favors the Ga column, the blochwave will actually maximize over the Ga atoms. Whilst channeling in the in the column containing As and Sb atoms will not have the blochwave crest over the atoms, causing the ratios between Ga and Sb to not change in a linear manner. Which ultimately results in ALCHEMI not being suitable for this particular specimen.
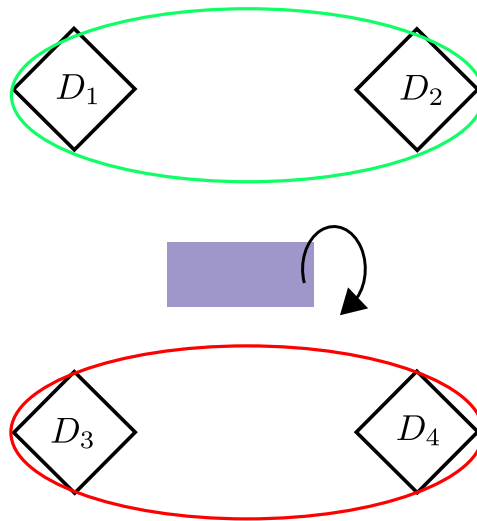
Figure 5.2: Detector positions relative to the nanowire

Statistical ALCHEMI

ALCHEMI gave some usable results, which correctly (within an error margin of 10%) gave the correct host atom of the impurity. However as this only applied to negative tilts, and the statistical approach (which takes all measurements into account) is then not expected to give the correct results. But as the experiment was performed with 4 different detectors it is off interest to see if the detectors give consistent results. The statistical AL-CHEMI was performed with and without a preset count C (determined by regression line w a preset). For the statistical ALCHEMI with and without a prefix, the results are wrong. However the statistical ALCHEMI without the prefix does however yield some interesting information. It seems to be consistent for detectors "on the same side" i.e yielding similar results for detectors 1,2 and for 3,4. Which can be seen in figure 5.2. Their absolute value appear to be correlated. This could mean that the detector position matter a lot when doing statistical ALCHEMI.

As reported by Kraxner et.al[23], shadowing by the specimen carrier and parts of the wire specimen itself (in particular for light elements) could lead to different results in the different detectors. In addition [23] stated that the following observations must be considered for proper quantitative evaluation of EDX spectra on a four quadrant EDX system. Using only one detector at full illumination will give correct quantification results but also a reduced collection efficiency. They also reported that the tilting of a specimen would create partial shadowing, resulting in different results for some detectors, mainly giving

the correct results for two detectors in which the orientation of the sample facing these two detectors, and an incorrect result for the others (which's generated X-rays would have to penetrate a large part of the specimen to reach the detectors). Placement and/or geomtry of the detector/s make a difference in the results of EDX, especially when it comes to measuring of channeling. In a paper by Ek et.al[24], they reported that the main effect causing inaccuracies in V/III wires atomic ratio of 50% were channeling, stating that for III-V nanowires it is not uncommon to see up to 50% deviations from the expected V/III atomic ratio of 1. Results these extreme are not observed in our results as the largest compositional deviations for the pure GaAs ZB case was observed at the tilts furthest away from the on-zone case i.e at tilts $\pm 5°$. If the deviations in the composition can be as severe as this report claims, the resulting channeling would be enormous around the zone axis. This does not correlate well to the results found in our experiment especially for the area 1 scenario for GaAs, the reason for the deviation could be the choice of zone axis and experimental errors.

5.2   Case 2: Bended nanowire segment

This model utilizes only a fitted model in the results.

Composition

The model had to be rebinned as each pixel did nor contain enough counts to make a complete spectra. The first spectra tried to utilize a rebinning of all vertical pixels, as the composition shows in figures 4.20, 4.21 and 4.22. The compositional variations are quite large for small step sizes, displaying the importance of having enough counts. There appears to be a trend at the end of the wire (a change in the general). The spectra was later rebinned to a 3 x 28 pixels, where each edge. The reason it was rebinned in 3 vertical pixels, was to explore what effect absorption and the detectors relative position to the point the X-rays are created. A clear compositional difference at the very edge i.e at position $2 + \mu m$, is observed for all edges. Indicating a clear compositional change, this is likely due to the excitation error becoming large enough at this particular section i.e it is off zone. The compositional variation at edge 1 is fluctuating more than the middle and edge 2 spectras. Most of the compositional variation is between As and Ga for edge 1. The general composition shift at the end, and has a decrease in Sb and an increase in As.

Channeling

The edge 1 channeling stands out from the rest, by displaying a stronger channeling effect. This edge is facing away from the detector which in turn means that the created x-rays will

have to traverse the material reach the detector, $As_{K\alpha}$ and $Ga_{K\alpha}$ are absorbed differently, thus causing extra variation in the ratio between As and Ga X-rays which reaches the detector. The reference for channeling was set at each edge's left most point. This is likely due to to the elements being absorbed at different rates.

Statistical ALCHEMI

As stated with case 1 the amount of Sb was likely to high for ALCHEMI to work. This appears to be the case for this nanowire as well. However the consistency of statistical ALCHEMI for the different edges are still of interest in regards to relative position of the detector. The statistical approach for the different edges give different results, meaning the relative detector placement is of likely great importance. This might differ for a specimen with a lower quantity of the impurity element. ALCHEMI and statistical ALCHEMI should likely be performed on specimens at which an equal amount of absorption can be expected.

5.3   Case 3: Beam rocking

The Beam rocking experiment was designed to mimic the method utilized in the experiments by Spence et.al[10] and Spence et.al[9] taking the result in an incoherent channeling pattern (ICP), this was done partially done leaving the results to be interpreted from a lower spatial resolution. Most of the [000] beam tilts show similar results, the 1 index is an outlier in this regard, but the index 8, 13 and 21 give very similar results in terms of composition and channeling. Indexes with the incident beam tilted to other zone axes for tilts 13-21 showcase much of the same behavior as the beam [000] cases, the same seems to be true for the channeling, where stronger channeling effects are appear at zone axis's.

The last plot where the K lines are plotted against the L lines, there does not appear to be as clear of correlation between the channeling effect of a given axis and the ratio between K and L lines. One would believe that the modelfitted would correct these values such as to make the ratios constant, but this does not appear to be the case. An error of roughly ± 0.1 in the ratios are observed, with the As K/L ratios varying to a larger degree than the Ga. What this means in all practicability is that the composition we calculate can give different /incorrect results due to the ratio between the k/L lines not being constant. The K/L lines do however follow some of the same trends and whether these trends stem from orientations or if they are mainly noise which happen to coincide is hard to determine. One would expect that the ratio between K/L lines be constant as a linear relationship between the excitation of K and L X-rays are to be expected. One might argue

that the model fitting could incorporate the ratio between K/L lines to a constant, which might lead to a better end result. This procedure would further alter the data and alienating the results from reality i.e changing the results to what the observer wants to see, instead of what is actually present. On another note, these variations could originate from absorption by the specimen itself. For a thick specimen electrons can penetrate deeply and could thus have X-rays originating from deeper within the sample which would cause a larger amount of L-line X-rays to be absorbed. In [25] the ratio Ag K_α/K_β was determined to deviate with a factor ± 0.004 and [26] reported a deviation of ± 0.044. In addition the paper by Gojska et.al[25] reported that Ag-Cu alloys, would cause Ag K_α/K_β ratio to grow rapidly beyond theoretical atom results when introduced to alloys of greater Cu concentration. Considering that the K ratios change it is believable that the same would apply for the K_α/L_α lines, considering the composition ($Ga \approx 50\%, As \approx 49\%$ and $Sb \approx 1\%$) a result of a few percentages (3% for As, 2% for Ga) can be reasonable. The standard AL-CHEMI gives great results for some tilts and the magnitude of the results are reasonable (atleast compared to the 4 detectors specimen tilting case). However not all the tilts give the expected results, and if only one tilt was considered to determine the occupational position of the impurity element (Sb) an incorrect result could be acquired. Comparitivly the ALCHEMI results on the beam tilting are more consistent and reasonable compared to the beam tilting specimen. However this is not a fair compraison as the specimen tilting was done with a material containing a relatively much larger quantity of the impurity element, which as stated earlier is likely a contributor in shifting the ALCHEMI results.

In a recent paper by Hansen et.al[27] reported that the relative ratios between a crystal consisting of Sn, Co,Ti had different relative ratios between different zone axes. This makes it possible to extract information about the crystal symmetry and space groups. Statistical ALCHEMI against the first referance spectra gave good results and predicted that $120\% + \pm 11\%$ of the impurity element resides on the As atom column. The result is unphysical but it is within a fair proximity of the actual case i.e 100% of Sb atoms on As column. The results would likely have been even better with a higher number of beam rocking areas preferably in a ICP where all pixels are compared against an off zone case. Spence et.al [9] measured the occupational fraction of Hf on a Ti Al material was found to be 1.03 ± 0.020 for occupation on the Ti column. They obtained great results, but as a comparison, this statistical result utilized 4582 spectras whilst the experiment utilized here had 21. Taking this into account the results provided here are very good. However the results seems to be very dependant upon the referance spectra, as the accuracy of an EDX scan off zone accuracy usually resides within $\pm 5at\%$. The quality of the ALCHEMI seems to be highly dependant upon the reference scan.

Chapter 6

Conclusion

The excitation errors effect around a channeling zone axis's effect on EDX were examined. The excitation error were obtained by three different methods. By physically rotating the specimen, by having the specimen itself bend and by changing the incident angle of the electron beam relative to the specimen. The strength of channeling were quantified, by utilizing a non channeling reference scan. The orientation effects on EDX quantification were not as severe as originally thought. It was found that the composition was most accurate (for the used k-factors) directly on the [110] axis of pure GaAs in a ZB strucutre. The largest compositional variations were found to be $\pm 5°$ off zone for the pure GaAs Zb (As $48at\%$, Ga $52at\%$ for the most negative tilt and As $43at\%$, Ga $57at\%$ for the most positive). For the pure GaAs in a WZ strucutre the channeling was strongest on the [110] zone, i.e the largest compositional variation was at the zone axis. For a GaAs ZB crystal with a Sb insert, larger deviations in the composition were found compared to the pure GaAs case especially around the [110] zone axis. The channeling from was found to be different around the zone axis for positive and negative tilts, which likely indicates channeling in different atomic rows. In general it was found that the clearest indication of channeling was in the number of counts emitted from the specimen, this was consistent across all cases and all areas. The channeling effect was highly dependant on the reference EDX spectra, if the created X-rays at a channeling orientation was partially absorbed by the specimen the resulting channeling effect would be higher. Indicating that caution should be taken when taking a reference spectra. ALCHEMI was attempted on a specimen with a high concentration of an impurity element, which likely failed due to large changes in the average potential which caused skewed EDX ratios. ALCHEMI was also done on the case where the beam was tilted, here the amount of a tertiary impurity element were low and the ALCHEMI procedure was partially successful and it was found

that a proper selection of reference spectra was required for good results ($p \approx 1 \pm 0.1$). Statistical ALCHEMI was also done, with good results for the beam rocking case ($p \approx 1.27 \pm 0.11$), but in this instance as well, a proper reference is needed. The results for statistical ALCHEMI would likely have been better if more data points had been utilized. The author would advice caution when doing EDX analysis as non-channeling conditions of some structures might have bigger deviations off zone than on (namely pure GaAs ZB). The work resulted in python code which can be open-source for determining the effects of channeling, ALCHEMI and statistical ALCHEMI.

Chapter 7

Further work

7.1 ALCHEMI

As only the specimen in case 3: rocking beam had a specimen actually suitable for AL-CHEMI and statistical ALCHEMI it would be of interest to redo case 1 and 2 with a suitable specimen. This would prove if ALCHEMI can be utilized by different techniques. In addition it should be attempted with even finer tilt angles. It should also be attempted on a ICP where a much larger set of spectras can be utilized in statistical ALCHEMI. The ICP should be done by a automatic data collection method unlike the experiments in this thesis (the automatic control was not as user friendly to date).

7.2 Diffraction and EDX

It would be very interesting to get complementary diffraction pattern to the EDX for on zone and close to on zone orientations. This would allow one to identify the exact excitation error and relate it to the elemental EDX ratios.

7.3 Space group identification

Channeling can potentially be utilized to identify a structures space group as reported by Hansen et.al [27]. This method compares the relative X-ray ratios between different channeling zone-axes. This would be a sensible subject in regards to the effects of channeling at different orientations.

Bibliography

[1] C. Kittel, *Introduction to Solid State Physics*. Wiley, 2005.

[2] O. S, Muto. M, "High-precision quantitative atomic-site-analysis of functional dopants incrystalline materials by electron-channelling-enhanced microanalysis," vol. 63, 2017, pp. 40–61.

[3] Ruska.E, "The emergence of the electron-microscope-connection between realization and 1 patent application, documents of an invention," vol. 95, 1986, pp. 3–28.

[4] R. Binning.G, "Scanning tunneling microscopy," vol. 30, 1986, pp. 355–369.

[5] J. J.C.H Spence, "Alchemi: a new technique for locating atoms in small crystals," 1983.

[6] J. Fultz, B. Howe, *Transmission Electron Microscopy and Diffractometry of Materials*, 4th ed. Springer, 2013.

[7] C. Williams, D. Carter, *Transmission Electron Microscopy*, 2nd ed. Springer, 2009.

[8] S. S. Hubbell, J.H., "Tables of x-ray mass attenuation coefficients and mass energy-absorption coefficients from 1 kev to 20 mev for elements z = 1 to 92 and 48 additional substances of dosimetric interest," "https://physics.nist.gov/PhysRefData/XrayMassCoef/ElemTab/z82.html", online;accessed 20 February 2020.

[9] Y. J.C.H Spence, M. Kuwabara, "Localization effects on quantification in axial and planar alchemi," vol. 26, 1988, pp. 103–112.

[10] D. S. J.C.H Spence, R.J Graham, "Cold alchemi: Impurity atom site location and th temperature dependance of dechannelling," vol. 62, 1986, pp. 153–163.

[11] Castaing.R, "applications of electron beams to a method of local chemical and crystallographic analysis," 1951.

[12] W. G.Cliff, "The quantitative analysis of thin specimens," vol. 103, pp. 203–207.

[13] https://www.rep.routledge.com/articles/thematic/alchemy/v-1.

[14] N. Pennycook.S.J, "Atom location by axial-electron-channeling," vol. 54, 1985, pp. 1543–1546.

[15] W. O. Rossouw.C.J, Turner.P.S, "Statistical-analysis of electron channeling microanalytical data for the determination of site occupancies of impurities," vol. 60, 1989, pp. 225–232.

[16] W. Rossouw.C.J, Turner.P.S, "Axial electron-channeling analysis of perovskite .1. theory and experiment for catio3," vol. 57, 1988, pp. 209–225.

[17] R. C. Bastow TJ, "Lattice site determination of dilute cu in -phase nial by 63 cu nuclear magnetic res-onance and x-ray emission channelling patterns," 1998.

[18] C. Williams, D. Carter, *Transmission Electron Microscopy*. Springer, 2016.

[19] D. S. W. F. Munshi.A.M, Helvoort.ATJ, "Controlling crystal phases in gaas nanowires grow by au-assisted molecular beam epitaxy."

[20] K. O. D. F. W. v. H. Todorovic.J, Moses.A.F, "Correlated micro-photoluminescence and electron microscopy studies of the same individual heterostructured semiconductor nanowires," vol. 326, 2011.

[21] J. N. J. A. J. D. G. A. H. B. H. D.Ren, L.Ahtapodov, "Single-mode near-infrared lasing in a gaassb-based nanowire superlattice at room temperature," vol. 18, 2018, pp. 2304–2310.

[22] D.M.Lundeby, "Improving the accuracy of tem-edx quantification by implementing the zeta-factor method," 2019.

[23] R. K. H. P. G. Kraxner.J, schäfer.M, "Quantitative edxs: Influence of geometry on a four detector system," vol. 172, 2016, pp. 30–39.

[24] L. W. M.Ek, S.Lehmann, "Electron channeling: challenges and opportunities for compostional analysis of nanowires by tem," 2020.

[25] E.-J. R. A.M.Gojska, K.Koziol, "Determination of the kβ/k intensity ratios of silver in ag-cu alloys," vol. 468, 2020, pp. 65–70.

[26] T. N.A.Khelil, "Proton-induced k-shell ionization cross sections for selected elements ag to la:0.6-2-0mev," vol. 11, 1975, pp. 893–900.

[27] J. V.Hansen, A.Kosinskiy, "Disinguishing space groups by electron channeling:centrosymmetric full-heusler or non-centrosymmetric half-heusler?" vol. A76, pp. 211–213.

A.1 Dynamical theory calculation

The following is based on chapter 13 of [6] The accelerated electron traveling through vacuum has an energy(E_0) given by

$$E_0 = \frac{\hbar^2 \chi^2}{2m} \tag{A.1}$$

Where $\hbar$ is the reduced Planch constant, m the electron mass and χ the wave vector amplitude in vacuum. As the high energy electron traverses a solid the the electron wavevector will be altered by the average potential of a solid (U_{00}). The energy of the electron within the solid thus becomes

$$E_{kin} = \frac{\hbar^2 \vec{k}^2}{2m} \tag{A.2}$$

The average potential of the solid can thus be expressed as,

$$U_{00} = \frac{\hbar^2}{2m} \left(\chi^2 - \vec{k}^2 \right) \tag{A.3}$$

U_{00} is negative i.e the electron wavevector increases as the incident electron traverses the solid by loosing potential energy and gaining kinetic energy.

The incident beam has a "spatial form" i.e modeled as $\exp\left(i\vec{k}\vec{r}\right)$, as it traverses a solid, a periodic crystal potential (consisting of fourier components U_g) will cause amplitudes from the incident plane wave to transfer to various diffracted beams i.e $\exp i(\vec{k} + \vec{g})\vec{r}$. The periodic crystal potential can be changed by crystal potential and impurities. The potential energy of the crystal can then be written as a combination of the average and periodic potentials.

$$V(\vec{r}) = \sum_{g \neq 0} U_g e^{i\vec{g}\vec{r}} + U_{00} \tag{A.4}$$

The Schrödinger equation is given as

$$\frac{-\hbar^2}{2m}\nabla^2\psi(\vec{r}) + V(\vec{r})\psi(\vec{r}) = E\psi(\vec{r}) \tag{A.5}$$

here $\psi(\vec{r})$ is the electron wavefunction, which can be expressed as a fourier series with reciprocal lattice vectors g.

$$\psi(\vec{r}) = \sum_g \phi(z)e^{i(k+g)\vec{r}} \tag{A.6}$$

$\phi(z)$ are the intensities of the forward and diffracted beams which depends on the thickness i.e depth of the beam inside the solid.

When solving the schrödinger equation a few approximations are done, as the incident high energy electrons are nearly perpendicular to z, and the reciprocal lattice vectors z dependance is set to 0 (i.e $g_z = 0$). Using this with eq() gives

$$\frac{\delta\psi}{\delta r} = \sum_g i((k_x + g_x) + (k_y + g_y) + (k_z + \frac{1}{i\phi_g(z)}\frac{\delta\phi_g(z)}{\delta z}))\phi_g(z)e^{(i(k+g)\vec{r}} \tag{A.7}$$

$$\frac{\delta^2\psi}{\delta^2 r} = -\sum_g \left(\left((k_x + g_x)^2 + (k_y + g_y)^2 + k_z^2\right)\phi_g(z) - \left(\frac{\delta^2\phi_g(z)}{\delta z^2} + i2k_z\frac{\delta\phi_g(z)}{\delta z}\right) \right)e^{i(k+g)\vec{r}} \tag{A.8}$$

Plugged into the schrödinger equation with $E = E_{kin}$ (the kinetic energy of the incident electron in vacuum) gives

$$\frac{\hbar^2}{2m}\sum_g \left((k_x + g_x)^2 + (k_y + g_y) + k_z^2\right)\phi_g(z)e^{i(k+g)r}$$

$$\frac{-\hbar^2}{2m}\sum_g \left(2ik_z\frac{\delta\phi_g}{\delta z} + \frac{\delta^2\phi_g}{\delta z^2}\right)e^{i(k+g)r}$$

$$+ \left(\sum_{g=0} U_g e^{igr} + U_{00}\right)\sum_g \phi_g(z)e^{i(k+g)r} \tag{A.9}$$

$$= \frac{\hbar^2}{2m}\chi^2\sum_g \phi_g(z)e^{i(k+g)r}$$

Multiplying with $\frac{2m}{\hbar^2}$ and $\exp i(k+g)r$, moving all terms to the left hand side as well as sorting terms with common ϕ_g functions gives

$$\sum_g \left((k_x + g_x)^2 + (k_y + g_y)^2 + k_z^2 - \chi^2 + \frac{2m}{\hbar^2} U_{00}) \phi_g(z) \right)$$

$$-\sum_g \left(2ik_z \frac{\delta \phi_g}{\delta z} + \frac{\delta^2 \phi_g}{2} \right) \quad \text{(A.10)}$$

$$+\frac{2m}{\hbar^2} \sum_{g'} \sum_{g'' \neq 0} \phi_{g'} U_{g''} e^{i(k+g'+g''-(k+g))} = 0$$

utilizing the orthogonalit relashionship which states

$$\int_{-l/2}^{l/2} e^{i2\pi(n'-n)k/l} dk = \begin{cases} 1 & \text{if n'=n} \\ 0 & \text{if n'} \neq n \end{cases}$$

(A.11)

 and integrating over all r, will thus cause all terms to be zero except for the terms where $k+g = k+g'+g''$. Using this and the potential energy A.3 term to make some eliminations thus grants, as well as assuming ϕ to change slowly with z i.e ($\frac{\delta^2 \phi}{\delta z^2} \approx 0$, and is neglected). solving for $\frac{\delta \phi_g}{\delta z}$

$$\frac{\delta \phi_g}{\delta z} = i \left(\frac{k_x^2 - (k_x + g_x)^2 + k_y^2 - (k_y + g_y)^2}{2k_z} \right) \phi_g(z) - \frac{i2m}{\hbar^2 2k_z} \left(\sum_{g' \neq g} \phi_{g'}(z) U_{g-g'} \right)$$

(A.12)

 This is only one of a set of coupled differential equations for the beam amplitudes. Between beam pairs the coupling is provided by the Fourier component of the crystal potential (i.e $U_{g-g'}$). Now we introduce the definition of the extinction distance ($\xi_g - g'$) (i.e how deep into the material the electron can penetrate given beam g and g'), and the beams excitation error (s_g).

$$\frac{1}{\xi_{g-g'}} = -\frac{2m}{\hbar^2 k_z} U_{g-g'} \quad \text{(A.13)}$$

$$s_g = \frac{k_x^2 - (k_x + g_x)^2 + k_y^2 - (k_y + g_y)^2}{2k_z} \quad \text{(A.14)}$$

Which then allows us to rewrite each ϕ_g as:

$$\frac{\phi_g}{\delta z} = i s_g \phi_g(z) + \sum_{g' \neq g} \frac{i}{2\xi_{g-g'}} \phi_{g'}(z) \tag{A.15}$$

In many materials an centrosymmetric real potential(V) is assumed i.e(V(r)=V(-r)), this in turn leads to the the extinction distance being written as

$$\xi_{g-g'} = \xi_{g'-g} \equiv \xi_{gg'} \tag{A.16}$$

solving for exact lauve condition

Assuming exact lauve conditions $s_g = 0$ and only consider one diffracted beam(ϕ_g) and the forward beam(ϕ_0). The equations reduce to

$$\frac{\delta\phi_0}{\delta z} = \frac{i}{2\xi_g} \phi_g(z) \tag{A.17}$$

$$\frac{\delta\phi_g}{\delta z} = \frac{i}{2\xi_g} \phi_0(z) \tag{A.18}$$

setting one into the other gives

$$\phi_0(z) = \frac{2\xi_g}{i} \frac{\delta\phi_g(z)}{\delta z} \tag{A.19}$$

Thus resulting in a harmonic oscillator differential equation.

$$\frac{\delta^2\phi_g(z)}{\delta z^2} - 4\xi_g^2 \phi_g(z) = 0 \tag{A.20}$$

Which has a solution on the form

$$\phi_0(z) = A_0 \cos\frac{z}{2\xi_g} + B_0 \sin\frac{z}{2\xi_g} \tag{A.21}$$

The diffracte beam will have a solution of the same form. To determine the factors A_g, B_g and A_0, B_0 (for the $\phi_0(z)$) we employ two assumptions,

1. outside the specimen we have no diffracted beam i.e $\phi_0(0) = 1$ for $z = 0$, in this case values $z < 0$ are unphysical as we are not traversing a medium, meaning that the $z = 0$ case applies for all values $z < 0$.

2. the amplitude of the two beam wavefunctions should be constant i.e for a normalized solution $|\phi_0(z)|^2 + |\phi_g(z)^2| = 1$.

An approperiate solution to these restrictions would be

$$\phi_0(z) = \cos\left(z/(2\xi_g)\right)$$
$$\phi_g(z) = i\sin\left(z/(2\xi_g)\right)$$
(A.22)

Which would result in a complete revival of the amplitude of the forward beam $\phi_0(z)$ at a depth of $2\pi\xi_g$ (this is dependent upon the structurefactor). The thing to take away from this is a complete energy transfer from one harmonic oscillator to another before the process itself reverses.

For cases which are not fulfilling the lauve conditions exactly, we can solve them numerically by assuming

$$\frac{\delta\phi}{\delta z} \approx \frac{\Delta\phi}{\Delta z}$$
(A.23)

Δz will serve as our baby steps through out the specimen and will be constant, thus giving the change in ϕ per distance Δz as

$$\Delta\phi_0(z) = \frac{i}{2\xi_g}\phi_g(z)\Delta z$$
$$\Delta\phi_g(z) = \frac{i}{2\xi_g}\phi_0(z)\Delta z + is_g\phi_g(z)\Delta z$$
(A.24)

For small s_g the extinction length dominates and for large s_g the intensity is distrubuted more like a circle. The equation has to be normalized to make sence. For cases where $s_g \neq 0$ the diffracted beam $\phi_g(z)$ will gain a real value as it traverses the medium. So far the electron probability have been assumed to be constant, however the real case will cause it to diminish due to absorption. This is implemented into the model by making ξ_g complex. This will be explained later

Another way of tackling this problem is to assume that the beams are composed of a superposition of bloch waves and to assume that the beams are planar as they traverse through the specimen. The beams (ϕ) are moving in slightly different directions, and the coupeling of these can be represented by blochwaves propagating at different speeds (but in the same direction). First we have make our beams planar, this can be modeled as a radial wave

$$\Phi_0(r) = \frac{\phi_0(z)}{\sqrt{V}}e^{ik_0 r}$$
(A.25)

$$\Phi_G(r) = \frac{\phi_g(z)}{\sqrt{V}}e^{i(k_0+g)r}$$
(A.26)

The bloch waves are naturally just the standard solution to the scrödinger equation on the form

$$\Psi(r) = \frac{A}{\sqrt{V}} e^{ikr} \tag{A.27}$$

with k being the wave vector and A the amplitude (which are unique for each blochwave). We choose to represent our new ϕ as a combination of two bloc waves for simplicity first. Assume that the our beams can be modeled as a superposition of these

$$\Phi_0(r) = C_0^0 \Psi^{(1)}(r) + C_0^1 \Psi^{(2)}(r) \tag{A.28}$$

$$\Phi_g(r) = C_g^0 \Psi^{(1)}(r) e^{igr} + C_g^1 \Psi^{(2)}(r) e^{igr} \tag{A.29}$$

Which by direct insertion gives

$$\Phi_0(r) = \frac{\phi_0(r)}{\sqrt{V}} e^{ik_0 r} = C_0^0 \frac{A_0}{\sqrt{V}} e^{ik_1 r} + C_0^1 \frac{B_0}{\sqrt{V}} e^{ik_2 r} \tag{A.30}$$

The k's for bloch wave 1 and 2 can be viewed as a deviation of the wavevector k

$$k_1 \equiv k + \gamma_1 \tag{A.31}$$

$$k_2 \equiv k + \gamma_2 \tag{A.32}$$

Which in turn allows us to write the equations as

$$e^{i(k_0 - k)r} \phi_0(z) = C_0^0 A_0 e^{i\gamma_1 r} + C_0^1 B_0 e^{i\gamma_2 r} \tag{A.33}$$

$$e^{i(k_0 - k)r} \phi_g(z) = C_g^0 A_0 e^{i\gamma_1 r} + C_g^1 B_0 e^{i\gamma_2 r} \tag{A.34}$$

Thus we have a represetation a coupeling between beams and bloch waves. Which is interesting in respects to alchemi as we can see if a bloch wave is maximized over a certain atom row.

Which we can write in matrix notation as

$$
\begin{bmatrix} \phi_0(z) \\ \phi_g(z) \end{bmatrix} = \begin{bmatrix} C_0^{(1)} & C_0^{(2)} \\ C_g^{(1)} & C_g^{(2)} \end{bmatrix} \begin{bmatrix} e^{i\gamma_1 z} & 0 \\ 0 & e^{i\gamma_2 z} \end{bmatrix} \begin{bmatrix} A_0 \\ B_0 \end{bmatrix}
\tag{A.35}
$$

It is of interest to identify the bloch waves for the $s_g = 0$ case as we later can use these to calculate the effect of the periodic potential. For this particular case it is reasonable to assume that $C_0^{(0)} = C_0^{(1)} = C_g^{(0)} = -C_g^{(1)} \equiv C$ which means both bloch waves in the two beam representation contributes equally. Which when paired with equation A.22 gives

$$
\frac{\phi_0(z)}{\sqrt{V}} e^{ik_0 r} = \frac{\cos(\frac{z}{2\xi})}{\sqrt{V}} e^{ik_0 r} = C^2 (\psi_1(r) + \psi_2(r))
$$
$$
\frac{\phi_g(z)}{\sqrt{V}} e^{i(k_0+g)r} = \frac{\sin(\frac{z}{2\xi})}{\sqrt{V}} e^{i(k_0+g)r} = C^2 (\psi_1(r) - \psi_2(r))
\tag{A.36}
$$

This gives a view on the form of the blochwaves i.e should be a trigonometric functions sin and cosin. Which then gives us the following bloch waves for $s_g = 0$

$$
\Psi^{(1)}(r) = \frac{1}{2\sqrt{2V}} (e^{ik_0 r} + e^{i(k_0+g)r})
$$
$$
\Psi^{(2)}(r) = \frac{1}{2\sqrt{2V}} (e^{ik_0 r} - e^{i(k_0+g)r})
\tag{A.37}
$$

The average periodic potential contribution(δU) can be estimated by a first order pertubation.

$$
\delta U^{(1)} = \int_V \phi^{(1)*}(r) \phi^{(1)}(r) d^3 r
\tag{A.38}
$$

The electron densities for the first and second bloch wave can be written as

$$
\psi^{(1)*}(r) \psi^{(1)}(r) = 1 + \cos(gr)
$$
$$
\psi^{(2)*}(r) \psi^{(2)}(r) = 1 - \cos(gr)
\tag{A.39}
$$

From equation A.4 we see that the potential part is given as

$$
V'(r) = \sum_{g' \neq 0} U_{g'} e^{ig' r}
\tag{A.40}
$$

Which gives

$$
\delta U^{(1)} = \int_V (1 + \cos(gr)) \sum_{g'0} U_{g'} e^{ig' r} d^3 r
\tag{A.41}
$$

The exponential term can be rewritten as

$$e^{ig'r} = cos(g'r) + isin(g'r) \qquad (A.42)$$

Which allows eq A.41 to be written as

$$\delta U^{(1)} = \sum_{g' \neq 0} U_{g'} \int_V cos(g'r) + cos(gr)cos(g'r) + isin(g'r) + cos(gr)isin(g'r) \quad (A.43)$$

The first, second and third terms will when integrated over the unitcell volume give 0 for ALL g'. The third term only gives non-zero values for values $g = \pm g'$.

$$\delta U^{(1)} = \frac{1}{V} \sum_{' \neq 0} U_{g'} \int_V cos(gr)cos(g'r)dr^3 = \frac{1}{2}(U_g - U_{-g}) \qquad (A.44)$$

Using the same approach to calculate for the second bloch wave, thus gives the average periodic potentials as

$$\delta U^{(1)} = \frac{1}{2}(U_g + U_{-g})$$
$$\delta U^{(2)} = -\frac{1}{2}(U_g + U_{-g})$$

$$(A.45)$$

Making the assumption of a centrosymetric potential i.e making $U_g = U_{-g}$, we observe that the average periodic potential of blochwave 2 is inversed of bloch wave 1.

Mentioned earlier was the fact that the fourier components of U_g where negative. This in turn makes the average periodic potential of bloch wave 2 larger than bloch wave 1. Also the average potential $(U_{00} + \delta U_g)$ for bloch wave 2 will be larger than the average crystal potential and vise versa for bloch wave 1. The physical interpretation of this is that bloch wave 1 has its wave peaks over positive atom cores, whilst bloch wave 2 has its wave peaks in the interstitial regions between said atom cores. Plugging this in to the equation of energy conversion A.3, for both of the two bloch waves. i.e making the average potential $\rightarrow$ the average periodic potential, and the specimen wavevector

$$\frac{\hbar^2}{2m}((k + \gamma_1)^2 - k^2) = U_g \rightarrow \gamma_1 = \frac{m}{\hbar^2 k}$$
$$\frac{\hbar^2}{2m}((k + \gamma_2)^2 - k^2) = -U_g \rightarrow \gamma_2 = -\frac{m}{\hbar^2 k}$$

$$(A.46)$$

Note that this is for the $s_g = 0$, case. we will now tackle the off zone case of the blochwaves. Returning to the original equation we derived for dynamical theory (eq:A.15) and still assuming a two beam condition gives the following equations for the forward and

the diffracted beam

$$\frac{i}{2\xi_g}\phi_g(z) = \frac{\delta\phi_0}{\delta z}$$

$$is - g\phi_g(z) + \frac{i}{2\xi_0}\phi_g(z) = \frac{\delta\phi_0}{\delta z}$$

(A.47)

The expected solution is on the form

$$\phi_0(z) = C_0^\gamma e^{i\gamma z}$$

$$\phi_g(z) = C_g^\gamma e^{i\gamma z}$$

(A.48)

Which plugged into our differential equation gives

$$\frac{i}{2\xi_g}C_g{}^{i\gamma z} = i\gamma C_0^\gamma e^{i\gamma z}$$

$$\frac{i}{2\xi_g}C_g{}^{i\gamma z} + is_g C_g^\gamma e^{i\gamma z} = i\gamma C_0^\gamma e^{i\gamma z}$$

(A.49)

The phase factors ($e^{i\gamma z}$) are canceled and we move the right hand side terms over to the left hand side, which then allows us to write the equations in a matrix notation which we can solve for the eigenvalues (γ_0/C_g^γ). We also observe that the imaginary parts are divided out.

$$\begin{bmatrix} -\gamma & \frac{1}{2\xi_g} \\ \frac{1}{2\xi_g} & s_g - \gamma \end{bmatrix} \begin{bmatrix} C_0^\gamma \\ C_g^\gamma \end{bmatrix} = \begin{bmatrix} 0 \\ 0 \end{bmatrix}$$

(A.50)

We are only interested in non-trivial solutions and these only exists when the determinant of the matrix is zero. Which then results in the following equation.

$$\gamma^2 - \gamma s_g - \frac{1}{4\xi_g^2} = 0$$

(A.51)

This particular quadric equation thus has these solutions for γ

$$\gamma^{(1)} = \frac{s_g}{2}(1 + \sqrt{1 + (s_g\xi)^{-2}}$$

$$\gamma^{(2)} = \frac{s_g}{2}(1 - \sqrt{1 + (s_g\xi)^{-2}}$$

(A.52)

Now that we have the actual values for the γ's we can determine the relationship between the coefficients $\frac{C_g^\gamma}{C_0^\gamma}$. This is simply a case of solving equation A.47 for the different γ's. e.g

$$\frac{C_g^{(1)}}{C_0^\gamma(1)} = 2\gamma\xi_g$$

(A.53)

Thus we have an expression for each of the coefficients and a way to link the beam approximation and the bloch wave representation. The only thing that remains is to normalize the coefficients. To avoid "unpleasant algebraic manipulations" a direct quote from the authors, a new dimensionless variable is introduced. (based on trigonometric relationships)

$$\beta \equiv cot^{-1}(s_g \xi_g)$$
$$s_g \xi_g = cot\beta$$

(A.54)

Inserting these into our coefficients, and considering some trigonometric geometries yields (why we use these will become apparent shortly)

$$\frac{C_g^{(1)}}{C_0^{(1)}} = cot\beta + \sqrt{cot^2\beta + 1} = cot(\beta/2) = \frac{cos(\beta/2)}{sin(\beta/2)}$$

(A.55)

$$\frac{C_g^{(2)}}{C_0^{(2)}} = cot\beta - \sqrt{cot^2\beta + 1} = -tan(\beta/2) = -\frac{sin(\beta/2)}{cos(\beta/2)}$$

(A.56)

This makes it easy to separate the coefficients and using our matrix representation (equaiton A.35) between the bloch waves and the beams thus becomes

$$\begin{bmatrix} \psi^{(1)} \\ \psi^{(2)} \end{bmatrix} = \begin{bmatrix} e^{-i\gamma^{(1)}z} & 0 \\ 0 & e^{-i\gamma^{(2)}z} \end{bmatrix} \begin{bmatrix} sin(\beta/2) & cos(\beta/2) \\ cos(\beta/2) & -sin(\beta/2) \end{bmatrix} \begin{bmatrix} \phi_0(z) \\ \phi_g(z) \end{bmatrix}$$

(A.57)

The only thing we lack to get a complete picture of the bloch waves representation is the boundrary conditions, from earlier we stated that outside the specimen before the incident beam interacts with the specimen ($z = 0$ conditions) only the forward beam contributes i.e $\phi_0 = 1$ and $\phi_g = 0$. solving this using our beam to bloch matrix notation gives the following ψ

$$\psi^{(1)} = sin(\beta/2)$$

(A.58)

$$\psi^{(2)} = cos(\beta/2)$$

(A.59)

This can then be used to express the amplitudes in the beam representation via the bloch waves.

$$\phi_0(z) = sin^2(\beta/2)e^{i\gamma^{(1)}z} + cos^2(\beta/2)e^{i\gamma^{(2)}z}$$
$$\phi_g(z) = cos(\beta/2)sin(\beta/2)e^{i\gamma^{(1)}z} - sin(\beta/2)cos(\beta/2)e^{i\gamma^{(2)}z}$$

(A.60)

If one Bloch wave comes to favor one specific atom column which will lead to an enhanced signal (EDX,EELS), thus when performing chemical analysis of a specimen the zone axis

is mostly ignored.

For samples with a thickness less than the extinction distance the following happens (as can be seen in this plot), kinematical thepry and dynamical thepry merges, this is also the case for large s.

A.1.1 kinematic theory of diffraction

utilizing A.15 and only accounting for one single scattering event (first born approximation) only accounting for the incident beam (g-beam), kinematical theory assumes that the incident beam wont diminish throughout the crystal(i.e $\phi_0 = 1$ for all z), giving

$$\frac{\phi_g}{\delta z} = is_g(z) + \frac{i}{2\xi_{g-0}}\phi_0(z) \tag{A.61}$$

Assuming $\phi_g(z)$ consist of two functions

$$\phi_g(z) = \psi_g(z) * +\gamma(z)$$
$$\frac{\delta\phi_g(z)}{\delta z} = \frac{\delta\psi_g(z)}{\delta z}\gamma(z) + \frac{\delta\gamma(z)}{\delta z}\psi_g(z) \tag{A.62}$$

comparing this our left hand side allows us to determine $\gamma(z)^{-is_g z}$ thus cancels out a term and reduces the equation to. Which makes sense as the wave equation outside/on the surface should have dependance on the material, the depth at which the scattering event thus constitutes the magnitude (which varies periodically through the material given no defects or impurities) of the excitation error

$$e^{s_g z}\frac{\delta\psi_g}{\delta z} = \frac{i}{2\xi_g} \tag{A.63}$$

There are ways to relate the dynamical theory to the structure factor, absorption and other effects, but this will not be detailed here. Rest can be looked up in [6].

A.2 Code

The code used to create all figures in this thesis are shown in their respective subsection. First some general functions and libraries utilized for all the dataset are presented.

A.2.1 General functions

```python
"""Libraries utilized"""
%matplotlib qt
import hyperspy.api as hs
import hyperspy.misc as hsm
import numpy as np
import pandas as pd
import matplotlib as mpl
import matplotlib.pyplot as plt
import os

def quantification(ms,ed):
    """Returns the composition of a model and spectra, the spectra
        must be fitted with the appropriate elements, this
        particular function only utilizes Ga,As and Sb for
        compositional calculations"""
    lines = ['As_Ka', "Ga_Ka", 'Sb_La']
    factors = [ 2.225, 1.930, 2.873]
    elements = ['As', 'Ga',  'Sb']
    out=[]
    medsi_q = []
    medsi = ms.get_lines_intensity()
    for line in lines:
        for peak in medsi:
            if line == peak.metadata.General.title[12:18].replace("
                ",""):
                medsi_q.append(peak)

    medsi_q
    msq=ed.quantification(intensities=medsi_q, method='CL',
        factors=factors)
    totp = 0
    for result in msq:
        name = result.metadata.General.title
        if name.startswith('atomic percent of'):
            name = name[18:]
            out.append(result.data[0])
        totp += result.data[0]
    return out

def channeling_effect(ms0,ms1,el1,el2):
"""Takes in two models ms0 and ms1, and two elemental lines el1
```

```python
     and el2. Returns the relative channeling effect between the
     models"""
    Y_r=ms0[el1].A.value/ms0[el2].A.value
    Y_c=ms1[el1].A.value/ms1[el2].A.value
    return abs(Y_r-Y_c)/Y_r*100

def Alchemi(ms0,ms1, element1,element2, element3, ratio=False):
"""Takes inn two models ms1 and ms0, and three elements, element1
    is the host element on which the occupational fraction will
    be calculated, element 2 is the other major element, and
    element 3 is the impurity element, returns the occupational
    fration, if ratio=True the elemental ratios will be printed"""
    A_0=ms0[element1].A.value
    A_1=ms1[element1].A.value

    B_0=ms0[element2].A.value
    B_1=ms1[element2].A.value

    C_0=ms0[element3].A.value
    C_1=ms1[element3].A.value

    R_a=A_0/A_1
    R_b=B_0/B_1
    R_c=C_0/C_1
    p=(R_c-R_b)/(R_a-R_b)
    if ratio==True:
        print("Ratio ",element1,": ", R_a)

        print("Ratio ",element2,": ", R_b)

        print("Ratio ",element3,": ", R_c)

        print("percentage of ",element3[:-3], "situated on",
            element1[:-3]," ", p*100, "%" )
    return p

"""Some help functions will follow which are utilized in
    statistical ALCHEMI"""

def data_matrix(X,Y, dim=1):
    """ returns a data matrix, (done mainly to get the formating
```

```python
            right for later functions, but can also be used to expand
            the X matrix 1 dimension to get an offset later in the
            regression"""
        I=[]
        if dim==2:
            for i in range(len(X)):
                I.append(1)
            X=np.array([I,X])
        else:
            X=np.array([X])
        y=np.array([Y])
        return X,y


def OLS(X,y):
    """Ordinary least squares of array X and Y, from datamatrix.
        returns the regression lines slope (and if dimensionality of
        datamatrix is 2 a constant offset"""
        w=np.linalg.pinv(X.T.dot(X)).dot(X.T.dot(y))
        return w


def plot_stat_alch(X,Y,dim,det):
    """Does statistical ALCHEMI, takes in X (number of counts from
        the host atom) Y ALCHEMI results (off multiple spectras), dim
        is for the dimensionality of the regression line i.e if you
        want a constant offset dim=2, else dim=1"""
        reg=[]
        x,y=data_matrix(X,Y,dim)
        w=OLS(x.T,y.T)
        #if len(w)==1:

            # print(round(w[0][0],4),'&', round(Error_mse(x,y,w),4),'\\\
                ')
        #else:
            # print(round(w[1][0],4),'&',round(w[0][0],4),'&',
                round(Error_mse(x,y,w),4), '\\\ ')
        if dim==2:
            for i in range(len(X)):
                reg.append(w[0]+w[1]*X[i])
            X_min=min(X)
            X_max=max(X)
            #print(X_min,X_max)
```

```
    p=(X_max+X_min)/2*w[1]+w[0]
    pm=X_max*w[1]+w[0]-p
    print('p= ',round(p[0],3), ' +-',round(pm[0],3),' C= ',
        round(w[0][0],3),'\\\\ ')

if dim==1:
    for i in range(len(X)):
        reg.append(w[0]*X[i])
    X_min=min(X)
    X_max=max(X)
    #print(X_min,X_max)
    p=(X_max+X_min)/2*w[0]
    pm=X_max*w[0]-p
    print('p=',round(p[0],3),' +-',round(pm[0],3), '\\\\ ')
plt.scatter(X,Y)
plt.plot(X,reg)
```

A.2.2 Case 1

The data for case 1 required some sorting of the incident data and is included here, in
addition to the functions for figures.

```
"""Get the path to the folder containing the files:"""
k=os.getcwd()

path=k+'\\ystein_EDX_data\\24_March_2015_Ton\\'
templist=[]
for filename in os.listdir(path):
    templist.append([path+filename, filename])

"""Filtering so, that only specific files remain. depending on
    input"""


def datalistarea_2(a,test,det):
    """
    a=area, test = list of data, det =detector (can take in list[]
        for detector1-4).
    Makes a list of files containing certain key words, i.e it
        acts as
    a filter to seperate out files that we don't want to deal with.
```

```python
    OPS. it will not return the list sorted after tilts.
    """
    tem=test[0][1][0:4]
    datalist=[]
    templist=[]
##pick area ou would like to exaime
    if isinstance(det,list):
        for i in range(len(test)):
            if tem in test[i][1]:
                for k in range(len(det)):
                    area="_D{}_{}.".format(det[k],a)
                    if area in test[i][1]:
                        #print(test[i][1])
                        templist.append(test[i][0])
                    else:
                        continue
            else:
                tem=test[i][1][0:4]
                if len(templist)>0:
                    datalist.append(templist)
                templist=[]
                for k in range(len(det)):
                    area="_D{}_{}.".format(det[k],a)
                    if area in test[i][1]:
                        templist.append(test[i][0])
        datalist.append(templist)



    else:
        area="_D{}_{}.".format(det,a)

        for i in range(len(test)):
            if tem in test[i][1]:
                if area in test[i][1]:
                    #print(test[i][1])
                    templist.append(test[i][0])
                else:
                    continue
            else:
                tem=test[i][1][0:3]
```

```python
            if len(templist)>0:
                datalist.append(templist)
            templist=[]
            if area in test[i][1]:
                #print(test[i][1])
                templist.append(test[i][0])
    datalist.append(templist)


    return datalist

    """Next sorts the list"""
def make_list(templist):
    """
    Sorts the list from datalist_area2
    """
    i=0
    tilts_n=templist[i:]
    tilts=[]
    if templist[1]==list:
        for i in range(len(tilts_n)):
            if '.emi' in tilts_n[i][1]:
                tilts.append(tilts_n[i])

        mtilts=[]
        for i in range(len(tilts)):
            if 'Tm' in tilts[i][1]:
                mtilts.append(tilts[i])
        ptilts=[]
        for i in range(len(tilts)):
            if 'Tp' in tilts[i][1]:
                ptilts.append(tilts[i])
        zerotilt=[]
        for i in range(len(tilts)):
            if 'T0_' in tilts[i][1]:
                zerotilt.append(tilts[i])
        tilt=['05','1_','2_','3_','5']
        mtilts_s=[]
        for k in range(1,len(tilt)+1):
            for i in range(len(mtilts)):
                if 'Tm'+tilt[-k] in mtilts[i][1]:
                    mtilts_s.append(mtilts[i])
```

```python
    else:
        for i in range(len(tilts_n)):
            if '.emi' in tilts_n[i][0]:
                tilts.append(tilts_n[i])

        mtilts=[]
        for i in range(len(tilts)):
            if 'Tm' in tilts[i][0]:
                mtilts.append(tilts[i])
        ptilts=[]
        for i in range(len(tilts)):
            if 'Tp' in tilts[i][0]:
                ptilts.append(tilts[i])
        zerotilt=[]
        for i in range(len(tilts)):
            if 'T0_' in tilts[i][0]:
                zerotilt.append(tilts[i])
        tilt=['05','1_','2_','3_','5']
        mtilts_s=[]
        for k in range(1,len(tilt)+1):
            for i in range(len(mtilts)):
                if 'Tm'+tilt[-k] in mtilts[i][0]:
                    mtilts_s.append(mtilts[i])
    return mtilts_s+zerotilt+ptilts


"""Get the sum of spectras from 4 detectectors"""

def get_sum_spectras(datalist,print_spec=False):
    """
    Summing together all the pixels, in map. If the format of the
        file is wrong,
    (it is a list) take the spectra instead. Change the type of
        the signal to EDS_TEM-
    Sum together equal detectors for a given tilt.
    """
    eds=hs.load(datalist[0])
    if type(eds)==list:
        if print_spec==True:
            print(datalist[0])
        eds=eds[0]
    eds=eds.sum()
```

```python
for i in range(1, len(datalist)):
    if print_spec==True:
        print(datalist[i])
    eds_temp=hs.load(datalist[i])
    if type(eds_temp)==list:
        eds_temp=eds_temp[0]
    eds_temp.set_signal_type("EDS_TEM")
    eds_temp=eds_temp.sum()
    eds+=eds_temp.sum()
eds.set_signal_type("EDS_TEM")
return eds


def Tot_count_tilt_area_plot(area,templist,det,
                    c=['tab:blue'],
                    fit=False):
"""
area=Area, templist = list of datafiles, det=detectors, c
    =Colors (need to input 4), fit= True/False to
    enable/Disable modelfit.

Counts the total tilts for Ga,As and Sb at a given tilt, for a
    given detector.
It can be done with or without modelfitting.
"""
values=make_list(templist)
data=datalistarea_2(area,values,det)
X=[-5, -3, -2, -1, -0.5, 0, 0.5, 1, 2, 3, 5]
C_tot=[]
ls='--'
k='Un-fitted'
if fit==True:
    ls='-'
    k='Fitted'
for i in range(len(X)):
    ed=get_sum_spectras(data[i])
    elements=["Ga", "As", "Sb", "Si", "Cu", 'Fe','O']
    ed.set_elements(elements)
    ed.change_dtype('float')
    ms = ed.create_model()
    if fit ==True:
        ms.fit()
```

```python
        C_tot.append(ms["As_Ka"].A.value+ms["Ga_Ka"].A.value+ms["Sb_La"].A.value)

    if isinstance(det,list):
        plt.plot(X,C_tot,linestyle=ls,color=c)
    else:
        plt.plot(X,C_tot,label=k+' det
            {}'.format(det),linestyle=ls,color=c)
    #plt.title('Counts area {} at different
        tilts'.format(area),fontsize=24)
    plt.xlabel(r'tilts $\degree$', fontsize=20)
    plt.ylabel('Counts', fontsize=20)
    plt.xticks(size = 20)
    plt.yticks(size = 20)
    #plt.legend(prop={'size': 20})


    return X,C_tot


    """Function to calculate the composition at a given area for
        set detectors e.g [1,2,4] will consider detector 1,2 and 4
        """
    def Composition_tilt_area_plot(area,templist,det,fit =False):
    values=make_list(templist)
    data=datalistarea_2(area,values,det)
    #X=make_tiltaxis(values)
    X=[-5, -3, -2, -1, -0.5, 0, 0.5, 1, 2, 3, 5]
    Y=[]
    Y1=[]
    Y2=[]
    As_C=[]
    Ga_C=[]
    Sb_C=[]
    ls='--'
    k='Un-fitted'
    if fit==True:
        ls='-'
        k='Fitted'
    for i in range(len(X)):
        ed=get_sum_spectras(data[i])
        elements=["Ga", "As", "Sb", "Si", "Cu", 'Fe','O']
        ed.set_elements(elements)
        ed.change_dtype('float')
```

```python
    ms = ed.create_model()
    if fit==True:
       ms.fit()
    C=quantification(ms,ed)
    As_C.append(C[0])
    Ga_C.append(C[1])
    Sb_C.append(C[2])
  if fit==True:
    plt.plot(X,As_C,label=r'$at \%$ As
        ',color='tab:blue',linestyle=ls)
    plt.plot(X,Ga_C,label=r'$at \%$ Ga ',color='tab:orange'
        ,linestyle=ls)
    plt.plot(X,Sb_C,label=r'$at \%$ Sb ',color='tab:green'
        ,linestyle=ls)
  else:
    plt.plot(X,As_C,color='tab:blue',linestyle=ls)
    plt.plot(X,Ga_C,color='tab:orange' ,linestyle=ls)
    plt.plot(X,Sb_C,color='tab:green' ,linestyle=ls)
 # if isinstance(det,list):
    #plt.title('Composition area {} at different tilts all
        detectrors {}'.format(area,k), fontsize=24 )
# else:
    #plt.title('Composition area {} at different tilts for
        detector {} {}'.format(area,det,k), fontsize=24 )
 plt.xlabel(r'tilts $\degree$', fontsize=30)
 plt.ylabel(r'$at\%$', fontsize=30)
 plt.xticks(size = 20)
 plt.yticks(size = 20)
 plt.legend(prop={'size': 20})


 """Channeling for a given area for a given detector at all
     tilts, plot"""
 def channeling_at_tilts(area,templist,det,fit
     =False,Ga_line='a'):
 values=make_list(templist)
 data=datalistarea_2(area,values,det)
 #X=make_tiltaxis(values)
 X=[-5, -3, -2, -1, -0.5, 0, 0.5, 1, 2, 3, 5]
 E=[]
 print(data[0])
 eds=get_sum_spectras(data[0])
```

```python
    elements=["Ga", "As", "Sb", "Si", "Cu", 'Fe','O']
    eds.set_elements(elements)
    eds.change_dtype('float')
    ms0=eds.create_model()
    if fit==True:
        ms0.fit()
    for i in range(len(X)):
        ed=get_sum_spectras(data[i])
        elements=["Ga", "As", "Sb", "Si", "Cu", 'Fe','O']
        ed.set_elements(elements)
        ed.change_dtype('float')
        ms = ed.create_model()
        if fit==True:
            ms.fit()
        E.append(channeling_effect(ms0,ms,"As_Ka","Ga_K{}".format(Ga_line)))

    k='Un-fitted'
    lstyle='--'
    if fit==True:
        k='Fitted'
        lstyle='-'

    if Ga_line=='a':
        col='tab:blue'
    else:
        col='tab:orange'
    plt.plot(X,E,linestyle=lstyle,color=col)
    #if isinstance(det,list):
    #   plt.title('Channeling effect at different tilts, Area {}
        all detectors'.format(area),fontsize=24 )
    #else:
    #   plt.title('Channeling effect at different tilts, Area {}
        Detector {}'.format(area,det),fontsize=24 )
    plt.xlabel(r'tilts $\degree$', fontsize=30)
    plt.ylabel(r'$E(\%)$', fontsize=30)
    plt.xticks(size = 20)
    plt.yticks(size = 20)
    plt.legend(prop={'size': 20})

"""ALCHEMI result for the different tilts i.e the number which
    should be plugged into the statistical ALCHEMI function"""
```

```python
def Alchemi_over_wire(Count_list, area, det, tilt1, fit=True,
    regression=False,tolerance=20):
    """"Gives ALCHEMI result for different tilts for a given area
        and detector(s), OG are the reference spetra and is
        allways set against the leftmost pixel,
    count_list is a list of the counts from the different areas
        (done to reduce computation time for multiple sequencial
        plots), area is the area of the wire, tilt1 is the
        reference tilt, regression is for statalch should be se to
        false in this case, tolerance filters out outliers"""
    if det==[1,2,3,4]:
        det=4
    Area_list=Count_list[area-1]
    Tilts=[-5, -3, -2, -1, -0.5, 0, 0.5, 1, 2, 3, 5]
    t1=[i for i, x in enumerate(Tilts) if x==tilt1]
    OG=[]
    X=[]
    Y=[]
    k=0
    if fit==True:
        k=1
    for i in range(len(Area_list[det][k])):
        OG.append(Area_list[det][k][i][t1[0]])
    for l in range(len(Area_list[0][0][0])):
        tilt_com=[]
        counts=0
        for i in range(len(Area_list[0][0])):

            tilt_com.append(Area_list[det][k][i][l])
            counts+=Area_list[det][k][i][l]
        X.append(counts)
        Y.append(
            ALCHEMI(OG,tilt_com, el, ratio=False))

    X,Y=remove_outliers(X,Y,tolerance)
    if det+1==5:
        p=plt.scatter(X,Y,label='Det All')
    else:
        p=plt.scatter(X,Y,label='Det {}'.format(det+1))
    plt.figure(figsize=(20,10))
```

```python
    plt.xlabel('N',fontsize=14)
    plt.ylabel('p',fontsize=14)#'f_{}'.format('As'),fontsize=20)
    #plot_stat_alch(X,Y,1,)
    #plt.legend(fontsize=20)
    plt.show()
    return X,Y
"""Simple function which performs statalch and returns the
    results, returns figures for both 1 dim and 2 dim inputs"""
def stat_alch_all_dets():
    det=[0,1,2,3]#[1,2,3,4]]
    dim=[1,2]
    area=2
    path=os.getcwd()
    for l in range(len(dim)):
        plt.figure(figsize=(20,10))
        for i in range(len(det)):
            #print('Detector {}, regression dim {}
                f_As'.format(det[i],dim[l]))
            #print(det[i]+1,' &')
            X,Y=Alchemi_over_wire(Count_list,area,det[i],5,True,20)
            plot_stat_alch(X,Y,dim[l],det[i])

        plt.title('Statistical ALCHEMI, regression dimension
            {}'.format(dim[l]),fontsize=24)
        outpath=os.path.join(path+'\\Data_figures\\Ton_4_detectors\\Stat_alch\\','
        plt.savefig(outpath)


    det=[1,2,3,4]
    for l in range(len(dim)):
        plt.figure(figsize=(20,10))
       # print('Detector {}, regression dim {}
            f_As'.format(det[i],dim[l]))
        #print(,' &')
        X,Y=Alchemi_over_wire(Count_list,2,det,5,True,20)
        plot_stat_alch(X,Y,dim[l],'all')

        plt.title('Statistical ALCHEMI, regression dimension
            {}'.format(dim[l]),fontsize=24)
        outpath=os.path.join(path+'\\Data_figures\\Ton_4_detectors\\Stat_alch\\','
        plt.savefig(outpath)
```

A.2.3 Case 2

Functions utilized to make the figures are given in this section

```python
"""Composition at different edges given by y"""
def composition_over_spectra(eds,fit=False, y=0,elements=["Ga",
    "As", "Sb"],length_wire=2.28):
    """eds input spectra/map, fit=true gives a gaussian model fit,
        elements are the elements which should be plotted, length
        of wire is to normalize the x axis. PLots the
        composition"""
    eds.set_elements(elements)
    eds.add_lines()
    eds.change_dtype('float')
    X=[0]*int(eds.axes_manager[0].size)
    l=''
    for i in range(len(X)):
        X[i]=i*length_wire/len(X)

    As_C=[]
    Ga_C=[]
    Sb_C=[]
    for i in range(len(X)):
        ed=eds.inav[i,y]
        ms=ed.create_model()
        if fit==True:
            ms.fit()
            l='modellfitted'
        C=quantification(ms,ed)
        As_C.append(C[0])
        Ga_C.append(C[1])
        Sb_C.append(C[2])
    plt.plot(X,As_C,label='As'.format(y))
    plt.plot(X,Ga_C,label='Ga'.format(y))
    plt.plot(X,Sb_C,label='Sb'.format(y))
    plt.xlabel(r'Position [$\mu$m]',fontsize=30)
    plt.ylabel(r'Composition At%',fontsize=30)
    #plt.title('Composition over the wire {}, height
        {}'.format(l,y),fontsize=24)
    plt.xticks(size = 20)
    plt.yticks(size = 20)
    plt.legend(prop={'size': 20})
```

```
    return X, As_C,Ga_C,Sb_C
"""Total number of counts at edge y"""
def Total_counts_at_height(eds,fit=False, y=0,elements=["Ga",
    "As", "Sb", "Si", "Cu", 'Fe','O'],length_wire=2.28 ):
    """eds input spectra/map, fit=true gives a gaussian model
        fit, elements are the elements which should be plotted,
        length of wire is to normalize the x axis.Plots the total
        number of counts at a given edge."""

    eds.set_elements(elements)
    eds.add_lines()
    eds.change_dtype('float')
    edge=["Edge 1", "Center", "Edge 2"]
    X=[0]*int(eds.axes_manager[0].size)
    l=''
    for i in range(len(X)):
        X[i]=i*length_wire/len(X)

    C=[]
    for i in range(len(X)):
        ed=eds.inav[i,y]
        ms=ed.create_model()
        if fit==True:
            ms.fit()
            l='modellfitted'
        C.append(ms["Ga_Ka"].A.value
            +ms["Sb_La"].A.value+ms["As_Ka"].A.value)
    plt.plot(X,C,label=edge[y])
    plt.xlabel(r'Position [$\mu$m]',fontsize=30)
    plt.ylabel('Total Counts', fontsize=30)
    #plt.title('Total Counts at height', fontsize=24)
    plt.legend(prop={'size': 20})
    plt.xticks(size = 20)
    plt.yticks(size = 20)
    return X, C

"""Channeling effect over the wire"""
def channeling_wire(eds,eds_random,y=0,length_wire=2.28):
    """eds spectra/map, eds_random is the spetra of a non
        channeling orientation, y is the edge, wire length is a
        normalization of the X-axis. plots the channeling effect
```

```python
       at a given height"""
    X=[0]*int(eds.axes_manager[0].size)
    E=[]
    ms0=eds_random.create_model()
    ms0.fit()


    edge=["Edge 1", "Center", "Edge 2"]
    for i in range(len(X)):
        X[i]=i*length_wire/len(X)
        print(X[i])
    for i in range(len(X)):
        ed=eds.inav[i,y]
        ms=ed.create_model()
        ms.fit()
        E.append(channeling_effect(ms0,ms,"As_Ka","Ga_Ka"))
    plt.plot(X,E,label=edge[y])
    #plt.title('Channeling effect',fontsize=24)
    plt.xlabel(r'tilts $\degree$', fontsize=30)
    plt.ylabel(r'$E(\%)$', fontsize=30)
    plt.legend(prop={'size': 20})
    plt.xticks(size = 20)
    plt.yticks(size = 20)
    return E


"""ALCHEMI over wire, to be plugged into statalch function"""
def Alchemi_over_wire(eds,OGpos,el,y):
    """eds is the map/spectra, OGpos is the nonchanneling
        orientation position on the wire, el is the element which
        the alchemi should be performed against (imprtant for stat
        alch)."""
    elements=["Ga", "As", "Sb"]# "Si", "Cu", 'Fe','O']
    eds.set_elements(elements)
    eds.add_lines()
    positions=eds.axes_manager[0].size
    eds.change_dtype('float')
    ed=eds.inav[0,y]#.create_model()

    ms0=ed.create_model()
    ms0.fit()

    X=[]
```

```
    Y=[]
    for k in range(1,positions):
        ed=eds.inav[k,y]
        ms=ed.create_model()
        ms.fit()
        X.append(ms[el].A.value)
        Y.append(
            p_st(ms0,ms,"As_Ka","Ga_Ka","Sb_La"))
    return X,Y


"""Stat alch at different edges"""
def stat_alch_at_height(dim,eds):
    y=[0,1,2]
    for i in range(len(y)):
        plt.figure(figsize=(20,10))
        print('height=',y[i])
        OG=[0,0]
        X,Y=Alchemi_over_wire(eds,OG,'As_Ka',y[i])
        X_1,Y_1=data_matrix(X,Y,dim)
        w=OLS(X_1.T,Y_1.T)
        plot_stat_alch(X,Y,w,dim)
        path=os.getcwd()
        outpath=k+'\\Data_figures\\\\Bend_wire\\bent_Stat_alch_height{}_dim{}'.for
        plt.savefig(outpath)
```

A.2.4 Case 3

The data for case 3 required some sorting of the incident data and is included here, in
addition to the functions for figures.

```
"""Get data"""
def get_list(series, set_name):
    k=os.getcwd()
    path=k+'\\Ton_data_rocking_mai\\EDXasEMSA\\Series_{}\\'.format(series)
    templist=[]
    for filename in os.listdir(path):
        if os.path.isfile(path+filename)==True:
            templist.append([path+filename])
    num_unsort=[]
    i=0
    for i in range(len(templist)):
```

```python
        path=templist[i][0]
        if os.path.isfile(path)==True:
            base=os.path.splitext(path)[0]
            name=base.split('\\')[-1]
            k=name[:len(set_name)]
            if k==set_name:
                if name[len(set_name):].isdigit()==True:
                    num_unsort.append([i,int(name[len(set_name):]),path])
                else:
                    num_unsort.append([i,0,path])
            i+=1

    num_sort=sorted(num_unsort, key=itemgetter(1))
    sorted_list=[]
    for i in range(len(num_sort)):
        sorted_list.append(num_sort[i][2])
    return sorted_list


"""Make a list of sorted data"""
def make_series_list(series_1,sorted_list):
    newlist=[]
    for i in range(len(series_1)):
        newlist.append(sorted_list[series_1[i]+1])
    return newlist


"""Find the reference spectras"""
def find_ref(ed,elements):
    C=np.Infinity
    for i in range(len(ed)):
        k= get_counts(ed_mod[i],elements)
        if k <C:
            C=k
            out=i
    return out


""""PLot channeling""""
def Channeling_plots(series, ref, el, listt,zerotilts, nr):
"""Sereies is special to this dataset, it was done in 3 sereis,
    ref is the reference spectra , zerotilts are on zone tilts,
    el are elements which should be compared in channeling, nr is
    to label the propper dataset, plots channeling"""
```

```python
    elements=["Ga", "As", "Sb", "Si", "Cu", 'Fe','O',"Al"]
    ed0=hs.load(ref)
    ed0.set_signal_type("EDS_TEM")
    ed0.add_elements(elements)
    ms0=ed0.create_model()
    ms0.fit()
    E=[]
    series_set=make_series_list(series,listt)
    X=[]
    num=1
    for i in range(len(series_set)):
        ed0=hs.load(series_set[i])
        ed0.set_signal_type("EDS_TEM")
        ed0.add_elements(elements)
        ms1=ed0.create_model()
        ms1.fit()
        E.append(channeling_effect(ms0,ms1,el[0],el[1]))
        X.append(num)
        num+=1
    fig, ax = plt.subplots(figsize=(20,10))
    plt.plot(X,E)
   # ax.set_title('Channeling effect for selected tilts, series
       {}'.format(nr),fontsize=24)
    ax.set_xlabel('Area Index',fontsize=30)
    ax.set_ylabel('Channeling effect E',fontsize=30)
    for i in range(len(zerotilts)):
        ax.axvline(x=zerotilts[i],linestyle='--',color='r')
    ax.set_xticks(X)
    ns=[]
    for i in range(len(series)):
        ns.append(series[i]+1)
    ax.set_xticklabels(ns)
    plt.xticks(size = 17)
    plt.yticks(size = 17)
    ax.tick_params(labelsize=20)
    ax.legend(prop={'size': 20})


"""Plot composition"""
def composition_plots(series,list1,nr,el,zerotilts):
"""series is particular to this dataset, list1 is a list of edx
```

```python
    spectras, el is elements, zero tilst are onzone locations. nr
    is to label the propper dataset. PLots compostion"""
elements=["Ga", "As", "Sb", "Si", "Cu", 'Fe','O',"Al"]
series_set=make_series_list(series,list1)
As=[]
Ga=[]
Sb=[]
Al=[]
X=[]
num=1
for i in range(len(series_set)):
    ed0=hs.load(series_set[i])
    ed0.set_signal_type("EDS_TEM")
    ed0.add_elements(elements)
    ms1=ed0.create_model()
    ms1.fit()
    C=quantification(ms1,ed0)
    print(C)
    As.append(C[1])
    Ga.append(C[0])
    Sb.append(C[2])

    X.append(num)
    num+=1
fig, ax = plt.subplots(figsize=(20,10))
if 'As' in el:
    plt.plot(X,As,label='As')
if 'Ga' in el:
    plt.plot(X,Ga,label='Ga')
if 'Sb' in el:
    plt.plot(X,Sb,label='Sb')
#if 'Al' in el:
#   plt.plot(X,Al,label='Al')
#ax.set_title('Channeling effect for selected tilts, series
    {}'.format(nr),fontsize=24)
ax.set_xlabel('Area Index',fontsize=30)
ax.set_ylabel(r'At\%',fontsize=30)
for i in range(len(zerotilts)):
    ax.axvline(x=zerotilts[i],linestyle='--',color='r')
ax.set_xticks(X)
ns=[]
```

```python
    for i in range(len(series)):
        ns.append(series[i]+1)
    ax.set_xticklabels(ns)

    ax.tick_params(labelsize=20)
    plt.xticks(size = 17)
    plt.yticks(size = 17)
    plt.legend(prop={'size': 20})

"""Funcitons below are utilized to plot the figures"""
def channeling_series_3(el):
    series=3
    set_name='Spectrum '
    Oref=8
    s1=[5,4,Oref,19,16]
    s2=[15,14,Oref,9,10]
    s3=[6,Oref,12,11]
    s4=[17,18,Oref,4]
    zerotilts=[1,8,13,21]
    el=["Ga_Ka","As_Ka","Al_Ka","Sb_La"]
    list1=get_list(series,set_name)
    non_channeling_ref=list1[1]
    #print(non_channeling_ref)
    S_all=range(0,21)
    S=[s1,s2,s3,s4]
    S=[S_all]
    for i in range(len(S)):
        Channeling_plots(S[i],non_channeling_ref,el,Oref,list1,series,zerotilts)
        k=os.getcwd()
        path=k+'\\Data_figures\\Rocking\\Series_{}\\Series_{},Channeling_tilts{}_r
        plt.savefig(path)


def composition_series_3(el):
    series=3
    set_name='Spectrum '
    Oref=4
    s1=[5,4,Oref,19,16]
    s2=[15,14,Oref,9,10]
    s3=[6,Oref,12,11]
    s4=[17,18,Oref,4]
```

```python
    zerotilts=[1,8,13,21]
    #el=["Ga_Ka","As_Ka","Al_Ka","Sb_La"]
    list1=get_list(series,set_name)
    non_channeling_ref=list1[0]
    S_all=range(0,21)
    S=[s1,s2,s3,s4]
    S=[S_all]
    for i in range(len(S)):
        composition_plots(S[i],list1,series,el,zerotilts)
        k=os.getcwd()
        path=k+'\\Data_figures\\Rocking\\Series_{}\\Series_{},Composition_tilts
            {}'.format(series,series,S[i])
        plt.savefig(path)


"""K vs L lines comparison"""
def K_v_L_plot(series,list1,nr,zerotilts):
"""series is specific to dataset, list1 is list of spectras, nr i
    for labeling, zerotilts are the position of zerotilts"""
    series_set=make_series_list(series,list1)
    As=[]
    Ga=[]
    X=[]
    num=1
    elements=["Ga", "As", "Sb", "Si", "Cu", 'Fe','O',"Al"]
    for i in range(len(series_set)):
        ed0=hs.load(series_set[i])
        ed0.set_signal_type("EDS_TEM")
        ed0.add_elements(elements)
        ms1=ed0.create_model()
        ms1.fit()
        As.append(ms1["As_Ka"].A.value/ms1["As_La"].A.value)
        Ga.append(ms1["Ga_Ka"].A.value/ms1["Ga_La"].A.value)
        X.append(num)
        num+=1
    fig, ax = plt.subplots(figsize=(20,10))
    #plt.figure(figsize=(20,10))
    print(X)
    for i in range(len(zerotilts)):
        ax.axvline(x=zerotilts[i],linestyle='--',color='r')
    plt.plot(X,As,label=r'$As K_\alpha/L_\alpha$'.format(series))
    plt.xlabel(r'Index', fontsize=18)
```

```python
    plt.ylabel(r'Ratio $\frac{K}{L}$',fontsize=18)
    plt.plot(X,Ga,label=r'$Ga K_\alpha/L_\alpha$'.format(series))
    ax.set_xticks(X)
    ns=[]
    for i in range(len(series)):
        ns.append(series[i]+1)
    ax.set_xticklabels(ns)
    plt.xticks(size = 17)
    plt.yticks(size = 17)

"""Automate the comparison of K vs L lines""".
def K_vs_L_lines(S,list1, series,zerotilts):
    # series_set=make_series_list(series,list1)
    non_channeling_ref=list1[0]
    #print(list1)
    for i in range(len(S)):
        K_v_L_plot(S[i],list1,series,zerotilts)
        #plt.title('K/L lines for selected tilts',fontsize=24)
        plt.legend(prop={'size': 20})
        plt.ticksize=20
        k=os.getcwd()
        path=k+'\\Data_figures\\Rocking\\Series_{}\\Series_{},K_vs_L_lines
            tilts {}'.format(series,series,S[i])
        plt.savefig(path)

""""specific ALCHEMI for this dataset, usabel for statalch"""
def ALCHEMI_at_tilts(series,list1,stat_alch=False):
    ref=[-1,-2]
    ref_list=make_series_list(ref,list1)
    series_set=make_series_list(series,list1)
    elements=["Ga", "As", "Sb", "Si", "Cu", 'Fe','O',"Al"]
    ed=hs.load(ref_list[0])
    #print(ref_list[0])
    ed.set_signal_type("EDS_TEM")
    ed.add_elements(elements)
    ms0=ed.create_model()
    ms0.fit()

    ed=hs.load(ref_list[1])
    #print(ref_list[0])
    ed.set_signal_type("EDS_TEM")
```

```python
    ed.add_elements(elements)
    ms02=ed.create_model()
    ms02.fit()

    p=[]
    p1=[]
    i=0
    X=[]
    for i in range(len(series_set)):
        ed0=hs.load(series_set[i])
        ed0.set_signal_type("EDS_TEM")
        ed0.add_elements(elements)
        ms1=ed0.create_model()
        ms1.fit()
        p.append(Alchemi(ms0,ms1,"As_Ka","Ga_Ka","Sb_La"))
        p1.append(Alchemi(ms02,ms1,"As_Ka","Ga_Ka","Sb_La"))

        X.append(ms1['As_Ka'].A.value)
        if p1[-1]!='Null' or p[-1]!='Null':
            print(series[i]+1, ' & ',round(p[-1],3), '&',
                round(p1[-1],3),'\\ ')
        else:
            print(series[i]+1, ' & ',p[-1], '&', p1[-1],'\\ ')
        i+=1
    if stat_alch==True:
        plt.figure(figsize=(20,10))
        plot_stat_alch(X,p,dim=1)
        plt.xticks(size = 17)
        plt.yticks(size = 17)
        plt.xlabel('N',fontsize=20)
        plt.ylabel('p',fontsize=20)
        #plt.legend(prop={'size': 20})

def ALCHEMI_series_3():
    series=3
    set_name='Spectrum '
    Oref=4
    s1=[5,4,Oref,19,16]
    s2=[15,14,Oref,9,10]
    s3=[6,Oref,12,11]
    s4=[17,18,Oref,4]
```

```
ref=-2
list1=get_list(series,set_name)
non_channeling_ref=list1[0]
S_all=range(0,21)
S=[s1,s2,s3,s4]
S=[S_all]
print('Tilt & p' )
for i in range(len(S)):
    ALCHEMI_at_tilts(S[i],list1,stat_alch=True)
k=os.getcwd()
path=k+'\\Data_figures\\Rocking\\Series_{}\\Series_{},ALCHEMI_tilts_{}'.forma
print(path)
plt.savefig(path)
```

A.3   Case 1: Sb insert in GaAs with 4 detectors

The results for the individual detectors for all cases.

A.3.1 Area 1

Composition
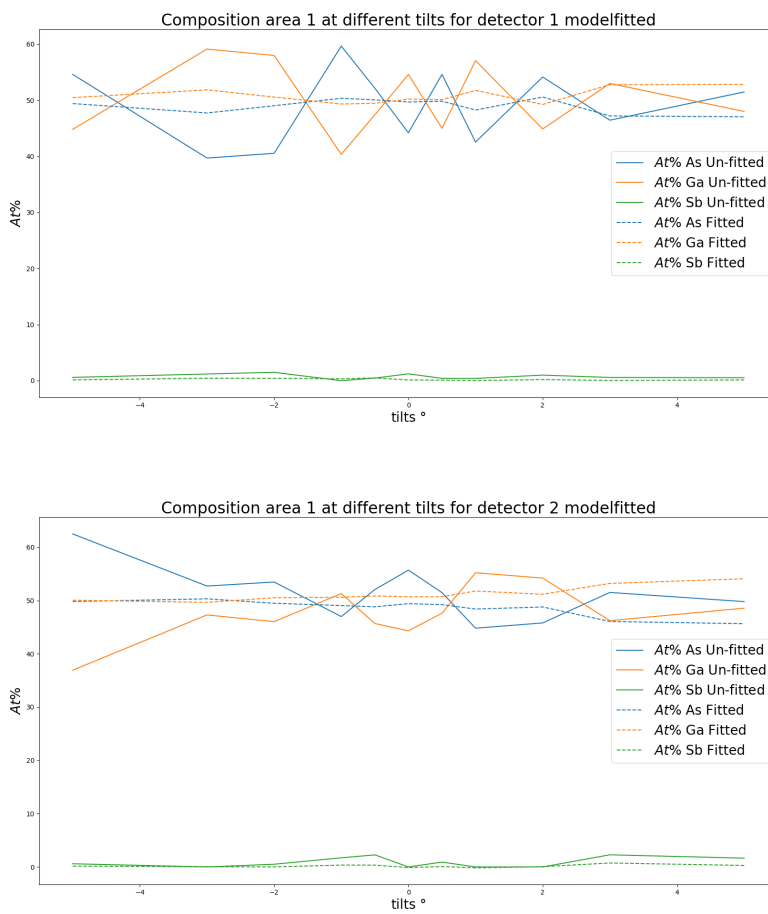
Figure A.1: Caption
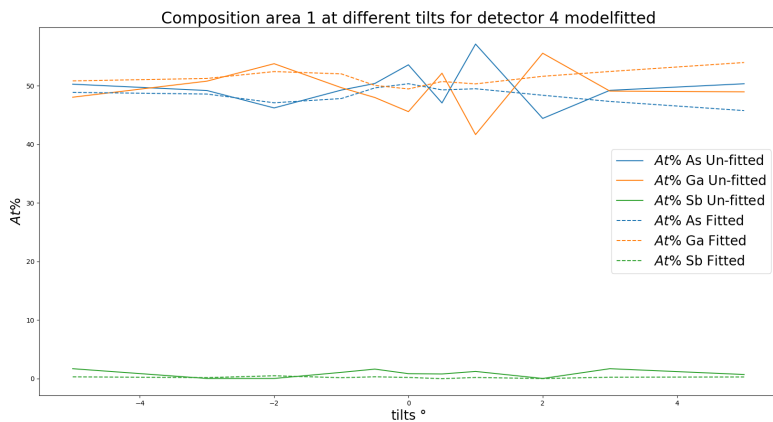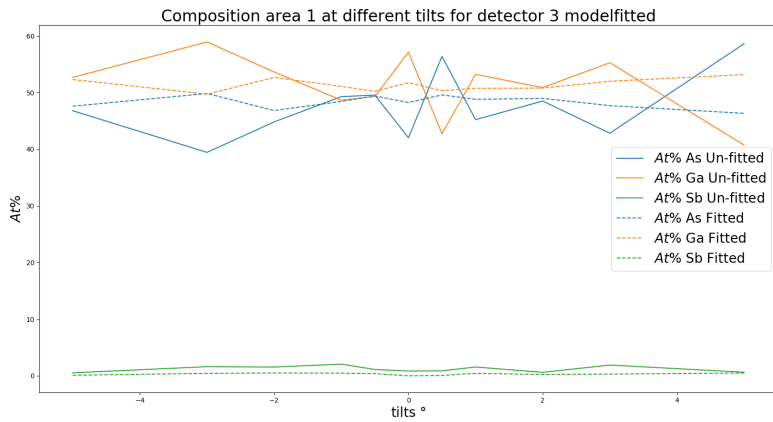
Figure A.2: Caption

Channeling
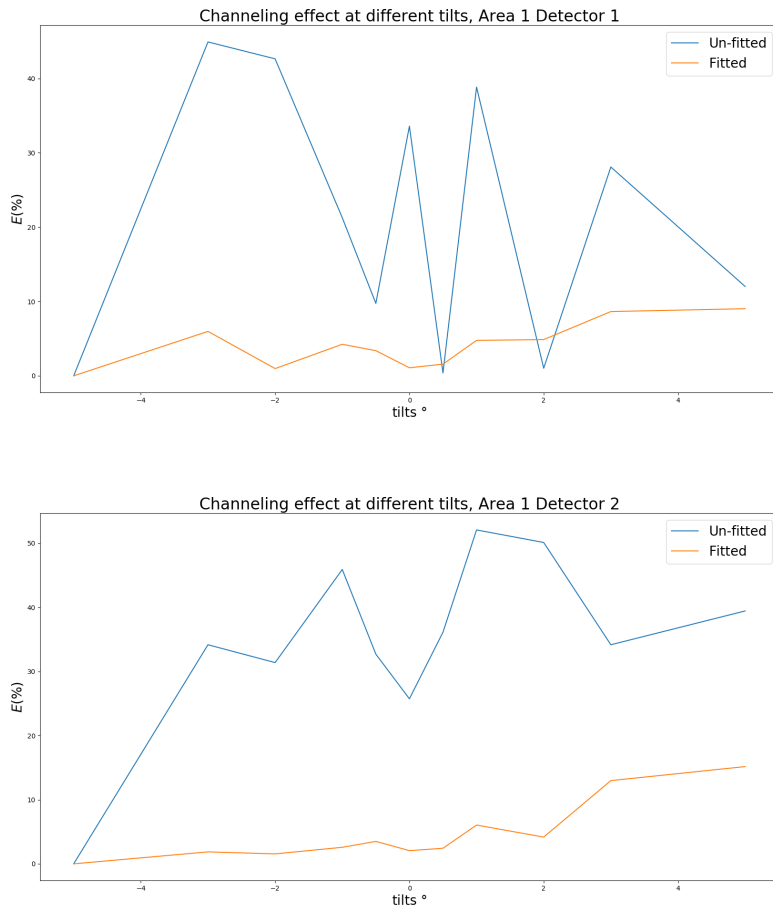
Figure A.3: Caption
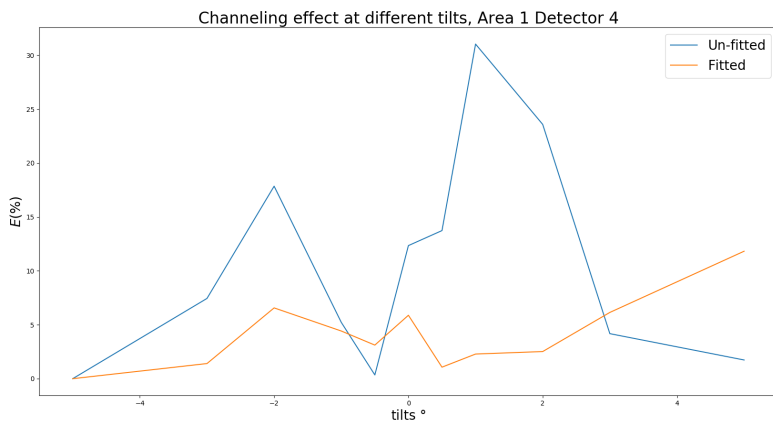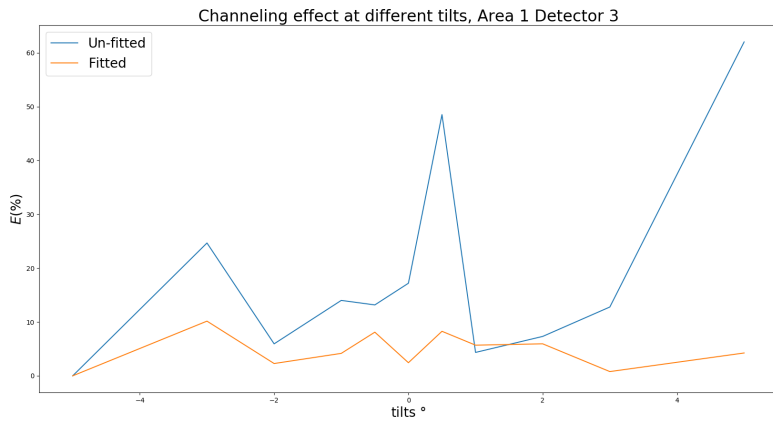
Figure A.4: Caption

Total Counts
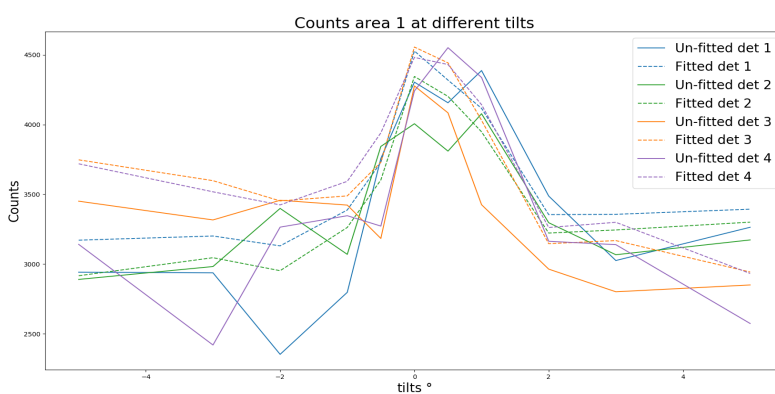
Figure A.5: Total number of counts at different tiltsfor the different detectors with a model fit at area 1

A.3.2 Area 2
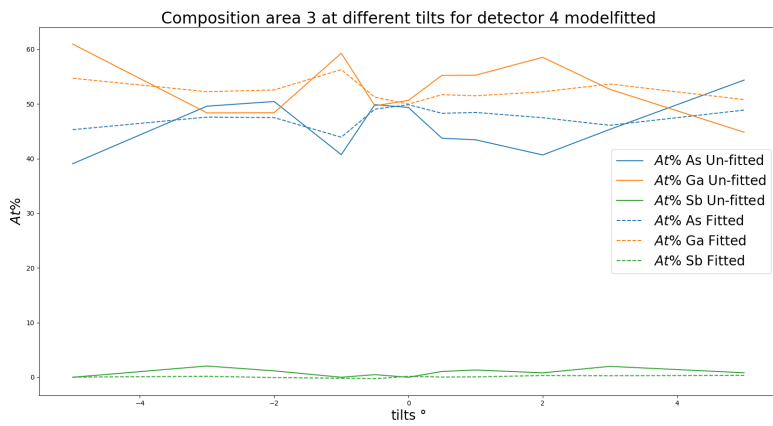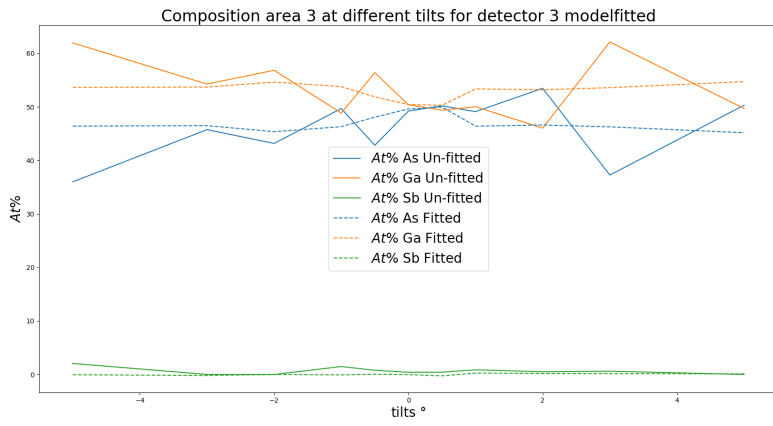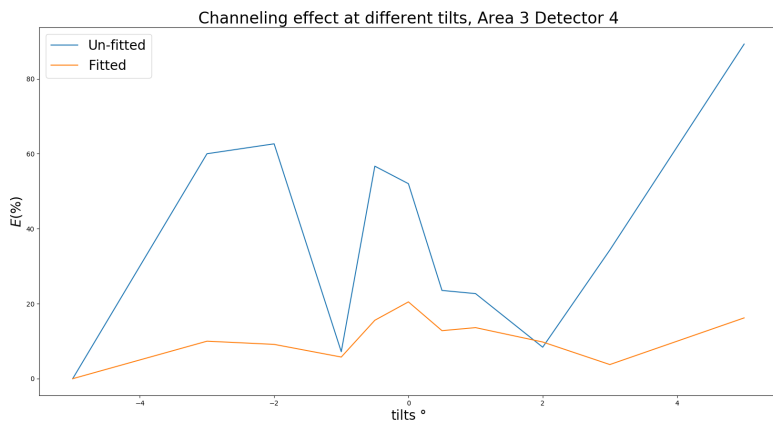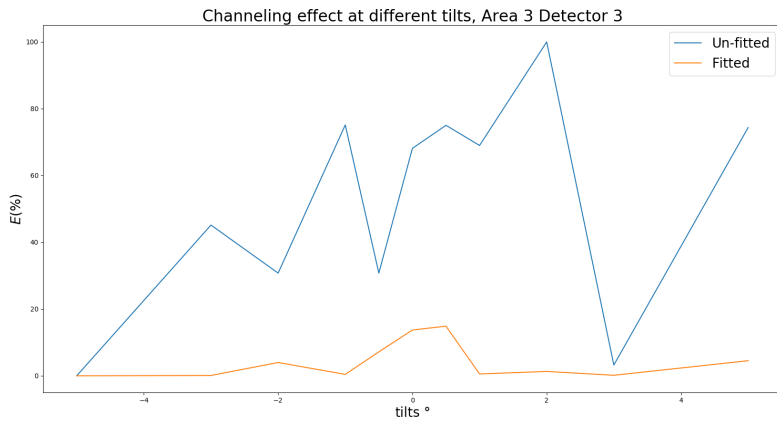
Composition
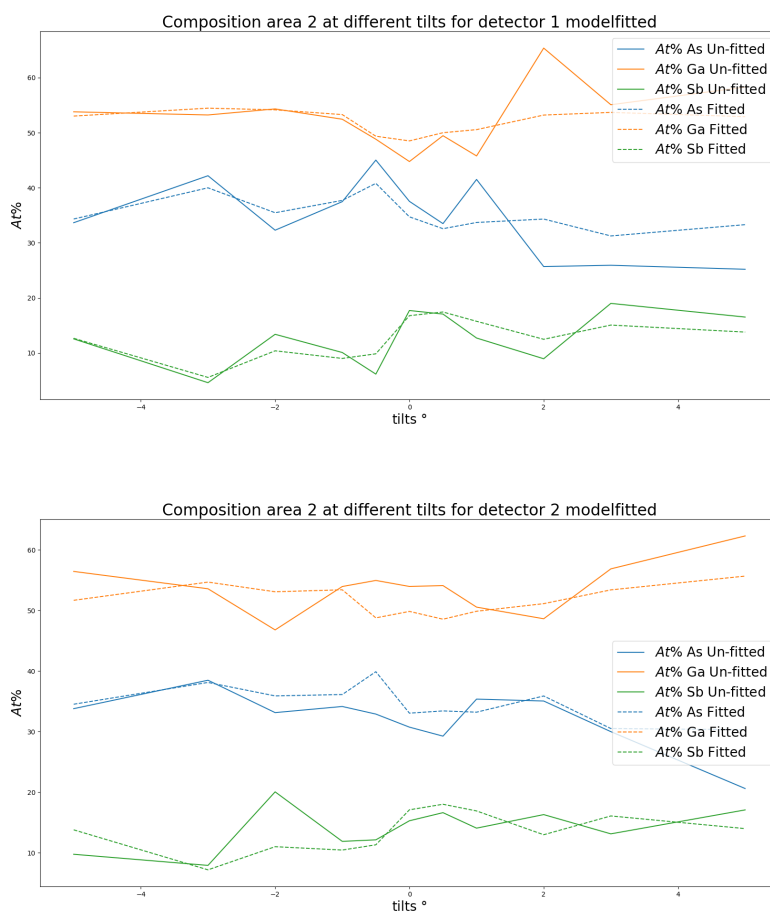
Figure A.6: Caption
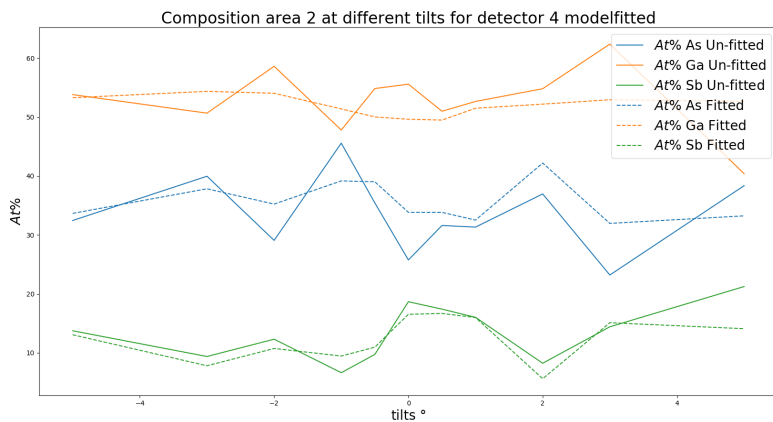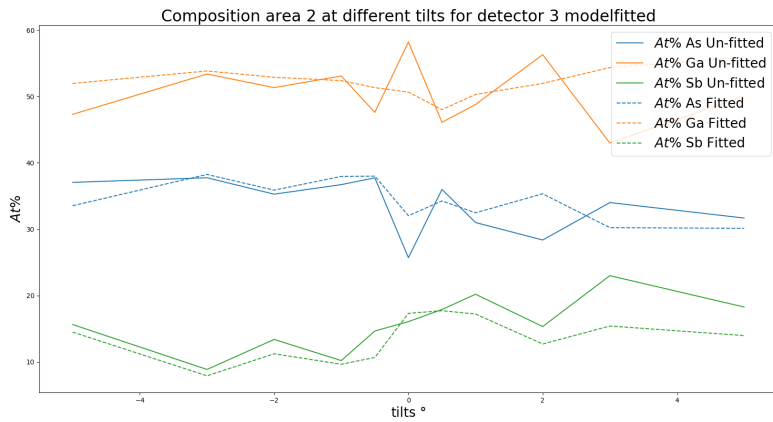
Figure A.7: Caption

Total Counts
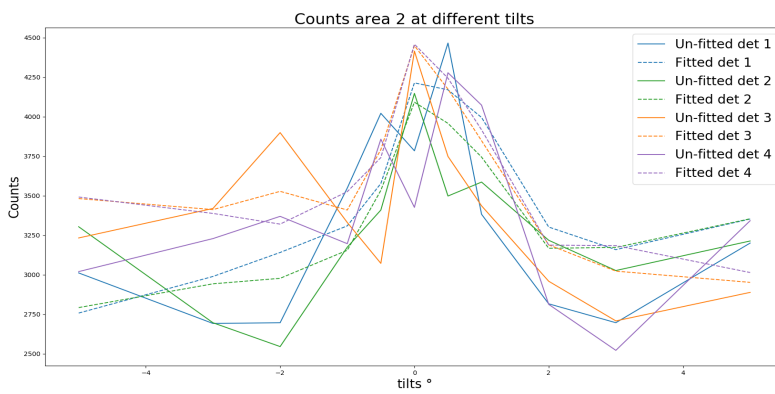
Figure A.8: Total number of counts at different tiltsfor the different detectors with a model fit at area 1

A.3.3 Area 3

Composition
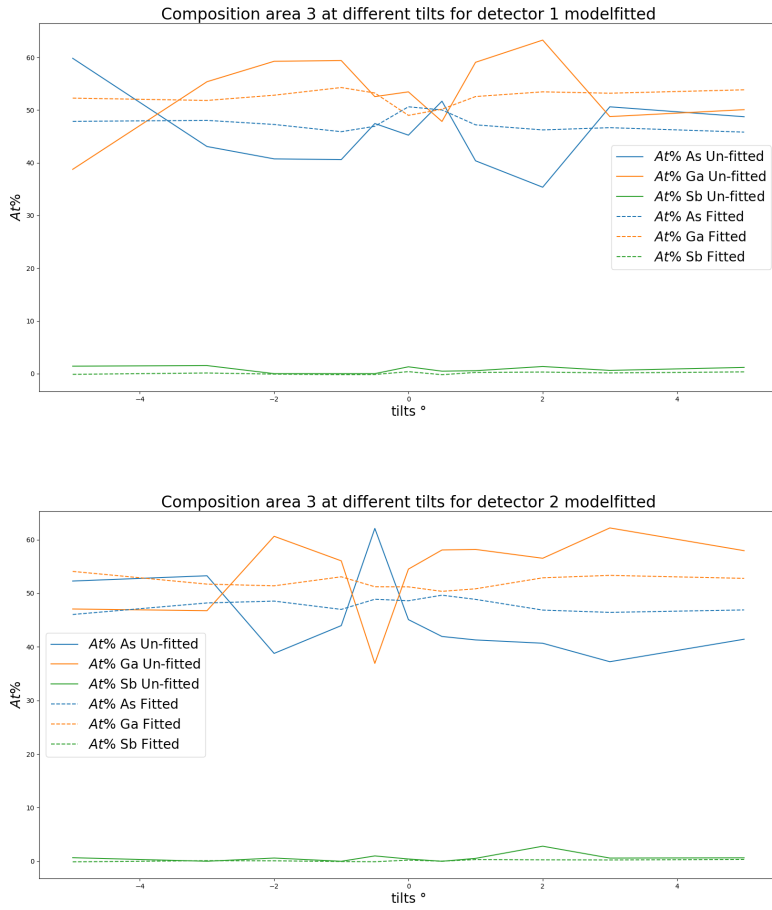
Figure A.9

Figure A.10

Channeling
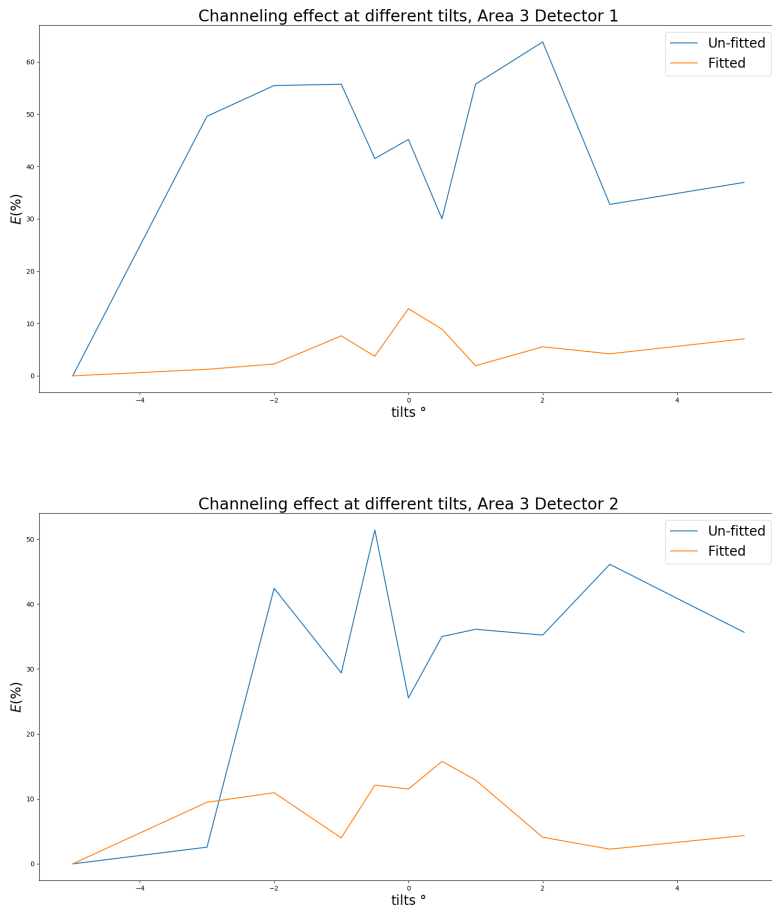
Figure A.11

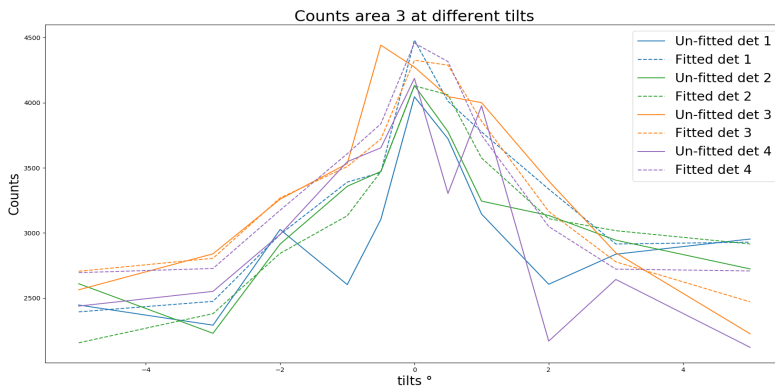**Figure A.12**

Total Counts

Figure A.13: Total number of counts at different tiltsfor the different detectors with a model fit at area 1

Øystein Rolstad